PRECLINICAL DEVELOPMENT OF ALPHA-PARTICLE THERAPEUTICS

By

Nathan Kauffman

A DISSERTATION

Submitted to
Michigan State University
in partial fulfillment of the requirements
for the degree of

Comparative Medicine and Integrative Biology– Doctor of Philosophy

2023

ABSTRACT

Internal radiation therapy is an alternative method to external beam radiation therapy for the treatment of cancer. Alpha (α)-particle based internal radiation therapy methods are being explored to improve the efficacy and toxicity compared to using beta (β-)-emitting isotopes. Two α-particle delivery platforms were developed; Pb-212-GlaS-Fc, which utilizes a systemic targeted approach, and Bi-212-MAA, which is a short-lived locoregionally delivered embolic radiopharmaceutical. Both of these radiopharmaceuticals were shown to be efficacious in treatment of cancer cells and be potential clinic therapeutics. Further, Bi-212-MAA was used as a platform to understand cellular and molecular responses of cancer to α-particle radiation. It was found that cancer cells are unable to utilize certain canonical radiation resistant responses, such as cell cycle control, when treated with α-particles. Additionally, cytokine production was dysregulated in these cells after treatment. These findings indicate that these two new delivery strategies have potential for translation to the clinic and that Bi-212-MAA can be used as a tool to elucidate additional molecular effects of α-particles on cancer cells.

TABLE OF CONTENTS

CHAPTER 1: CURRENT TRENDS IN INTERNAL RADIATION THERAPY

(Previously published as: Kauffman, N.; Morrison, J.; O'Brien, K.; Fan, J.; Zinn, K.R. Intra-Arterial Delivery of Radiopharmaceuticals in Oncology: Current Trends and the Future of Alpha-Particle Therapeutics. *Pharmaceutics* **2023**, *15*, doi:10.3390/pharmaceutics15041138.)

Introduction

Radiation therapy is a pillar of oncological care. External-beam radiation therapy is a well-established modality of tumor therapy that has gone through many technological advancements to improve accuracy, safety, and efficiency. Even with these advancements, the external beam has limitations, such as treating tumors near sensitive or mobile organs, deep-seated tumors, or wide-spread metastases [1–3]. Efforts to deliver radiation treatment in these situations have led to alternative radiotherapy technologies. Brachytherapy and Selective Internal Radiation Therapy (SIRT) place radioactive sources or drugs near or within tumors [4–6]. An emerging alternate approach is the cancer-targeted intravenous delivery of small peptides or antibodies that are radiolabeled with beta (β-)-emitters to address situations where an external beam is contraindicated. Variations on this theme include a "pretargeting" approach where an unlabeled antibody–avidin conjugate is administered and allowed to "pretarget" tumors over multiple days, followed by injection of radiolabeled biotin that quickly binds the pretargeted conjugate in the tumor, with any unbound radiolabeled biotin rapidly cleared to minimize the radiation dose to normal tissues [7–10]. This original strategy has been extended to include click chemistry instead of the avidin–biotin approach and can also be applied to cross the blood–brain barrier [11,12]. Certain thyroid cancers express a specific transporter for iodide that can be exploited for imaging and therapy. One of the oldest and most accepted treatments for thyroid cancer uses I-123-iodide for SPECT imaging and dosimetry, followed by I-131-iodide for radiation therapy [13,14]. This concept of imaging first, then selecting the appropriate therapy, has evolved into "radiotheranostics" and is rapidly advancing by using novel targeting strategies and new therapeutic radioisotopes. The purpose of this review is to discuss the current landscape of radiotheranostics, which has recently been FDA-approved for intravenous injection for imaging and therapy but is now under intensive evaluation for intra-arterial (IA) dosing. In addition, the potential of new radioisotopes that decay by α-particle emissions will be explored.

Radiotheranostics

Theranostics is a modern term that refers to the use of a diagnostic agent first to identify patients with targetable diseases, followed by treating those same patients with a therapeutic agent that is analogous to the diagnostic agent [15]. In nuclear medicine applications for cancer, the agent can be referred to as a radiotheranostic. It typically has a chelator molecule that binds one radioisotope for imaging and a second radioisotope for the therapeutic treatment of the cancer [16]. This concept is shown in Figure 1.1. The same chelator may be used to tightly bind both the imaging radioisotope and therapeutic radioisotope separately, or different chelators may be used for each. This strategy allows for an initial imaging session with Positron Emission Tomography (PET), Single-Photon Emission Computed Tomography (SPECT), or gamma camera imaging to confirm the high uptake or proper targeting of the agent in an individual patient's tumor before proceeding to a therapeutic radioisotope in a later treatment session. The main pillar of radiotheranostics, which involves the use of a radioisotope with a lower radiation dose for screening before committing to the desired therapeutic radioisotope, is not a new concept and has been used widely in nuclear medicine. This is highlighted in Tables 1.1 and 1.2, which summarize FDA-approved radiopharmaceuticals.

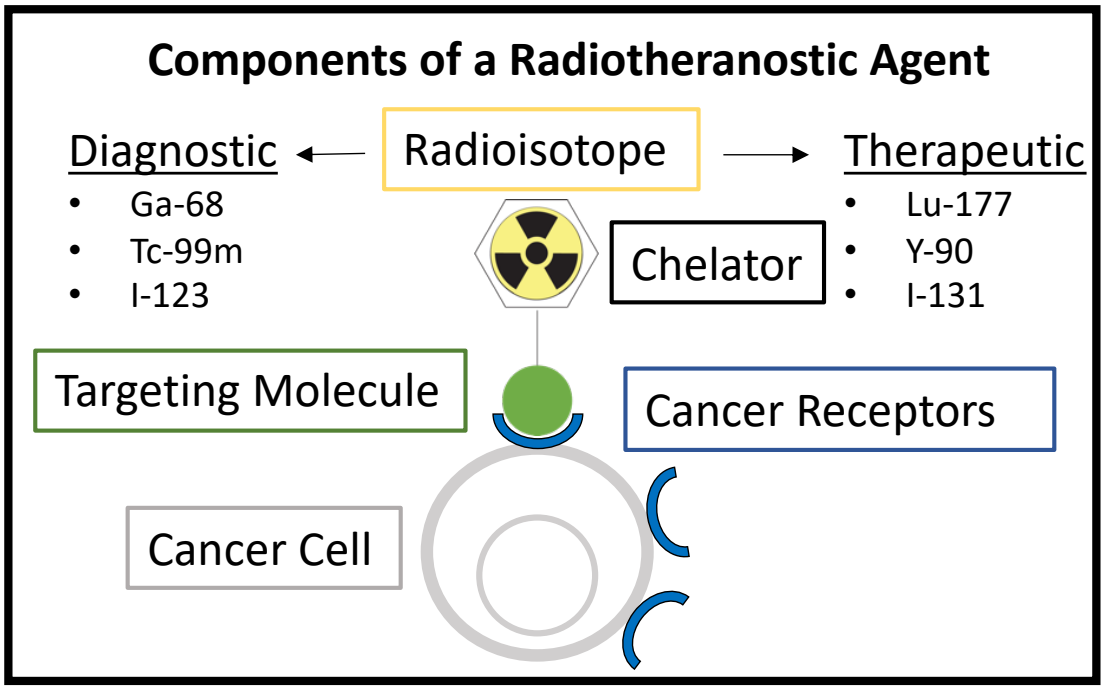

Figure 1.1 | Components of a radiotheranostic, showing the same targeting molecule being used for either diagnostic or therapeutic applications depending on the radioisotope.

Table 1.1 | FDA-approved Radiotheranostic Combinations.

Imaging Agent	Therapeutic Agent	Cancer Indication
I-123-Iodide (Sodium Iodide I-123)	I-131 Iodide (Hicon)	Hyperthyroidism and selected cases of thyroid carcinoma
I-123-iobenguane (MIBG, Adreview)	I-131 iobenguane (Azedra)	Pheochromocytoma and paraganglionoma
Ga-68-DOTATATE (Netspot) Ga-68-dotatoc Ga-68-gozetotide (Locametz and Illuccix) Cu64-DOTATATE (Detectnet)	Lu-177-DOTATATE (Lutathera)	Somatostatin-positive Neuroendocrine tumors
Ga-68-PSMA-11 F-18-piflufolastat (Pylarify)	Lu177- vipivotide tetraxetan (PSMA-617; Pluvicto)	PSMA-positive metastatic castration-resistant prostate cancer; for patients previously treated with androgen receptor pathway inhibition and taxane-based chemotherapy

Table 1.2 | Other FDA-approved Radiation Therapeutics.

Imaging Agent	Therapeutic Agent	Cancer Indication
Tc-99m-medronate (MDP)	Sr-89 chloride (Metastron)	Bone metastases; areas of altered osteogenesis, typically increased osteoblastic activity
	Ra-223 dichloride (Xofigo)	Castration-resistant prostate cancer, symptomatic bone metastases, and no known visceral metastatic disease
Tc-99m-MAA	Y-90-loaded glass microspheres (Theraspheres) Y-90-resin microspheres (SIR-Spheres)	Hepatocellular carcinoma, off-label use for liver metastasis
In-111-Zevalin (the FDA removed the requirement for this scan prior to Y-90-Zevalin therapy in 2011)	Y-90 ibritiumomab tiuxetan (Zevalin)	Lymphoma
	P-32 Colloid	Cavitary metastases of cancer

The two drug combinations that match the modern definition of radiotheranostics are Gallium-68-DOTATATE/Lutetium-177-DOTATATE (Netspot/Lutathera) and Ga-68-PSMA-11/Ga-68-PSMA-617 (Ga 68 PSMA-11/Pluvicto). Netspot/Lutathera utilizes DOTATATE to target somatostatin receptor-positive neuroendocrine tumors. PET imaging with Ga-68-DOTATATE confirms targeting and high levels of the agent in the tumors to subsequently justify multiple cycles of Lu-177-DOTATATE for β-radiation therapy. Lutathera was approved by the FDA in 2018 after the impressive success of the Phase 3 NETTER-1 trial, where progression-free survival at 20 months post-treatment was 65.2% in the Lu-177-DOTATATE arm and 10.8% in the standard-therapy arm [17].

Following development of somatostatin-receptor imaging/therapy very closely was the targeting of the prostate-specific membrane antigen (PSMA) for the diagnosis of castration-resistant prostate cancers. Ga-68-PSMA-11 (Ga 68 PSMA-11) was FDA-approved in 2020, followed by F-18-piflufolastat (Pylarify) in 2021. Subsequently, Lu-177-PSMA-617 (Pluvicto) was approved in March 2022 for therapeutic applications [18,19]. PSMA-617 targets PSMA and becomes internalized into cancer cells [20]. Major side effects can result from this therapy due to the off-targeting of the molecule; these include xerostomia, renal damage, and bone marrow ablation. An improvement in total body distribution and the targeting of tumors by alternate delivery techniques or improved PSMA drug pharmacodynamics/kinetics can not only decrease these side effects but also lead to a better tumor response.

Nearly all current FDA-approved radiopharmaceutical drugs for imaging and therapeutic applications are required to be injected intravenously per their label indications, except for I-213 and I-131 (oral). These cancer-seeking drugs have a biological half-life long enough to bind and accumulate in tumor tissue with sufficient clearance to provide appropriate tumor levels over the background for imaging and to reduce toxic effects on normal tissues [21]. The few radiotheranostic agents available and the narrow range of applicable tumor indications for each drug highlight the challenges in developing them and obtaining FDA approval and insurance reimbursement [22–24]. Radiotheranostics have the potential for “off-label” routes of administration under defined conditions, such as during approved clinical trials. Alternate forms of delivery could increase the specificity of targeting agents and increase the tumor-to-healthy-tissue dosing profile [25,26]. Image-guided IA delivery is an established method for a variety of

cancer drug therapies, including radioisotope therapy such as yttrium-90, and would thus be applicable for radiotheranostics.

Interventional Oncology

Interventional oncology (IO) encompasses a variety of minimally invasive procedures utilizing fluoroscopy, ultrasound, or Computed Tomography (CT) imaging guidance to deliver local therapy to tumors [27]. IO procedures are performed by a subspecialized physician who is board certified in Interventional Radiology (IR). Figure 1.2 shows a typical IR angiosuite and an overview of a Y90 radioembolization procedure. The two main treatment options in IO are ablation and embolization. Ablation consists of tumor destruction achieved through direct medication injection, heating, freezing, or electroporating the tumor tissue. Embolization is a procedure that targets tumors via their arterial blood supply. After navigating a catheter into the appropriate artery, a variety of treatment agents can be directly injected into a tumor. Embolization particles can be mixed with chemotherapy, contain radioactive sources, or simply block the blood supply to the tumor to cause tissue ischemia and destruction. These IO therapies can be used individually, in combination, or with other oncologic treatments to achieve the desired goal.

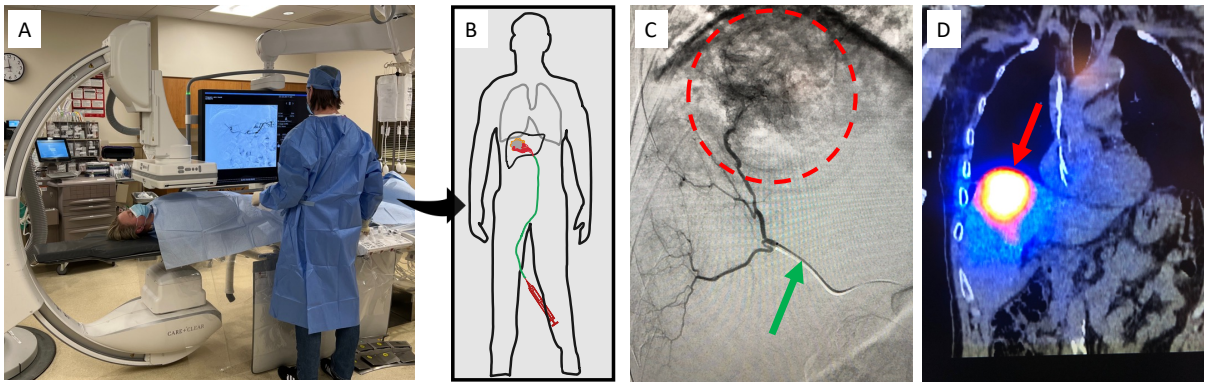

Figure 1.2 | Overview of a fluoroscopy suite and Y90 procedure. Patients are placed on a bed underneath a fluoroscopy machine (**A**), which allows the physician to use image guidance to guide a catheter to the point of interest (**B**). Fluoroscopic imaging (**C**) allows visualization of a radio-opaque catheter (green arrow), which can be used to inject contrast dye that outlines the vessels feeding the tumor (red circle). Once in the proper location, therapeutic Y90 can then be delivered, and follow-up SPECT imaging (**D**) can confirm retention in the tumor.

Patients who are candidates for IO procedures typically have tumors that are limited in size and/or spread of disease. In most oncologic centers, patients are evaluated by a multidisciplinary group of physicians, also known as a “Tumor Board”, to determine the optimal

treatment pathway. In many scenarios, IO procedures can be curative. Interventional oncologic procedures can also be utilized to decrease a patient's tumor burden and make them a candidate for other curative treatments such as surgical resection or transplantation. In the absence of a curative treatment option, IO procedures can also be employed for palliative purposes to prolong life and treat malignancy-related pain and other symptoms. IO therapies are minimally invasive and well tolerated, with most performed under sedation on an out-patient basis. This allows for a larger population of patients to be treated compared to more invasive alternatives.

Radioembolization

One of the most common IA cancer therapies is the delivery of radioactive, embolic particles directly into tumors, also known as SIRT or Transarterial Radioembolization (TARE). Currently, two types of particles are FDA-approved for use in this procedure: SIR-sphere and Therasphere. Both utilize small embolic beads labeled with yttrium-90 to lodge within tumor-specific arterial vasculature and deliver a therapeutic dose to a tumor with β-radiation. As both these particles use yttrium-90 as the therapeutic agent, the treatment is also sometimes referred to as Y90. The only FDA-approved indication for Y90 is unresectable liver cancer, which can be primary hepatocellular carcinoma or liver metastases from a different primary tumor location [28].

The clinical trial that led to SIR-sphere approval was a phase 3 randomized trial comparing the responses of patients with colorectal cancer metastases to the liver treated with either chemotherapy alone or a combination of SIRT and chemotherapy. Improvements were seen in partial and complete responses, tumor volume, and serum levels of the carcinoembryonic agent [29]. Multiple trials have since confirmed the long-term efficacy of radioembolization, which has already been well summarized [30]. There are many current trials exploring the advancements in radioembolization, including Y90 combination therapies and improved Y90 dosimetry [31–34]. Two other areas of interest are the radioembolization of extrahepatic tissues and the development of novel radioembolics.

Mouli et al. performed an initial study in dogs to explore the use of Y90 in the prostate [35]. The study was performed in 14 male castrated beagles with induced prostatic hyperplasia. The treated dogs showed a significant decrease in the treated hemigland compared to the untreated contralateral hemigland control. They also showed no clinical signs of toxicity. Further, histology showed radiation-induced cell death in the treated prostate gland tissue, while

radiography and gross observation of the extraprostatic organs showed no changes. This result indicates that the prostate, although a very different tissue compared to the liver, is amenable to Y90. The success of future therapeutic studies could open the door for additional targets, such as breast cancer, which has been shown to be targetable with IA-delivered chemotherapy [36].

Other radioembolics being investigated are Iodine-131 lipiodol, Rhenium-188 lipiodol, Rhenium-188 microspheres, and Ho-166 microspheres [28]. In Europe, Ho-166-labeled microspheres are emerging as a third option next to SIR-spheres and Theraspheres [37]. Ho-166 is an attractive option mainly for its partial gamma (γ) emission (6.7%). While pure β-emitters are typically seen as the most ideal therapeutic agent, having some γ emission, such as in the case of Ho-166, allows for better imaging and thus tracking of the microspheres when compared to Y90. Better tracking is available for both the scout imaging session before therapy and the therapy delivery itself. Due to Y90′s poor imaging qualities, technetium-99m-labeled macroaggregated albumin (MAA) is used for scouting and calculating liver shunts to the venous system. MAA is similar in size to Y90 spheres but is not a perfect predictor for Y90 distribution. Since Ho-166 has inherent imaging properties, it can be used at a low dose to predict its own deposition profile and dosimetry upon therapeutic delivery. Post-treatment, Ho-166 deposition can be more accurately imaged with SPECT/CT compared to Y-90 since Y-90 does not have γ emissions but relies on Bremsstrahlung radiation instead, which is not ideal.

Overall, radioembolics are a promising prospect because they are receptor-agnostic, which means they do not rely on the high expression of a cancer-specific biological marker relative to healthy tissues to achieve therapeutic effect. Since cancers are highly heterogeneous across both tissue types and individual patients, having a diverse range of tools is highly beneficial. A recent review of reports investigating new β-emitting microparticles highlights the interest in developing new radioembolics at the preclinical level [38]. Alternatively, combining the specificity of selective IA delivery with cancer receptor binding may prove to be the best option when available.

Intra-Arterial Delivery of Radiopeptides

The IA delivery of receptor-targeted radiopharmaceuticals has also gained interest at the clinical level [39]. Radiotheranostics delivered via IA administration have the potential to both increase the amount of targeted cancer binding and decrease the uptake in non-target tissues, thereby reducing toxicity. Although Lu-177-DOTATATE (Lutathera) and Lu-177-PSMA-617

(Pluvicto) have only recently become FDA-approved, these agents, along with similar analogues, are already being evaluated in several clinical trials to determine the potential advantages of IA delivery using the same dosing levels as IV (Table 1.3).

Table 1.3 | DOTATATE- and PSMA-Related Radiopeptides Delivered via IA in Clinical Trials.

Study Name [Reference Number]	Radiopharmaceutical Used	Phase	# of Participants
Intra-arterial Lutetium-177-dotatate for Treatment of Patients With Neuro-endocrine Tumor Liver Metastases (LUTIA) [NCT03590119]	Lu-177-DOTATATE	2/3	26
Lutathera in People With Gastroenteropancreatic (GEP), Bronchial, or Unknown Primary Neuroendocrine Tumors That Have Spread to the Liver [NCT04544098]	Lu-177-DOTATATE	1	10
Intra-arterial Hepatic (IAH) Infusion of Radiolabeled Somatostatin Analogs in GEP-NET Patients With Dominant Liver Metastases (LUTARTERIAL) [NCT04837885]	Lu-177-DOTATATE	2	20
Personalized PRRT of Neuroendocrine Tumors (P-PRRT) [NCT02754297]	Lu-177-Octreotate	2	300
Comparison of Hepatic Intra-arterial vs. Systemic Intravenous 68Ga-PSMA PET/CT for Detection of Hepatocellular Carcinoma [NCT05111314]	Ga-68-Gozetotide	1	10
Pharmacokinetics of IA and IV Ga68-PSMA-11 Infusion [NCT04976257]	Ga-68-PSMA-11	1	5

Figure 1.3 summarizes the paradigm of IA delivery of a radioembolic and a radiotheranostic, with the embolic drug becoming lodged within the vasculature and the radiopeptide entering the tumoral space to target cancer cells. The IA delivery method results in higher radiopeptide binding in tumors compared with IV delivery. This has been demonstrated in multiple clinical trials across a variety of cancer types and tissue locations.

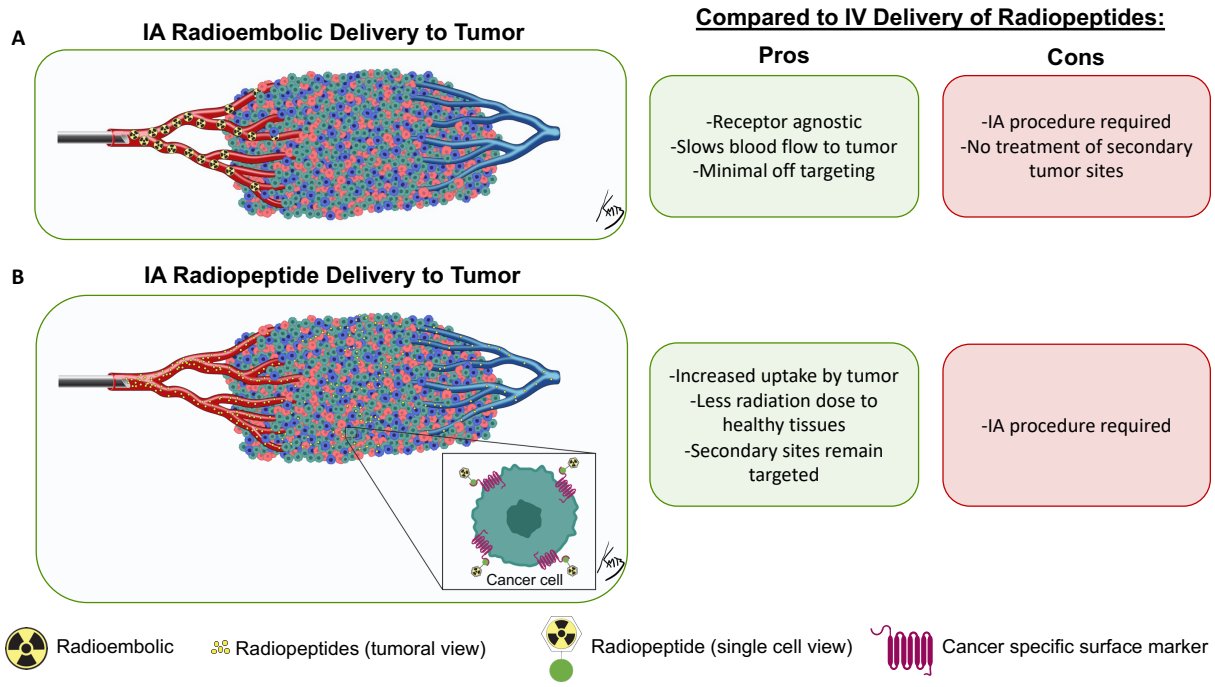

Figure 1.3 | Overview of the IA delivery paradigm of radioembolics and radiopeptides. The radioembolic (**A**) becomes lodged in the smaller arterial vessels and will not cross over into the venous system. Conversely, radiopeptides (**B**) will enter the tumor space and bind to specific cancer receptors. Not all radiopeptides will be retained in the tumor and will instead travel systemically through the venous system. This allows for a higher accumulation of the radiopeptide in the tumor while still giving a systemic dose for satellite tumor-site treatment. In the tumor diagram, green cells are tumor cells expressing the specific marker, while red and blue cells are non-targeted tumor microenvironment cells. Figure 1.3 tumor vasculature: © Kevin Brennan 2023.

Kratochwil et al. demonstrated improvement in therapeutic efficacy using the IA delivery of Y-90-DOTATOC to treat metastatic neuroendocrine tumors to the liver [40]. Y-90-DOTATOC is a somatostatin-receptor targeting ligand with a β-emitting radioisotope, making it functionally similar to Lu-177-DOTATATE (Lutathera). The IA delivery of DOTATOC was first proven with a Ga-68-labeled agent, and IA showed a 3.7-fold increase in tumor accumulation compared with IV dosing.

With the knowledge gained from the IA imaging study, Kratochwil et al. performed a therapeutic trial in 15 patients with unresectable neuroendocrine tumor metastasis to the liver [41]. The patients received hepatic artery-infused DOTATOC labeled with either Y-90 or Lu-177 after confirmation of targeting with IA In-111-DOTATOC imaging. One patient had a complete response, eight had partial remission, and six had stable disease according to RECIST criteria.

These results are promising, but without a comparison to IV therapy, it cannot be determined if the increased comparative uptake seen on imaging with IA delivery would lead to better tumor responses.

Thakral et al. performed a similar trial comparing IA to IV delivery of Lu-177-DOTATATE to neuroendocrine metastases [42]. A total of 29 patients were enrolled in the study; 15 patients received a single IA dose and the other 14 received a single IV dose. A threefold increase in tumor uptake was seen with IA compared to IV delivery, and no significant difference was seen in the absorbed dose to other healthy organs. Further, no patients in the IA group experienced any adverse events. These results mirror the findings from Kratochwil et al.

Prostate cancer has been investigated as a target for both Y90 and IA delivery of radiotheranostics. Sayman et al. compared the ratio of the absorbed dose of Lu-177-PSMA in prostate lesions compared to healthy organs in the IA and IV delivery techniques [43]. Four patients were given IV treatment one week before receiving the same therapy through IA delivery. The patients were imaged with SPECT/CT to determine the total dose in lesions vs. healthy organs after each delivery technique. Improvements were seen in the ratio of radiation dose delivered to the dominant prostate lesion compared to the liver, bone marrow, healthy prostate, and whole body. When looking at the direct dominant lesion accumulation in IA vs. IV, only a 1.2-fold increase was observed. It was hypothesized that the initial IV treatment "stunned" the tumor and prevented a high uptake in the IA treatment. The critical advantage found in IA delivery was the lower dose present in healthy tissues compared to IV.

Two studies showed improvement in the accumulation of radiopharmaceutical drugs in meningioma with IA delivery. Verburg et al. compared IV and IA uptake of Ga-68-DOTATATE in four patients with inoperable meningiomas [44]. Compared to IV baseline uptake, patients averaged 2.7-fold more uptake in their respective tumors on PET/CT imaging after IA dosing. No change in toxicity was noted. More recently, Vonken et al. performed a similar study on four patients with meningiomas and compared IV and IA uptake of Lu-177-HA-DOTATATE [45]. Patients averaged a nearly five-fold increase in lesion accumulation of Lu-177 on SPECT/CT imaging with IA delivery. The technical success of the IA procedure was 100%, and no differences in adverse effects were found.

Averaging the reported ratio data from these five studies results in approximately three-fold more accumulation of IA delivered radiopharmaceuticals in tumor tissue compared to IV dosing. Summarized data and the calculated average are reported in Figure 1.4.

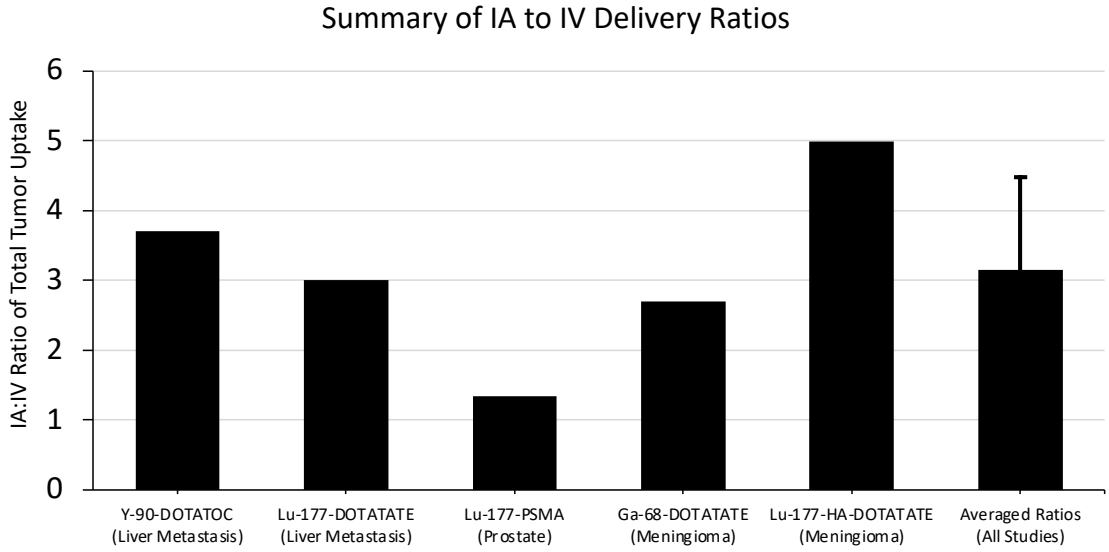

Figure 1.4 | Summary of findings comparing IA and IV delivery of radiopharmaceuticals to tumors. The ratios from all studies were averaged, and the standard deviation of the average is reported here. The authors of the corresponding studies are as follows: Kratochwil et al. (Y-90-DOTATOC) [40], Thakral et al. (Lu-177-DOTATATE) [42], Sayman et al. (Lu-177-PSMA) [43], Verburg et al. (Ga-68-DOTATATE) [44], and Vonken et al. (Lu-177-HA-DOTATATE) [45].

It is important to mention the recently finished LUTIA trial (official title: "Intra-arterial Lutetium-177-dotatate for Treatment of Patients With Neuro-endocrine Tumor Liver Metastases"). This trial employed a within-patient design where one liver lobe was treated IA and the opposite liver lobe received an IV treatment downstream from the IA infusion site [46]. The results of this trial in 26 patients have not been released yet, but they should give a great sense of the effectiveness of IA delivery of cancer receptor-targeted therapy.

Risks and Cost Comparison of IA vs. IV Delivery of Radiopharmaceuticals

Part of the attraction of IV-delivered radiopharmaceuticals is their low risk and low cost, as the procedure is essentially identical to any other IV-delivered drug. In comparison, IA procedures incur a much greater cost and have associated risks. Advancing a catheter into a deep arterial space requires a trained interventional radiologist, a large group of trained staff, intraprocedural imaging, and peri-procedural care. This adds additional costs and requires additional planning and utilization of critical procedural spaces. Additionally, image guidance

procedures result in radiation exposure and additional risks compared to IV. Fluoroscopy-guided techniques require repeated X-ray exposures to visualize catheter advancement and position, but the total X-ray radiation dose is kept to a minimum as much as possible. IA procedures can rarely cause side effects, the most severe of which are vessel damage or hemorrhage.

Further, not all patients or tumors may be candidates for such a procedure. Some tumors may not have ideal vascular access or arterial components to make an IA procedure beneficial. Some tumor arteries can be tortuous, making it difficult to gain access and leading to poor target delivery. Embolics specifically need to be carefully placed in tumor-specific areas to prevent creating ischemia in healthy tissue. Additionally, leakage of embolics out of the tumor space could lead to accumulation and dosage in the lungs.

Alpha-Particle Therapy

Further driving the potential of radiotheranostics is the application of radioisotopes that decay by alpha (α)-particle emission in addition to radioisotopes that have only β-emission. Ra-223 dichloride is the only FDA-approved radiopharmaceutical that decays with α-particle emissions. The Ra-223 ionic chemical form binds most metastatic bone lesions with altered osteogenesis and has been used to treat many men with painful prostate bone metastases. All remaining FDA-approved radiopharmaceuticals rely on β-energy for radiation therapy. The β-decay occurs when a neutron converts to a proton and an electron and the high-energy electron (β-) is ejected from the nucleus. Radioisotopes decaying with β-emissions include I-131, Lu-177, and Y-90 and are used for a variety of reasons, including their half-life, purity, and ease of commercial production. One issue has arisen with β-emitting radiopharmaceuticals as our understanding has improved for applications in the preclinical and clinical settings: the penetration range of β-, while allowing for crossfire in non-targeted cancer cells, can deliver high and toxic radiation doses to the surrounding healthy tissues [47].

Alpha (α)-particles, which comprise two neutrons and two protons, are emitted from large unstable radioisotopes during decay. A comprehensive review of targeted α-particle therapy was recently published. It highlights not only current radiopharmaceuticals but also basic radiation biology [48]. Briefly, α-emitting radionuclides have not been widely used at the clinical level because of their low commercial availability and lack of pure α-emitting nuclides. Alpha (α)-particles are attractive from a cancer biology standpoint because of three major benefits

compared to those that decay by only β-emissions: high linear energy transfer (LET), short penetration range, and efficiency in hypoxic environments.

Alpha (α)-particles have a linear energy transfer of 100 keV/μm compared to the 0.2 keV/μm of β-particles in tissue. The higher LET means a larger portion of the total radiation dose is delivered over an equal pathlength. Alpha (α)-particles can deliver up to 1000× more dose to cells than β-particles, even with the same number of radioactive decays. This high energy allows for double rather than single-strand DNA breaks, leading to increased cell death. Cancer cells can adapt to single-stranded DNA breaks and survive, but struggle when double-strand breaks occur. An incredible example of this occurred when β-resistance was overcome with α-particle therapy with Ac-225-PSMA [49]. As shown in Figure 1.5, Lu-177-PSMA was unable to debulk tumors or decrease PSA levels in this patient, but repeated doses of Ac-225-PSMA led to complete tumor eradication and a return to normal levels of PSA. Improvements in neuroendocrine cancer therapy are also seen when an α-particle emitter is used instead of β-radiation [50,51].

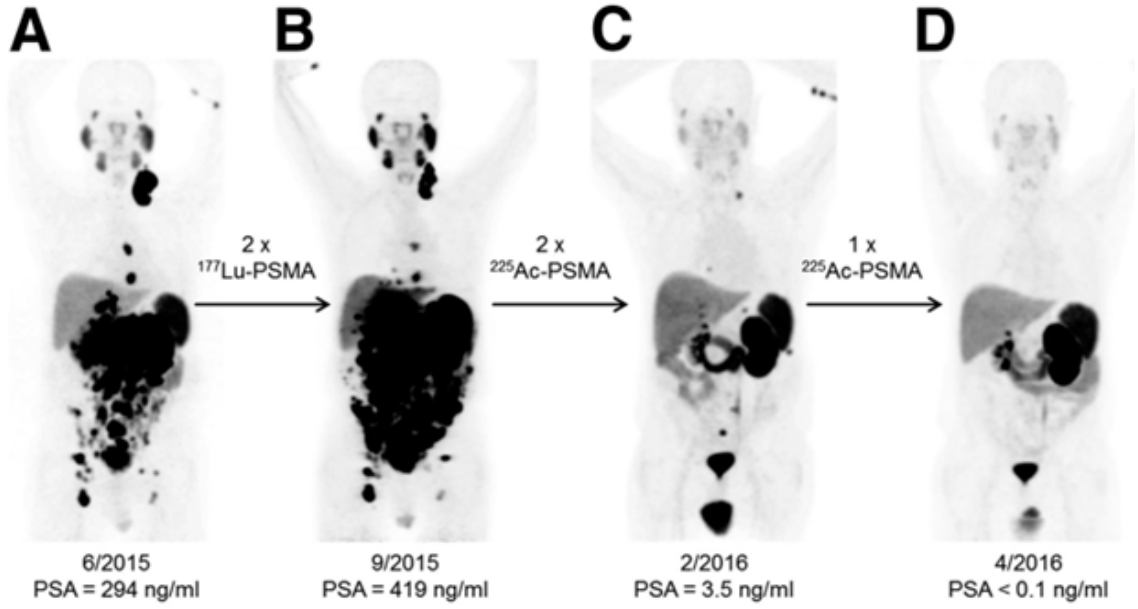

Figure 1.5 | Alpha (α)-particle therapy overcomes β-resistant cancer. This imaging was performed using Ga-68-PSMA-11 PET/CT scanning. Kratochwil, C. et al. reports, "In comparison to initial tumor spread (**A**), restaging after 2 cycles of β-emitting ^{177}Lu-PSMA-617 presented progression (**B**). In contrast, restaging after second (**C**) and third (**D**) cycles of α-emitting ^{225}Ac-PSMA-617 presented impressive response." This research was originally published in *The Journal of Nuclear Medicine* [49].

The short pathlength of α-particles is another advantage. Alpha (α)-particles deliver their energy over 40–90 μm of tissue, while β-penetrate 0.5–12 mm. Sensitive tissues near solid tumor locations, including prostate cancers, can be heavily irradiated during β-therapy. The range of α-particles is still large enough to cross multiple cell diameters, allowing for a local crossfire effect on non-targeted cells, but limiting the dose to healthy tissue [52].

Hypoxia, a hallmark of cancer, is notorious for causing resistance to a variety of cancer treatments [53]. Radioisotopes with primary β-emissions are no different and are not very effective to treat highly hypoxic tumors. The lower-energy radiation used in external-beam and β-therapies relies to a large degree on the formation of free radicals to induce cancer cell death. Conversely, α-particles rely solely on double-stranded breaks, thus making oxygen levels in the tumor environment irrelevant.

Many investigators have taken note of the advantages of using α-particles for cancer treatment [54]. Table 4 summarizes clinical trials utilizing α-particles for a multitude of cancer types. The variety of radionuclides and the total number of trials highlight the enthusiasm for using α-particles for therapy under the radiotheranostic paradigm.

Table 1.4 | All Active Trials Utilizing Available α-Particle Radionuclides for Cancer Therapy. Studies can be found by using the clinicaltrials.gov search tool with radionuclide terms formatted as in the following example: At-211 OR 211At OR Astatine-211.

α-Emitting Nuclide	**Number of Trials**	**Cancers Targeted across All Nuclides**
At-211	8	Myeloma Leukemia
Ac-225	25	Thyroid Ovarian
Bi-213	2	Neurological Non-malignant Neoplasm
Th-227	4	Colorectal Prostate
Pb-212	8	Lung Bladder
Ra-223	104	Gastric Breast Liver Bone

Alternate Delivery Strategy for Alpha-Particles

With only one FDA-approved radiopharmaceutical with α-particle emissions, it is clear that α-emitting radiopharmaceuticals have not been successfully translated to clinical settings in spite of significant research in this area. There are a variety of radioisotopes with α-particle emissions that have unique physical and chemical properties that can be matched to their intended use, such as a specific half-life or desired chelator. Alternate delivery methods allow for the additional tailoring of the overall treatment strategy. The delivery methods of α-particles in the clinical setting include IA, intraperitoneal, and intravesical.

The strongest example supporting the use of a radioisotope with α-particle emissions delivered by an alternate route was from Kratochwil et al., who used Bi-213-DOTATOC-delivered IA to overcome previous resistance to Y-90-DOTATOC therapy [55]. Patients underwent an interventional procedure to deliver therapy to the hepatic artery, meaning the treatment went to most of the liver. Further, the leakage of therapy into the systemic system allowed for treatment of disseminated sites, which is shown in Figure 1.6. While this study did not compare IA to IV as closely as others, it represents a major advancement in understanding both α-particle therapy and IA delivery of radiopharmaceuticals.

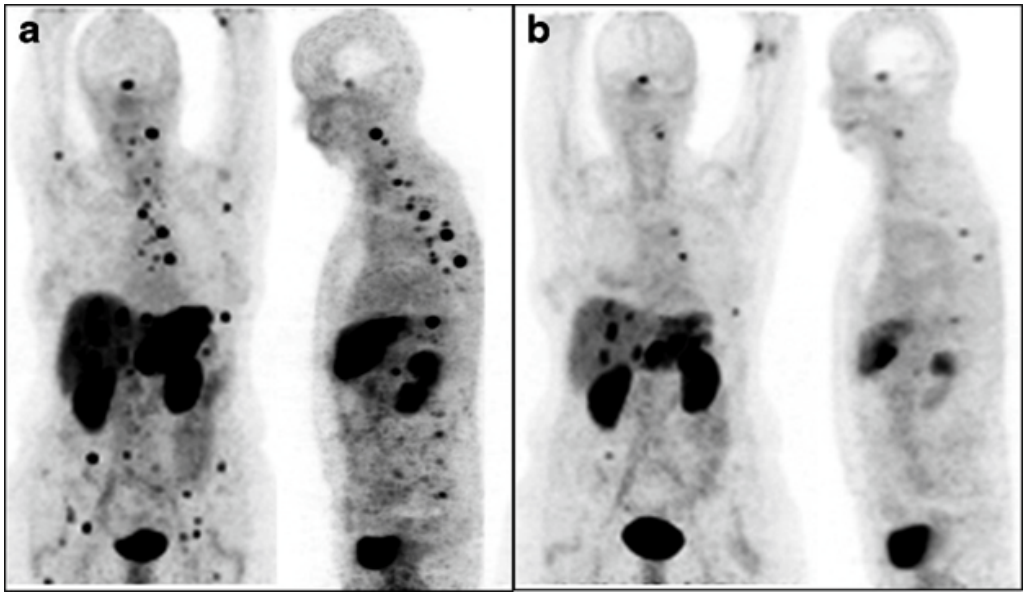

Figure 1.6 | Intra-arterial Bi213-DOTATOC overcomes Y90-DOTATOC resistance. Ga-68-DOTATOC-PET imaging shows bulky liver disease and widespread lesions before treatment (**a**). Reduction in both primary liver and metastatic disease was seen on imaging six months after administration of Bi-213-DOTATOC into the common hepatic artery (**b**). This research was originally published in the *European Journal for Nuclear Medicine and Molecular Imaging* [55]. Accessed on 1 February 2023 https://creativecommons.org/licenses/by/4.0/legalcode.

The intraperitoneal delivery of α-particle radiopharmaceuticals can increase the targeting of peritoneal-confined disease while decreasing systemic toxicity. Meredith et al. showed the peritoneal retention of Pb-212-TCMC-Trastuzumab delivered directly into the peritoneal cavity [56]. In a dose-escalation phase 1 trial with 18 patients, single-dose therapy resulted in stable disease in several patients in the higher dose cohorts with no drug-related toxicities. This is a promising delivery strategy as it targets locally disseminated disease without total-body radiation.

Intravesical delivery for bladder cancer is a known concept that has shown synergy with radionuclide therapy. Autenrieth et al. showed the efficacy of Bi-213-labeled anti-EGFR antibody after intravesical delivery for the treatment of muscle-invasive bladder cancer [57]. The therapy was delivered through a urinary catheter into the bladder, allowing direct exposure to the tumor with no leakage into the bloodstream. The treatment was safe, with no toxicities reported, and the total dose delivered to the bladder wall was within tolerable limits. Further, the dose contribution of α, β-, and γ emissions to the bladder wall was calculated, showing that approximately 76% of the dose was from β- and 21% was from α. Even though α-particles have a much higher LET, only the decays that occur within microns of the wall will result in α-particle energy deposition, whereas β-particles have a range on the millimeter scale. The much larger range of β- results in multiple-fold more energy deposition events, outweighing the higher LET of α-particles.

Recently, external-beam radiation therapy combined with immunotherapy resulted in a systemic immune response against cancer, also known as the abscopal effect. Specifically, tumors irradiated with three fractionated doses (8 Gy each) showed synergy with anti-CTLA4 antibodies against both the irradiated tumor and a secondary untreated tumor [58]. Locoregionally delivered radiation therapy could be used to replicate the three-dose approach in cases where an external beam was contraindicated. Both embolic agents and biologically targeted radiopharmaceuticals can be delivered in this fashion, and some success has already been seen using low doses of repeated Lu-177 radiopeptide therapy to stimulate anti-cancer immune function when combined with immunotherapy [59].

Embolic radiopharmaceuticals mirror the external beam in that no cancer receptors are targeted, while IA-delivered radiopharmaceuticals targeting cancer receptors have the advantage of reaching higher tumor accumulation than via IV dosing with reduced dosing to normal tissues.

Further research is needed with radiopharmaceuticals that decay quickly to recapitulate the fast and fractionated radiation therapies that are possible with an external beam. Table 1.5 outlines currently available short-lived α-particle emitters that could serve this purpose. Long-lived radioisotopes would give a gradually declining radiation treatment across their decay, thus abrogating the fractionated approach. Additionally, α-particle radiation's inherent effects on cancer immunogenicity are becoming better understood, and it may be the most ideal radiation type for inducing synergy with the immune system [60].

Table 1.5 | Source and Decay Properties of Short-lived Radionuclides that Emit an α-Particle. Accessed February 4 2023 https://periodictable.com/Isotopes/085.211/index3.full.dm.html.

Source (Parents)	**Nuclide (Half-Life)**	**Decay Mode (%)**	**Daughters (Half-Life)**	**Daughters' Decay Mode (%)**	**Other Daughters**
Cyclotron: Bi-209(α,2n)At-211	At-211 (7.2 hr)	α (41.8%) 5.98 MeV	Bi-207 (32.9 yr)	β+ 1.37 MeV	
		EC (58.2%)	Po-211 (0.5 ms)	α (100%) 7.59 MeV	Pb-207 (Stable)
Generator: Ra-224 (3.6 d)→Fr-224→Ra-224-Rn-220→Po-216→Pb-212(10.6 h)→Bi-212 (Pb-212 or Bi-212 can be eluted)	Bi-212 (60.55 m)	β- (64.1%) 0.8 MeV	Po-212 (0.3 ms)	α (100%) 8.8 MeV	Pb-208 (Stable)
		α (35.9%) 6.1 MeV	Tl-108 (3.05 m)	β- (100%) 0.6 MeV	Pb-208 (Stable)
Generator: Ac-225 (10 d)→Fr-221→ At-217→Bi-213 (Bi-213 eluted)	Bi-213 (45.6 m)	β- (97.9%) 1.42 MeV	Po-213 (3.72 ms)	α (100%) 8.5 MeV	Pb-209 (3.2 h-100% β- 0.6 MeV)→Bi-209 (1.8×10^{19} yr)
		α (2.09%) 5.9 MeV	Tl-209 (2.2 m)	β- (100%) 3.97 MeV	Pb-209 (3.2 h-100% β- 0.6 MeV)→Bi-209 (1.8×10^{19} yr)
Generator: Rn-222 (3.8 d)→ Po-218 (3.1 m)→ Pb-214 (27 m; 100% β-, 1.02 MeV)→ Bi-214 (Pb-214 and Bi-214 are in equilibrium when recovered and used together, or when Bi-214 is purified)	Bi-214 (19.9 m)	β-(99.97%) 3.27 MeV	Po-214 (0.16 ms)	α 7.8 MeV	Pb-210 (22 yr)
		α (0.021%) 5.62 MeV	Tl-210 (1.3 m)	β- 5.4 MeV	Pb-210 (22 yr)
		β-, α (0.003%) 11.1 MeV	Pb-210 (22 yr)		

Radioisotopes that decay by only α-particle emissions (no β-) are an attractive option but rare to find. One example is At-211 (7 h half-life), which is an α-emitter without any β-emission. However, it is important to note At-211's source is a cyclotron equipped with an α-particle beam rather than a generator. Generators can be located at multiple sites or regional radiopharmacies and eluted by trained staff on an "as-needed" basis. This contrasts with a cyclotron, which must have a fixed location to produce the radioisotope followed by the transportation of the radioisotope to sites that do not have access to the cyclotron. This logistical issue makes it harder, but not impossible, for At-211 to be a longer-term option for fractionated therapy approaches. As an example, a Pb-212 generator can be eluted every 3 h to harvest Bi-212, with approximately 88% of the maximum activity being available at each elution. This allows not only for multiple patients to be treated per day, but for a single patient to reliably receive multiple treatments over a specific fractionated schedule. IA procedures can be easily performed on an in-patient or out-patient basis. The short half-life of the desirable radioisotopes means radiation dosing to the cancer in a short time interval, and patients become non-radioactive quickly as well, reducing radiation exposure to family members. Thus, it is an attractive strategy to use local generator-based radioisotope systems for the manufacturing of radiopharmaceuticals for immediate use with IA procedures. This method for a locoregional fractionated therapy strategy for cancer has the potential to achieve better outcomes, especially when combined with short-lived radioisotopes that emit α-particles during decay.

Conclusion

The future of radiotheranostics looks promising as more agents gain FDA approval and costs are covered by insurance reimbursement. The current process of obtaining reimbursement approval from the Centers for Medicare and Medicaid Services (CMS) is complicated and time-consuming, and often required before insurance companies will cover the costs of radiopharmaceuticals and imaging and the physicians' fees. This is a significant problem that delays helping the maximum number of patients. Ideally, a streamlined process should allow for FDA approval to be simultaneous with reimbursement approvals. An additional problem is building the infrastructure, including installing cyclotrons to produce the radioisotopes, hot cells to safely handle the high levels of radiation, and radiopharmacies for cGMP manufacturing of the final radiopharmaceutical drugs. The process is often delayed by compliance approvals that involve multiple regulatory agencies as well as supply chain issues.

Off-target radiation damage to normal tissues is another significant problem with the current generation of therapeutic agents. For example, radiation doses to the kidneys from the normal excretion of Lutathera (Lu-177-DOTATATE) during the treatment of neuroendocrine tumors may limit future treatments beyond the initial four-dose schedule. The same may be true for patients with prostate cancer who are treated with Pluvicto (Lu-177-vipivotide tetraxetan) in terms of the dose to the salivary glands. Generally speaking, patients with high doses to normal tissues may not be eligible for additional rounds of therapy if they relapse and need additional therapy. The alternate approaches to delivering these radiopharmaceuticals by the IA route may help with this issue, especially if tumor uptake levels can be realized with lower total doses that translate into lower doses to normal tissues.

Cancer targeting with IV and/or IA delivery of radiopharmaceuticals addresses many of the drawbacks of external-beam radiation therapy. Continued research will yield advances in delivery strategies and radioisotope choices. Radioisotopes that decay by α-particle emissions cause double-stranded DNA breaks in tumors that are not easily repaired by cancer cells. When α-particle emitters are delivered to tumors in optimal dose schedules and combined with immunotherapy, a systemic immune response can be the result, which has a huge potential to improve patient outcomes.

BIBLIOGRAPHY

1. Baskar, R.; Lee, K.A.; Yeo, R.; Yeoh, K.W. Cancer and radiation therapy: Current advances and future directions. *Int. J. Med. Sci.* **2012**, *9*, 193–199. https://doi.org/10.7150/ijms.3635.

2. Ma, L.; Men, Y.; Feng, L.; Kang, J.; Sun, X.; Yuan, M.; Jiang, W.; Hui, Z. A current review of dose-escalated radiotherapy in locally advanced non-small cell lung cancer. *Radiol. Oncol.* **2019**, *53*, 6–14. https://doi.org/10.2478/raon-2019-0006.

3. Razvi, Y.; Chan, S.; Zhang, L.; Tsao, M.; Barnes, E.; Danjoux, C.; Sousa, P.; Zaki, P.; McKenzie, E.; DeAngelis, C.; et al. A review of the Rapid Response Radiotherapy Program in patients with advanced cancer referred for palliative radiotherapy over two decades. *Support. Care Cancer* **2019**, *27*, 2131–2134. https://doi.org/10.1007/s00520-018-4474-9.

4. Chargari, C.; Deutsch, E.; Blanchard, P.; Gouy, S.; Martelli, H.; Guerin, F.; Dumas, I.; Bossi, A.; Morice, P.; Viswanathan, A.N.; et al. Brachytherapy: An overview for clinicians. *CA Cancer J. Clin.* **2019**, *69*, 386–401. https://doi.org/10.3322/caac.21578.

5. Kennedy, A.; Brown, D.B.; Feilchenfeldt, J.; Marshall, J.; Wasan, H.; Fakih, M.; Gibbs, P.; Knuth, A.; Sangro, B.; Soulen, M.C.; et al. Safety of selective internal radiation therapy (SIRT) with yttrium-90 microspheres combined with systemic anticancer agents: Expert consensus. *J. Gastrointest. Oncol.* **2017**, *8*, 1079–1099. https://doi.org/10.21037/jgo.2017.09.10.

6. Ragde, H.; Grado, G.L.; Nadir, B.; Elgamal, A.A. Modern prostate brachytherapy. *CA Cancer J. Clin.* **2000**, *50*, 380–393. https://doi.org/10.3322/canjclin.50.6.380.

7. Altai, M.; Membreno, R.; Cook, B.; Tolmachev, V.; Zeglis, B.M. Pretargeted Imaging and Therapy. *J. Nucl. Med.* **2017**, *58*, 1553–1559. https://doi.org/10.2967/jnumed.117.189944.

8. Paganelli, G.; Chinol, M. Radioimmunotherapy: Is avidin-biotin pretargeting the preferred choice among pretargeting methods? *Eur. J. Nucl. Med. Mol. Imaging* **2003**, *30*, 773–776. https://doi.org/10.1007/s00259-002-1090-0.

9. Pastorino, S.; Baldassari, S.; Ailuno, G.; Zuccari, G.; Drava, G.; Petretto, A.; Cossu, V.; Marini, C.; Alfei, S.; Florio, T.; et al. Two Novel PET Radiopharmaceuticals for Endothelial Vascular Cell Adhesion Molecule-1 (VCAM-1) Targeting. *Pharmaceutics* **2021**, *13*, 1025. https://doi.org/10.3390/pharmaceutics13071025.

10. Verhoeven, M.; Seimbille, Y.; Dalm, S.U. Therapeutic Applications of Pretargeting. *Pharmaceutics* **2019**, *11*, 434. https://doi.org/10.3390/pharmaceutics11090434.

11. Rondon, A.; Degoul, F. Antibody Pretargeting Based on Bioorthogonal Click Chemistry for Cancer Imaging and Targeted Radionuclide Therapy. *Bioconjugate Chem.* **2020**, *31*, 159–173. https://doi.org/10.1021/acs.bioconjchem.9b00761.

12. Shalgunov, V.; Lopes van den Broek, S.; Vang Andersen, I.; García Vázquez, R.; Raval, N.R.; Palner, M.; Mori, Y.; Schäfer, G.; Herrmann, B.; Mikula, H.; et al. Pretargeted imaging

beyond the blood—Brain barrier. *RSC Med. Chem.* **2023**, *14*, 444–453. https://doi.org/10.1039/d2md00360k.

13. Mazzaferri, E.L.; Kloos, R.T. Current Approaches to Primary Therapy for Papillary and Follicular Thyroid Cancer. *J. Clin. Endocrinol. Metab.* **2001**, *86*, 1447–1463. https://doi.org/10.1210/jcem.86.4.7407.

14. Valerio, L.; Pieruzzi, L.; Giani, C.; Agate, L.; Bottici, V.; Lorusso, L.; Cappagli, V.; Puleo, L.; Matrone, A.; Viola, D.; et al. Targeted Therapy in Thyroid Cancer: State of the Art. *Clin. Oncol.* **2017**, *29*, 316–324. https://doi.org/10.1016/j.clon.2017.02.009.

15. Kelkar, S.S.; Reineke, T.M. Theranostics: Combining imaging and therapy. *Bioconjugate Chem.* **2011**, *22*, 1879–1903. https://doi.org/10.1021/bc200151q.

16. Aboagye, E.O.; Barwick, T.D.; Haberkorn, U. Radiotheranostics in oncology: Making precision medicine possible. *CA Cancer J. Clin.* **2023**. https://doi.org/10.3322/caac.21768.

17. Hennrich, U.; Kopka, K. Lutathera((R)): The First FDA- and EMA-Approved Radiopharmaceutical for Peptide Receptor Radionuclide Therapy. *Pharmaceuticals* **2019**, *12*, 114. https://doi.org/10.3390/ph12030114.

18. Pathmanandavel, S.; Crumbaker, M.; Nguyen, A.; Yam, A.O.; Wilson, P.; Niman, R.; Ayers, M.; Sharma, S.; Eu, P.; Martin, A.J.; et al. The Prognostic Value of Posttreatment (68)Ga-PSMA-11 PET/CT and (18)F-FDG PET/CT in Metastatic Castration-Resistant Prostate Cancer Treated with (177)Lu-PSMA-617 and NOX66 in a Phase I/II Trial (LuPIN). *J. Nucl. Med.* **2023**, *64*, 69–74. https://doi.org/10.2967/jnumed.122.264104.

19. Zhang, H.; Koumna, S.; Pouliot, F.; Beauregard, J.M.; Kolinsky, M. PSMA Theranostics: Current Landscape and Future Outlook. *Cancers* **2021**, *13*, 4023. https://doi.org/10.3390/cancers13164023.

20. Kratochwil, C.; Giesel, F.L.; Stefanova, M.; Benesova, M.; Bronzel, M.; Afshar-Oromieh, A.; Mier, W.; Eder, M.; Kopka, K.; Haberkorn, U. PSMA-Targeted Radionuclide Therapy of Metastatic Castration-Resistant Prostate Cancer with 177Lu-Labeled PSMA-617. *J. Nucl. Med.* **2016**, *57*, 1170–1176. https://doi.org/10.2967/jnumed.115.171397.

21. Sgouros, G.; Bodei, L.; McDevitt, M.R.; Nedrow, J.R. Radiopharmaceutical therapy in cancer: Clinical advances and challenges. *Nat. Rev. Drug Discov.* **2020**, *19*, 589–608. https://doi.org/10.1038/s41573-020-0073-9.

22. Ailuno, G.; Iacobazzi, R.M.; Lopalco, A.; Baldassari, S.; Arduino, I.; Azzariti, A.; Pastorino, S.; Caviglioli, G.; Denora, N. The Pharmaceutical Technology Approach on Imaging Innovations from Italian Research. *Pharmaceutics* **2021**, *13*, 1214. https://doi.org/10.3390/pharmaceutics13081214.

23. Bolzati, C.; Dolmella, A. Nitrido Technetium-99 m Core in Radiopharmaceutical Applications: Four Decades of Research. *Inorganics* **2019**, *8*, 3. https://doi.org/10.3390/inorganics8010003.

24. Velikyan, I. 68Ga-Based radiopharmaceuticals: Production and application relationship. *Molecules* **2015**, *20*, 12913–12943. https://doi.org/10.3390/molecules200712913.

25. Huang, R.; Boltze, J.; Li, S. Strategies for Improved Intra-arterial Treatments Targeting Brain Tumors: A Systematic Review. *Front. Oncol.* **2020**, *10*, 1443. https://doi.org/10.3389/fonc.2020.01443.

26. Tepe, G.; Duda, S.H.; Kalinowski, M.; Kamenz, J.; Brehme, U.; Hanke, H.; Claussen, C.D.; Bares, R.; Baumbach, A.; Dinkelborg, L.M. Local intra-arterial drug delivery for prevention of restenosis: Comparison of the efficiency of delivery of different radiopharmaceuticals through a porous catheter. *Investig. Radiol.* **2001**, *36*, 245–249.

27. Degrauwe, N.; Hocquelet, A.; Digklia, A.; Schaefer, N.; Denys, A.; Duran, R. Theranostics in Interventional Oncology: Versatile Carriers for Diagnosis and Targeted Image-Guided Minimally Invasive Procedures. *Front. Pharm.* **2019**, *10*, 450. https://doi.org/10.3389/fphar.2019.00450.

28. Bozkurt, M.F.; Salanci, B.V.; Ugur, O. Intra-Arterial Radionuclide Therapies for Liver Tumors. *Semin. Nucl. Med.* **2016**, *46*, 324–339. https://doi.org/10.1053/j.semnuclmed.2016.01.008.

29. Gray, B.; Van Hazel, G.; Hope, M.; Burton, M.; Moroz, P.; Anderson, J.; Gebski, V. Randomised trial of SIR-Spheres plus chemotherapy vs. chemotherapy alone for treating patients with liver metastases from primary large bowel cancer. *Ann. Oncol.* **2001**, *12*, 1711–1720. https://doi.org/10.1023/a:1013569329846.

30. Kallini, J.R.; Gabr, A.; Salem, R.; Lewandowski, R.J. Transarterial Radioembolization with Yttrium-90 for the Treatment of Hepatocellular Carcinoma. *Adv. Ther.* **2016**, *33*, 699–714. https://doi.org/10.1007/s12325-016-0324-7.

31. Facciorusso, A.; Bargellini, I.; Cela, M.; Cincione, I.; Sacco, R. Comparison between Y90 Radioembolization Plus Sorafenib and Y90 Radioembolization alone in the Treatment of Hepatocellular Carcinoma: A Propensity Score Analysis. *Cancers* **2020**, *12*, 897. https://doi.org/10.3390/cancers12040897.

32. Lewandowski, R.J.; Gabr, A.; Abouchaleh, N.; Ali, R.; Al Asadi, A.; Mora, R.A.; Kulik, L.; Ganger, D.; Desai, K.; Thornburg, B.; et al. Radiation Segmentectomy: Potential Curative Therapy for Early Hepatocellular Carcinoma. *Radiology* **2018**, *287*, 1050–1058. https://doi.org/10.1148/radiol.2018171768.

33. Vouche, M.; Lewandowski, R.J.; Atassi, R.; Memon, K.; Gates, V.L.; Ryu, R.K.; Gaba, R.C.; Mulcahy, M.F.; Baker, T.; Sato, K.; et al. Radiation lobectomy: Time-dependent analysis of future liver remnant volume in unresectable liver cancer as a bridge to resection. *J. Hepatol.* **2013**, *59*, 1029–1036. https://doi.org/10.1016/j.jhep.2013.06.015.

34. Zhan, C.; Ruohoniemi, D.; Shanbhogue, K.P.; Wei, J.; Welling, T.H.; Gu, P.; Park, J.S.; Dagher, N.N.; Taslakian, B.; Hickey, R.M. Safety of Combined Yttrium-90 Radioembolization and Immune Checkpoint Inhibitor Immunotherapy for Hepatocellular

Carcinoma. *J. Vasc. Interv. Radiol.* **2020**, *31*, 25–34. https://doi.org/10.1016/j.jvir.2019.05.023.

35. Mouli, S.K.; Raiter, S.; Harris, K.; Mylarapu, A.; Burks, M.; Li, W.; Gordon, A.C.; Khan, A.; Matsumoto, M.; Bailey, K.L.; et al. Yttrium-90 Radioembolization to the Prostate Gland: Proof of Concept in a Canine Model and Clinical Translation. *J. Vasc. Interv. Radiol.* **2021**, *32*, 1103–1112.e1112. https://doi.org/10.1016/j.jvir.2021.01.282.

36. Zhang, W.; Liu, R.; Wang, Y.; Qian, S.; Wang, J.; Yan, Z.; Zhang, H. Efficacy of intraarterial chemoinfusion therapy for locally advanced breast cancer patients: A retrospective analysis of 28 cases. *OncoTargets Ther.* **2013**, *6*, 761–765. https://doi.org/10.2147/OTT.S44882.

37. Klaassen, N.J.M.; Arntz, M.J.; Gil Arranja, A.; Roosen, J.; Nijsen, J.F.W. The various therapeutic applications of the medical isotope holmium-166: A narrative review. *EJNMMI Radiopharm. Chem.* **2019**, *4*, 19. https://doi.org/10.1186/s41181-019-0066-3.

38. Bakker, R.C.; Lam, M.; van Nimwegen, S.A.; Rosenberg, A.; van Es, R.J.J.; Nijsen, J.F.W. Intratumoral treatment with radioactive beta-emitting microparticles: A systematic review. *J. Radiat. Oncol.* **2017**, *6*, 323–341. https://doi.org/10.1007/s13566-017-0315-6.

39. Feuerecker, B.; Scheidhauer, K.; Schwaiger, M.; Mustafa, M. Intra-arterial radiopeptide therapy of hepatic metastases of neuroendocrine tumors: A systematic review. *Clin. Transl. Imaging* **2017**, *5*, 89–99. https://doi.org/10.1007/s40336-016-0220-9.

40. Kratochwil, C.; Giesel, F.L.; Lopez-Benitez, R.; Schimpfky, N.; Kunze, K.; Eisenhut, M.; Kauczor, H.U.; Haberkorn, U. Intraindividual comparison of selective arterial versus venous 68Ga-DOTATOC PET/CT in patients with gastroenteropancreatic neuroendocrine tumors. *Clin. Cancer Res.* **2010**, *16*, 2899–2905. https://doi.org/10.1158/1078-0432.CCR-10-0004.

41. Kratochwil, C.; Lopez-Benitez, R.; Mier, W.; Haufe, S.; Isermann, B.; Kauczor, H.U.; Choyke, P.L.; Haberkorn, U.; Giesel, F.L. Hepatic arterial infusion enhances DOTATOC radiopeptide therapy in patients with neuroendocrine liver metastases. *Endocr. Relat. Cancer* **2011**, *18*, 595–602. https://doi.org/10.1530/ERC-11-0144.

42. Thakral, P.; Sen, I.; Das, S.S.; Manda, D.; Cb, V.; Malik, D. Dosimetric analyses of intra-arterial versus standard intravenous administration of 177Lu-DOTATATE in patients of well differentiated neuroendocrine tumor with liver-dominant metastatic disease. *Br. J. Radiol.* **2021**, *94*, 20210403. https://doi.org/10.1259/bjr.20210403.

43. Sayman, H.B.; Gulsen, F.; Sager, S.; Akgun, E.; Yeyin, N.; Bilgic, S.; Toplutas, K.N.; An, F.; Beytur, F.; Oklu, R.; et al. Selective Intra-Arterial Lutetium-177-Labeled Prostate-Specific Membrane Antigen Therapy for Castration-Resistant Prostate Cancer: Initial Results. *J. Vasc. Interv. Radiol.* **2022**, *33*, 342–345. https://doi.org/10.1016/j.jvir.2021.10.016.

44. Verburg, F.A.; Wiessmann, M.; Neuloh, G.; Mottaghy, F.M.; Brockman, M. Intraindividual comparison of selective intraarterial versus systemic intravenous 68Ga-DOTATATE

PET/CT in patients with inoperable meningioma. *Nuklearmedizin* **2019**, *58*, 23–27. https://doi.org/10.1055/a-0802-5039.

45. Vonken, E.P.A.; Bruijnen, R.C.G.; Snijders, T.J.; Seute, T.; Lam, M.; Keizer, B.; Braat, A. Intraarterial Administration Boosts (177)Lu-HA-DOTATATE Accumulation in Salvage Meningioma Patients. *J. Nucl. Med.* **2022**, *63*, 406–409. https://doi.org/10.2967/jnumed.121.262491.

46. Ebbers, S.C.; Braat, A.; Moelker, A.; Stokkel, M.P.M.; Lam, M.; Barentsz, M.W. Intra-arterial versus standard intravenous administration of lutetium-177-DOTA-octreotate in patients with NET liver metastases: Study protocol for a multicenter, randomized controlled trial (LUTIA trial). *Trials* **2020**, *21*, 141. https://doi.org/10.1186/s13063-019-3888-0.

47. Bodei, L.; Cremonesi, M.; Grana, C.M.; Fazio, N.; Iodice, S.; Baio, S.M.; Bartolomei, M.; Lombardo, D.; Ferrari, M.E.; Sansovini, M.; et al. Peptide receptor radionuclide therapy with (1)(7)(7)Lu-DOTATATE: The IEO phase I-II study. *Eur. J. Nucl. Med. Mol. Imaging* **2011**, *38*, 2125–2135. https://doi.org/10.1007/s00259-011-1902-1.

48. Tafreshi, N.K.; Doligalski, M.L.; Tichacek, C.J.; Pandya, D.N.; Budzevich, M.M.; El-Haddad, G.; Khushalani, N.I.; Moros, E.G.; McLaughlin, M.L.; Wadas, T.J.; et al. Development of Targeted Alpha Particle Therapy for Solid Tumors. *Molecules* **2019**, *24*, 4314. https://doi.org/10.3390/molecules24234314.

49. Kratochwil, C.; Bruchertseifer, F.; Giesel, F.L.; Weis, M.; Verburg, F.A.; Mottaghy, F.; Kopka, K.; Apostolidis, C.; Haberkorn, U.; Morgenstern, A. 225Ac-PSMA-617 for PSMA-Targeted alpha-Radiation Therapy of Metastatic Castration-Resistant Prostate Cancer. *J. Nucl. Med.* **2016**, *57*, 1941–1944. https://doi.org/10.2967/jnumed.116.178673.

50. Delpassand, E.S.; Tworowska, I.; Esfandiari, R.; Torgue, J.; Hurt, J.; Shafie, A.; Nunez, R. Targeted alpha-Emitter Therapy with (212)Pb-DOTAMTATE for the Treatment of Metastatic SSTR-Expressing Neuroendocrine Tumors: First-in-Humans Dose-Escalation Clinical Trial. *J. Nucl. Med.* **2022**, *63*, 1326–1333. https://doi.org/10.2967/jnumed.121.263230.

51. Shi, M.; Jakobsson, V.; Greifenstein, L.; Khong, P.L.; Chen, X.; Baum, R.P.; Zhang, J. Alpha-peptide receptor radionuclide therapy using actinium-225 labeled somatostatin receptor agonists and antagonists. *Front. Med.* **2022**, *9*, 1034315. https://doi.org/10.3389/fmed.2022.1034315.

52. Sgouros, G.; Roeske, J.C.; McDevitt, M.R.; Palm, S.; Allen, B.J.; Fisher, D.R.; Brill, A.B.; Song, H.; Howell, R.W.; Akabani, G.; et al. MIRD Pamphlet No. 22 (abridged): Radiobiology and dosimetry of alpha-particle emitters for targeted radionuclide therapy. *J. Nucl. Med.* **2010**, *51*, 311–328. https://doi.org/10.2967/jnumed.108.058651.

53. Muz, B.; de la Puente, P.; Azab, F.; Azab, A.K. The role of hypoxia in cancer progression, angiogenesis, metastasis, and resistance to therapy. *Hypoxia* **2015**, *3*, 83–92. https://doi.org/10.2147/HP.S93413.

54. Strosberg, J.; Herrmann, K.; Bodei, L. The Future of Targeted alpha-Therapy Is Bright, but Rigorous Studies Are Necessary to Advance the Field. *J. Nucl. Med.* **2023**, *64*, 219–220. https://doi.org/10.2967/jnumed.122.264805.

55. Kratochwil, C.; Giesel, F.L.; Bruchertseifer, F.; Mier, W.; Apostolidis, C.; Boll, R.; Murphy, K.; Haberkorn, U.; Morgenstern, A. (2)(1)(3)Bi-DOTATOC receptor-targeted alpha-radionuclide therapy induces remission in neuroendocrine tumours refractory to beta radiation: A first-in-human experience. *Eur. J. Nucl. Med. Mol. Imaging* **2014**, *41*, 2106–2119. https://doi.org/10.1007/s00259-014-2857-9.

56. Meredith, R.F.; Torgue, J.J.; Rozgaja, T.A.; Banaga, E.P.; Bunch, P.W.; Alvarez, R.D.; Straughn, J.M., Jr.; Dobelbower, M.C.; Lowy, A.M. Safety and Outcome Measures of First-in-Human Intraperitoneal alpha Radioimmunotherapy with 212Pb-TCMC-Trastuzumab. *Am. J. Clin. Oncol.* **2018**, *41*, 716–721. https://doi.org/10.1097/COC.0000000000000353.

57. Autenrieth, M.E.; Seidl, C.; Bruchertseifer, F.; Horn, T.; Kurtz, F.; Feuerecker, B.; D'Alessandria, C.; Pfob, C.; Nekolla, S.; Apostolidis, C.; et al. Treatment of carcinoma in situ of the urinary bladder with an alpha-emitter immunoconjugate targeting the epidermal growth factor receptor: A pilot study. *Eur. J. Nucl. Med. Mol. Imaging* **2018**, *45*, 1364–1371. https://doi.org/10.1007/s00259-018-4003-6.

58. Vanpouille-Box, C.; Alard, A.; Aryankalayil, M.J.; Sarfraz, Y.; Diamond, J.M.; Schneider, R.J.; Inghirami, G.; Coleman, C.N.; Formenti, S.C.; Demaria, S. DNA exonuclease Trex1 regulates radiotherapy-induced tumour immunogenicity. *Nat. Commun.* **2017**, *8*, 15618. https://doi.org/10.1038/ncomms15618.

59. Aicher, A.; Sindrilaru, A.; Crisan, D.; Thaiss, W.; Steinacker, J.; Beer, M.; Wiegel, T.; Scharffetter-Kochanek, K.; Beer, A.J.; Prasad, V. Short-Interval, Low-Dose Peptide Receptor Radionuclide Therapy in Combination with PD-1 Checkpoint Immunotherapy Induces Remission in Immunocompromised Patients with Metastatic Merkel Cell Carcinoma. *Pharmaceutics* **2022**, *14*, 1466. https://doi.org/10.3390/pharmaceutics14071466.

60. Perrin, J.; Capitao, M.; Allard, M.; Chouin, N.; Gouard, S.; Marionneau-Lambot, S.; Louvet, C.; Donnadieu, E.; Bruchertseifer, F.; Morgenstern, A.; et al. Targeted Alpha Particle Therapy Remodels the Tumor Microenvironment and Improves Efficacy of Immunotherapy. *Int. J. Radiat. Oncol. Biol. Phys.* **2022**, *112*, 790–801. https://doi.org/10.1016/j.ijrobp.2021.10.013.

CHAPTER 2: OLIGOMERIZATION OF THE PROTEIN S DERIVATIVE GLAS-FCMUT INCREASED DELIVERY OF ALPHA-PARTICLE THERAPY TO MOUSE BREAST CANCER CELLS

Introduction

The tumor microenvironment plays a critical role in cancer progression and therapy resistance [1-3]. One component of the tumor microenvironment that has been shown to contribute to cancer progression is phosphatidylserine (PS), a phospholipid that is normally located on the inner leaflet of the plasma membrane but becomes exposed on the surface of cancer cells and tumor blood vessels [4,5]. PS exposure in the tumor microenvironment can contribute to cancer progression in several ways. It can act as an immunosuppressant, preventing immune cells from recognizing cancer cells, thus promoting immune evasion. Additionally, PS exposure can promote angiogenesis, which is necessary for tumor growth and metastasis [4-6].

Targeting PS is a promising approach for cancer therapy. Bavituximab is a monoclonal antibody that targets PS on the surface of cancer cells and tumor blood vessels [4,7]. By binding to PS, bavituximab can promote an anti-tumor immune response through multiple mechanisms, such as antibody dependent cellular cytotoxicity, and inhibit angiogenesis, thus reducing the ability of cancer cells to survive and grow [7]. In clinical trials, bavituximab showed promising results in terms of efficacy, safety, and tolerability [8,9].

GlaS-Fc is a novel derivative of Protein S, a protein that functions in anti-coagulation and apoptosis cell clearing through PS binding [10,11]. GlaS-Fc was designed specifically for targeting PS. In addition to the Gla domain, GlaS-Fc contains four EGF-like domains and a carboxyl-terminal IgG Fc domain. Due to the presence of the Fc domain, it forms a ~110 kDa dimer that exceeds the renal clearance threshold, leading to longer *in vivo* circulation times than the 53 kDa monomer. In this manuscript, GlaS-Fc's affinity for PS on cancer cells was investigated. This approach takes advantage of the fact that dying cancer cells often expose increased PS on their surface, making them a highly specific target for the PS-targeted protein. The efficacy of this approach in preclinical models of cancer was demonstrated, highlighting its potential as a promising strategy for improving the effectiveness of radiation therapy and reducing side effects.

Methods

GlaS-Fc formulation

GlaS-Fc is a modified version of a base protein called GlaS (Supplementary Figure 2.1). Initial experiments were performed using GlaS where it was found that unlabeled GlaS could not prevent AnnexinV-PE from binding and actually increased the binding efficacy of Cy5-GlaS (Supplementary Figure 2.2). While investigating this phenomena, GlaS-Fc was created by attaching a mutated murine IgG2a Fc region to GlaS to increase protein size to 53 kDa. GlaS-Fc forms a ~110 kDa dimer through interactions of the Fc domain. The mutated Fc (I253A) cannot interact with FcRn but retains all other functions. It was found that this increase in size increased biological half-life and reduced renal binding in mice (Supplementary Figure 2.3). With the goal of eventually using the GlaS platform for *in vivo* experiments, it was deemed critical to identify which GlaS version had the best potential for *in vivo* study. Therefore, GlaS-Fc was the version chosen for testing the *in vitro* binding characteristics to cancer cells.

GlaS-Fc protein was stably expressed in CHO K1 cells and grown in roller bottles seeded with a stable cell pool at 3 x 106 cells/ml in media supplemented with 60 ng/ml vitamin K required for post-translational gamma-carboxylation glutamic acids within the N-terminal Gla domain (Supplementary Figure 2.1). Media was harvested, clarified by centrifugation, concentrated 10X and diafiltered into Tri Buffered saline (TBS) containing 300mM Betaine and frozen until purification could be initiated. Production of Gla-Fc was monitored by anti Gla Western blot. Purification of the GlaS-Fc protein entailed a three-step process. Thawed media was first loaded onto a Protein G column which binds the Fc domain. The column was then washed with TBS containing 0.5M NaCl to remove weakly bound proteins and then eluted with pH 5 glycine. Eluted fractions were immediately neutralized with Tris. Gla-Fc containing fractions were pooled, diluted, adjusted to pH 5.5 and loaded onto a sulfate column (Thermo). After washing to baseline in 50mM NaCL pH 5.5, the column was eluted with a linear gradient of 50mM - 1 M NaCl, pH 5.5. GlaS-Fc containing fractions were pooled and characterized for purity by SE-HPLC and SDS-PAGE. Following concentration to 3 ml, preparative SEC on SuperDex 200 was run with a mobile phase of 20mM HEPES, 150mM NaCl, 10mM CaCl2, and pH 7.2. The final fractions were pooled, 1% sucrose was added and stored frozen at -80°C.

GlaS-Fc conjugation to Cy5 dye

Conjugation of GlaS-FC with Cy5 for fluorescent and flow cytometry studies was done using Amersham (GE Healthcare) products. GlaS-FC (1 mg) in sodium phosphate buffer (50mM, 7.4 pH) was added to Cy5 kit and incubated rocking at room temperature for 1 hour. The solution was then dialyzed in 1x phosphate buffered saline (PBS) using 10,000 kDa cutoff Slida-a-Lyzer dialysis membranes (Fisher Scientific) for 2 hours at 4°C. The membranes were placed into fresh PBS and dialyzed overnight to remove unbound dye. Bradford assay was used to determine final protein concentration.

GlaS-Fc Conjugation and Radiolabeling with Pb-212

GlaS-Fc was buffer exchanged into 0.1M carbonate buffer (pH 9.3) using slide-a-lyzer cassette and added to a vial containing lyophilized TCMC-SCN (Macrocyclics) at a 10:1 molar ratio. The reaction took place at room temperature protected from light with slight rocking for 2 hours. Free TCMC was removed by buffer exchanging GlaS-Fc-TCMC into 0.1 M ammonium acetate (pH 7.0).

A Ra-224/Pb-212 generator (10 mCi) was provided by Oak Ridge National Lab (The isotopes used in this research were supplied by the U.S. Department of Energy Isotope Program, managed by the Office of Isotope R&D and Production). The column was washed with 2 M HCl to remove all Ra-224 daughters for digestion and radiolabeling. The dried Pb-212 isotope was collected from glass vials using 0.1M HNO_3 and then buffered with 1M ammonium acetate (pH 5.4).

For radiolabeling, 270 μCi (CRC-25R, Capintec, calibration #158) of buffered Pb-212 was added to 400 μg of purified GlaS-Fc-TCMC and placed onto a shaker set at 40°C and 500 rpm for 1 hour. The reaction took place under 0.1% ascorbic acid for radioprotection. Pb212-GlaS-Fc was purified into 1x PBS using 7K MWKO Zeba spin column (Thermo Fisher). Purity was confirmed using instant thin layer chromatography (iTLC) on paper silica gel impregnated strips using 10 mM EDTA in 0.15 M NH_4OAc as the mobile phase. Strips were cut in half and measured on gamma counter (Wizard2, Perkin Elmer) to determine purity percent. Specific activity (μCi/μg) was determined by measuring uCi of Pb-212 into the final sample and measuring protein concentration with Bradford assay.

Cell lines

4T1, MCF, and EO771 cells were purchased from ATCC. Cells were cultured in complete media (RPMI for 4T1 or DMEM for MCF7 and EO771 with 10% FBS, 1% penicillin/streptomycin and 1% L-glutamine, Thermo Fisher Scientific) and incubated at 37°C with 5% CO_2. Cells were subcultured upon reaching 90% confluency and reseeded at 20% confluency.

For generation of stably luciferase expressing cell lines, both 4T1 and EO771 cells were transduced by PLV-10170-pLV-CAG-Firefly luciferase-PGK-Puro lentivirus (Cellomics Technology) and luciferase positive clones were selected using puromycin (Thermo Fisher Scientific).

Flow cytometry binding assay

Flow cytometry was performed using Sytox Blue (Thermo Fisher #S34857), and GlaS-Fc conjugated to Cy5. 4T1 or MCF7 cells were plated into clear 24 well plates at 25% confluency 2 days before experimentation. H_2O_2 (2mM) was added to half of the wells 2 hours prior to fluorophore addition, with the plate on a rocker to ensure even distribution of H_2O_2. Cells were dissociated with Versene (ThermoFisher), washed once with 1x PBS + 1% FBS, then resuspended in AnnexinV Binding Buffer (BioLegend #422201) at a concentration of $1x10^6$ cells/ml. 1000 ng of unlabeled GlaS-Fc was added to the blocking condition tubes and were incubated at room temperature for 10 minutes. 20 ng of Cy5-GlaS-Fc was then added to the appropriate tubes and incubated at 37°C for 15 minutes. 200 µl of Annexin V Binding buffer was added to each tube for adequate analysis volume. Cells were strained into a 12x75 mm tube with MiFlow cell strainers (Sigma #BAH136800040-50EA). Sytox Blue (0.5 µL) was added to the appropriate tubes and then analyzed on a Cytek Aurora cytometer. Gating was done to exclude debris, doublets, and dead cells (Sytox +) and spectral unmixing was done based on Cy5 signal.

Fluorescent microscopy binding assay and analysis

MCF7 or 4T1 cells were plated into black, 96 well, tissue culture treated plates at 25% confluency two days before experimentation. Cells were measured at ~90% confluency at the start of the assay. Cells were incubated with 2 mM H_2O_2 for 2 hours. The H_2O_2-containing media solution was aspirated and the cells were washed once with 1x DPBS. Complete media was added to the cells to make the final volume of each well 100 µl after all additives. This was followed by addition of 1 µg of unlabeled GlaS-Fc, or no additives, suspended in media. After a

15 minute incubation, 50 ng of labeled Cy5-GlaS-Fc suspended in media was added to the appropriate conditions and incubated for 1 hr with rocking at 37°C 5% CO_2. The wells were then aspirated and washed with 1x DPBS. 50 µl of clear DMEM with 10% FBS was added to the cells for imaging.

Imaging was done on a Nikon Eclipse TS2R fluorescence microscope. Images were acquired at 20x with a 500 ms exposure time. Filters for the fluorescence were Cy5.5 (filter #49022). Images were then imported to Adobe Photoshop to be combined for viewing. The original fluorescent images were run through ImageJ to determine fluorescence intensity and aggregation size using the Analyze Particles tool. The summary and each individual image's raw data were exported and graphed. Particles of 100 and 1000 pixels were considered medium and large sized, respectively.

Pb-212-GlaS-Fc survival assay and analysis

A survival assay was performed by first seeding $2x10^3$ 4T1 Luc+ cells per well into a 96-well plate. 18 hours later, cells were treated with either 2 mM H_2O_2 or media as an untreated control. After 2 hours incubation, media was removed and replaced with unlabeled GlaS-Fc at 0.5, 1.0, or 2.0 nM concentrations while cells given media were used as an untreated control. After 10 minutes, cells were treated with 125 nCi of Pb-212-GlaS-Fc (Protein concentration of 0.1 nM) while cells given media were used as an untreated control. 24 hours later, media was removed and replaced with fresh media. Cells were imaged at 24, 48, and 72 hours post Pb-212-GlaS-Fc treatment using IVIS Lumina bioluminescence imaging (BLI) with autoexposure setting. Data were analyzed using ROI and radiance (photon/second). Pb-212-GlaS-Fc treated conditions were normalized to the corresponding control sample based on concentration of unlabeled GlaS-Fc added. The normalized pair was then normalized again to the 0 nM unlabeled control in either the untreated or H_2O_2 treated condition.

Statistical analysis

Statistical analysis was performed using GraphPad. One-way analysis of variance (ANOVA) with Dunnett's test was used to compare the experimental groups to the control group. One-way ANOVA was used for all other cross group analyses. Data are reported as mean ± standard error of the mean (SEM). P-values < 0.05 were considered statistically significant.

Results

Addition of unlabeled GlaS-Fc increases total binding of Cy5-GlaS-Fc

Cy5 labeled GlaS-Fc was added to 4T1 and MCF7 cancer cells and assayed with flow cytometry to determine specific binding and establish optimal concentration for future experiments. Interestingly, adding unlabeled GlaS-Fc to block binding sites did not block Cy5-GlaS-Fc binding, nor did it diminish total binding. Rather, addition of unlabeled GlaS-Fc increased the binding of Cy5-GlaS-Fc in both untreated and H_2O_2 treated cells (Figure 2.1A and 2.1B). Synergy was seen between the addition of unlabeled GlaS-Fc and treatment with H_2O_2, used as a stimulator of PS expression.

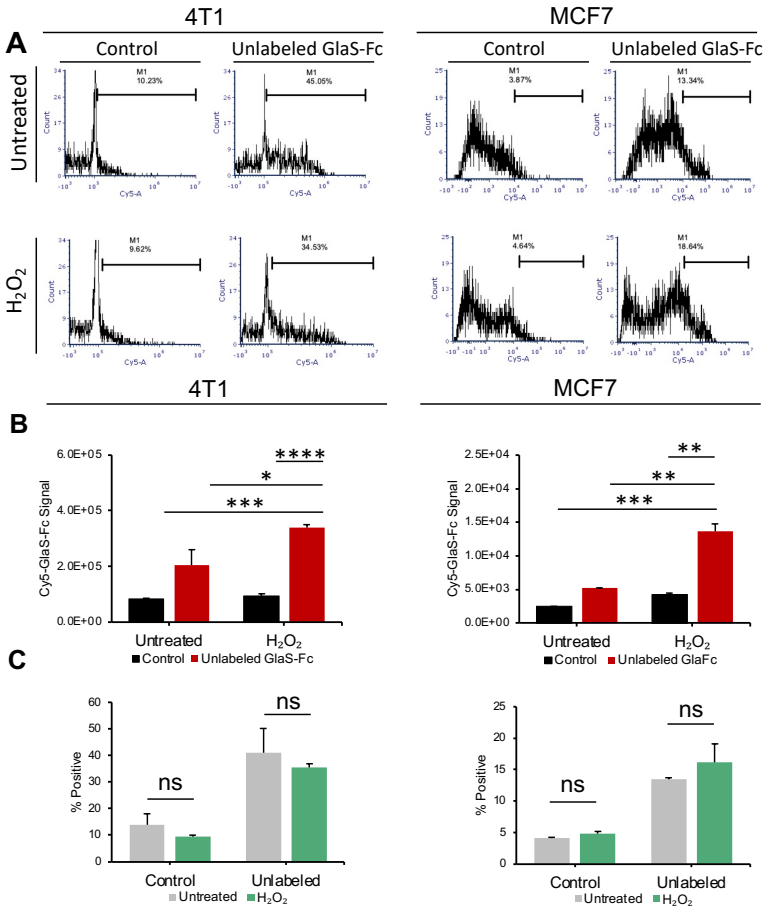

Figure 2.1 | Unlabeled GlaS-Fc increased total binding and intensity of Cy5-GlaS-Fc. (A,B) Representative histograms of Cy5 gating of 4T1 and MCF7 cells treated with Cy5-GlaS-Fc **(A)** with averaged total Cy5 fluorescence data **(B)** comparing unlabeled GlaS-Fc and H_2O_2 treated conditions (n = 3). Both 4T1 and MCF7 cells showed greatest binding of Cy5-GlaS-Fc in the combined unlabeled and H_2O_2 treated condition. **(C)** Comparison of the percent of total cells in the Cy5 positive gate across all conditions. No significant changes were seen between the averages of the paired untreated and H_2O_2 treated samples in the control or unlabeled GlaS-Fc conditions. ns, not significant; *, $P < 0.05$; **, $P < 0.01$; ***, $P < 0.001$; ****, $P < 0.0001$.

To further understand the synergy between H_2O_2 and unlabeled GlaS-Fc, the percentage of positive cells within each analyzed sample was averaged and compared within the untreated or H_2O_2 treated condition (Figure 2.1C). There was no significant difference caused by unlabeled GlaS-Fc in the percentage of positive cells in the Cy5-GlaS-Fc positive gate in either the untreated or H_2O_2 treated samples. This indicates that the unlabeled GlaS-Fc and H_2O_2 synergy does not increase the total number of cells positive for Cy5-GlaS-Fc, but rather increases the density of Cy5-GlaS-Fc binding and intensity of signal coming from an individual cell.

GlaS-Fc forms large oligomers to increase intensity of binding events

To investigate how the increase in intensity per individual cell was occurring, fluorescent microscopy was used to visualize the binding of Cy5-GlaS-Fc to cells (Figure 2.2A). By quantifying the total signal in each condition, we were able to replicate our findings from the flow cytometry assay with synergy observed between unlabeled GlaS-Fc and H_2O_2 (Figure 2.2B). The combined conditions appeared to have both more total visual binding events but also larger-sized binding events (Figure 2.2A). To quantify the shift in binding event size, the size of each individual binding event was measured and compared to the total number of medium (100 pixel) sized events (Figure 2.2C) and large (1000 pixel) events (Figure 2.2D). There was again a synergy between unlabeled GlaS-Fc plus H_2O_2, with this condition having significantly more and larger events compared to the other groups (Figure 2.2C and 2.2D). These large observed binding complexes were referred to as oligomers.

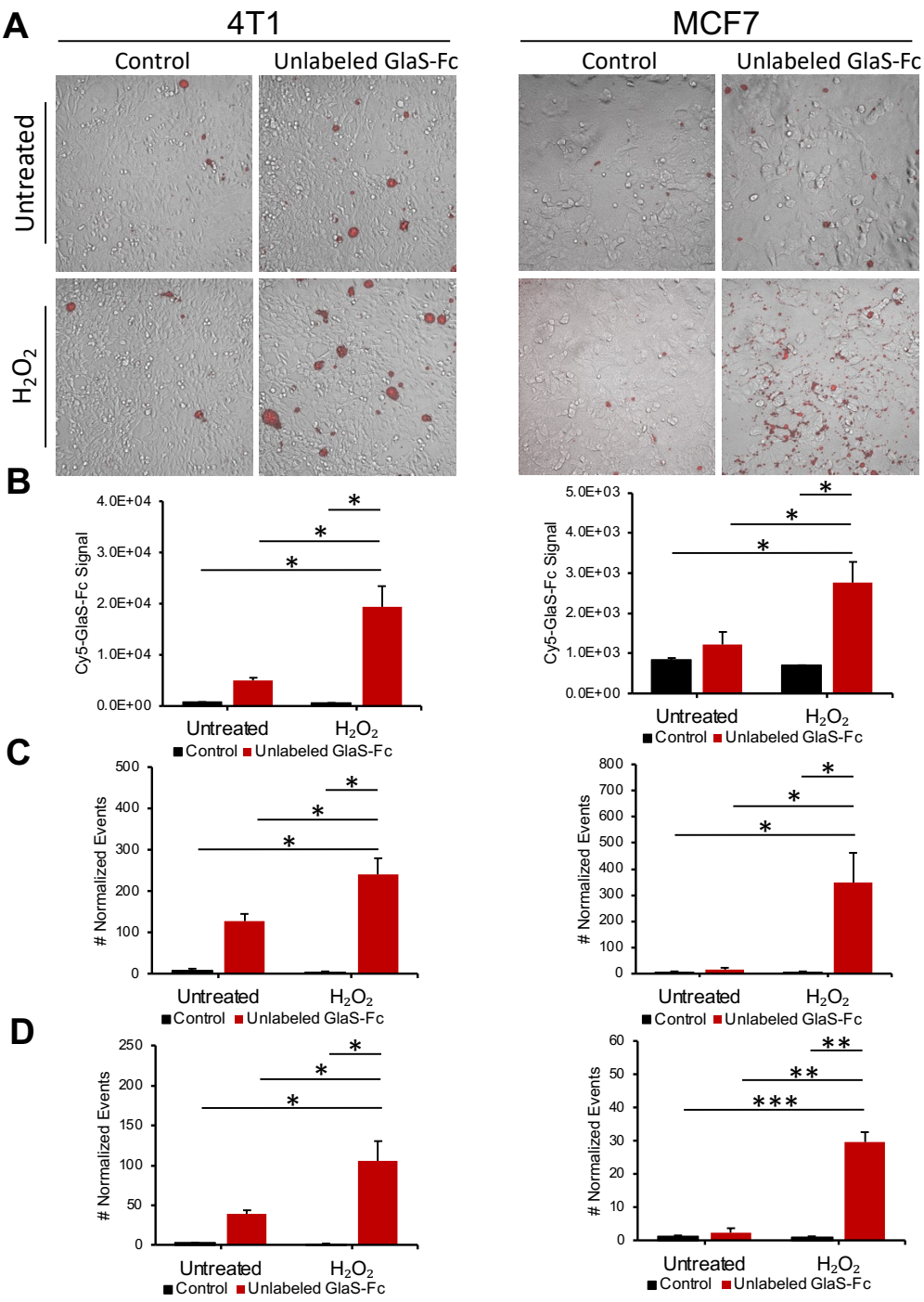

Figure 2.2 | GlaS-Fc and Cy5-GlaS-Fc cooperated to increase size of Cy5-GlaS-Fc binding events. (A,B) Representative microscopy images of 4T1 and MCF7 cells treated with Cy5-GlaS-Fc **(A)** with averaged integrated density data **(B)** comparing unlabeled GlaS-Fc and H_2O_2 treated conditions (n = 3). Both 4T1 and MCF7 cells showed greatest binding of Cy5-GlaS-Fc in the combined unlabeled and H_2O_2 treated condition. **(C,D)** Comparison of total Cy5 positive events above either 100 **(C)** or 1000 **(D)** pixel size. Both 4T1 and MCF7 cells showed significantly more large events in the combined unlabeled and H_2O_2 treated condition compared to all other conditions. *, $P < 0.05$; **, $P < 0.01$; ***, $P < 0.001$.

Higher resolution microscopy was employed to further understand what the GlaS-Fc oligomers looked like and how they behaved. In a single sample study using STORM imaging, we repeated our previous findings where unlabeled GlaS-Fc increases both the total amount of Cy5-GlaS-Fc bound and increases event size (Figure 2.3A). Furthermore, due to the higher resolution and colocalization algorithm software, we were able to show that there are many individual oligomers on the cell rather than a single large aggregate (Figure 2.3B).

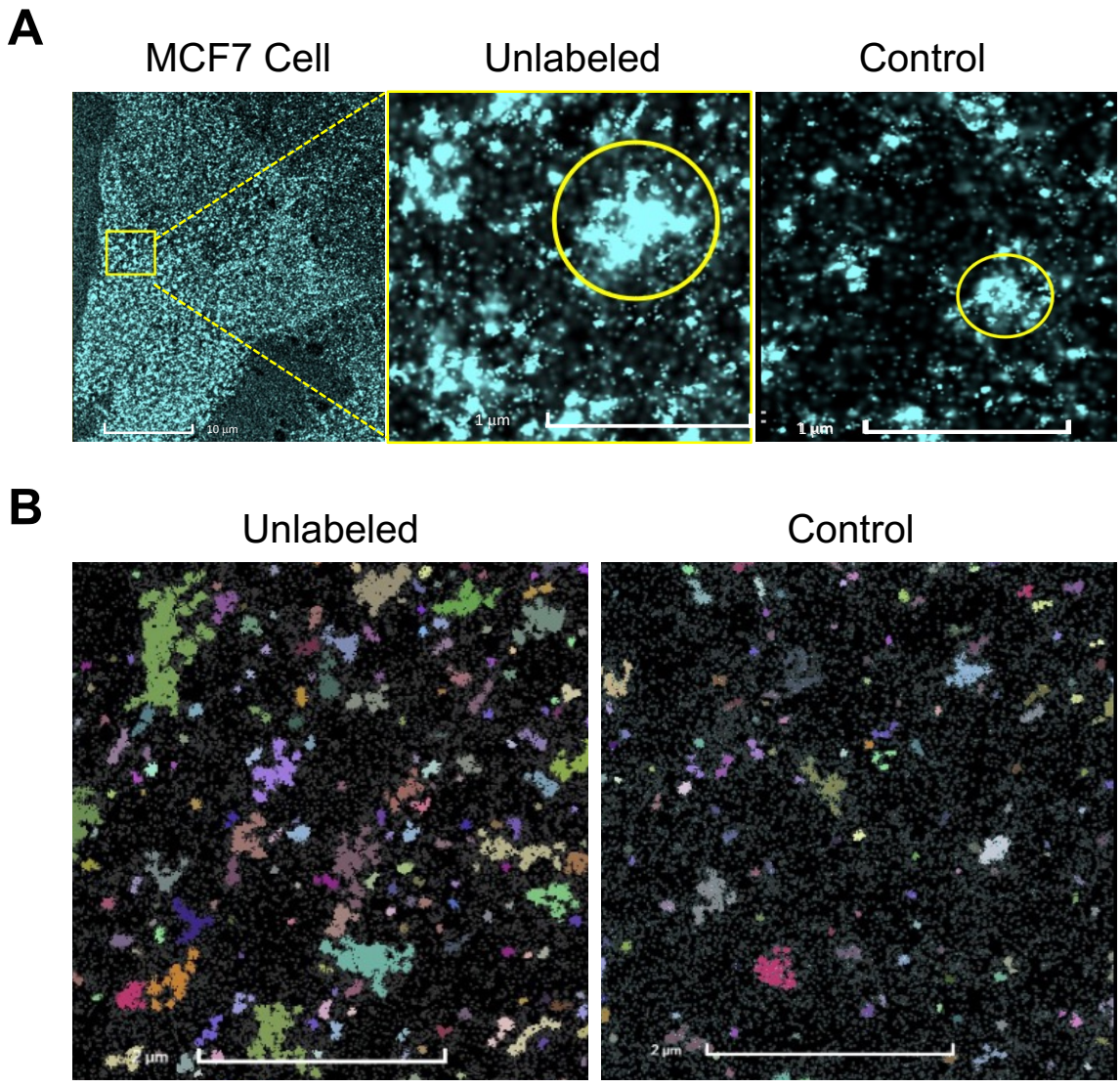

Figure 2.3 | GlaS-Fc formed distinct aggregates on the cell surface. (A,B) STORM imaging showed increased that the addition of unlabeled GlaS-Fc increased aggregate size **(A)** as well as formation of more independent aggregates **(B)** compared to control. The high resolution images showed that the increase in cell binding by Cy5-GlaS-Fc occurred from both an increase in the size and number of independent aggregates rather expansion of a single large aggregate.

Synergy of unlabeled GlaS-Fc and cell surface PS stimulation increases Pb-212-GlaS-Fc radiotherapy efficacy

We theorized that the increased binding synergy of unlabeled GlaS-Fc and H_2O_2 might lead to better therapeutic results if a treatment radioisotope was attached to GlaS-Fc. Pb-212 is an alpha (α)-particle emitting radioisotope with a 10 hour half-life. Alpha (α)- particles penetrate only microns into tissue and cross approximately 4 cancer cell diameters [12]. This means that Pb-212 must be brought into close proximity of cancer cells to deliver effective radiation therapy. The effect of unlabeled GlaS-Fc and H_2O_2 on Pb-212-GlaS-Fc treatment efficacy was tested in 4T1 cells. Reduction in 4T1 cell growth was seen in nearly all conditions at the 48- and 72-hour time points but not the 24-hour time point (Figure 2.4A-C). Pb-212-GlaS-Fc caused significant cell growth reduction in the 0 nM unlabeled condition in untreated cells at 72 hours compared to control. However, there was no difference in the same condition in the H_2O_2 treated cells, meaning no effect of Pb-212-GlaS-Fc was seen in this group.

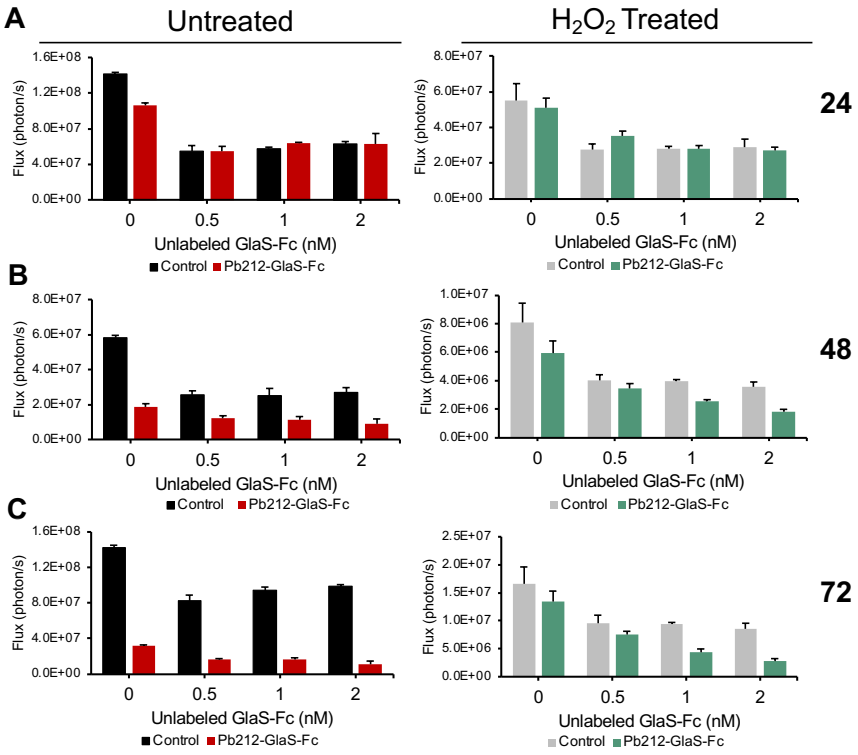

Figure 2.4 | Unlabeled GlaS-Fc and increased PS expression synergized with Pb-212-GlaS-Fc alpha-particle therapy to increase treatment efficacy. **(A-C)** Total luciferase signal was used to assess cell number of both 4T1 and MCF7 cells at 24 **(A)**, 48 **(B)**, and 72 **(C)** hours post treatment with Pb-212-GlaS-Fc (n = 3). A dose response to unlabeled GlaS-Fc was only seen in the Pb-212-GlaS-Fc treated conditions. ns, not significant; *, $P < 0.05$; **, $P < 0.01$; ***, $P < 0.001$; ****, $P < 0.0001$.

Addition of Pb-212-GlaS-Fc in the untreated cells caused 77% reduction of growth in the 0 nM unlabeled condition and 89% in the 2nM condition. Conversely, the H_2O_2 treated cells had 22% reduction in the 0 nM condition and 67% reduction in the 2 nM condition. To present this difference in efficacy graphically, we controlled for reduction of cell growth due to H_2O_2 and GlaS-Fc itself by first normalizing the percent change in growth between the control and Pb-212-GlaS-Fc condition at each level of unlabeled GlaS-Fc and then normalizing those values to the 0 nM GlaS-Fc control. This was done separately between untreated and H_2O_2 groups so that each group had its own control to normalize to. Normalizing the data in this way again revealed synergy between unlabeled GlaS-Fc and increased PS expression via H_2O_2 (Figure 2.5). While there was a significant difference between the 0 nM and 2 nM unlabeled condition in untreated cells, the effect size was negligible compared to the effect size seen in the corresponding H_2O_2 treated 0 nM and 2 nM unlabeled pair (1.15- vs 3.25-fold change). While efficacious therapy of Pb-212-GlaS-Fc was seen at 72 hours in the untreated cells, no difference was seen in the H_2O_2 treated cells. It appears that the combination of increased PS density and GlaS-Fc concentration is able to treat cells that were otherwise not targeted by H_2O_2 (Figure 2.6).

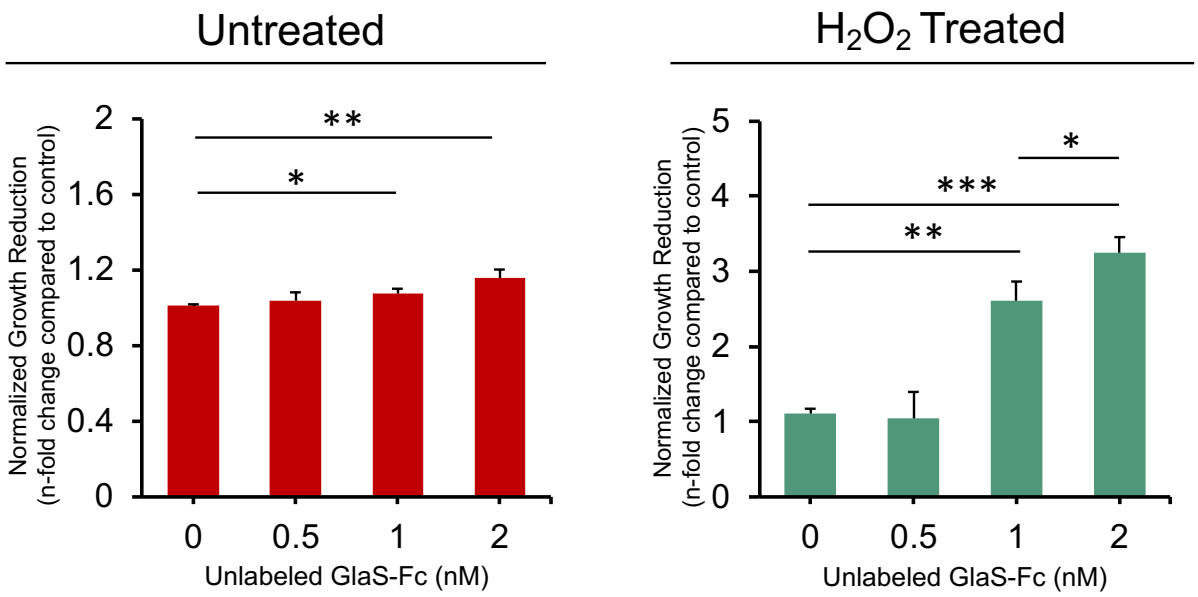

Figure 2.5 | A greater effect of unlabeled GlaS-Fc is seen in the H_2O_2 treated condition. Normalized data showed that synergy of unlabeled GlaS-Fc and Pb-212-GlaS-Fc was only seen in the H_2O_2 condition. While there was a significant difference in growth between 0 nM and 2 nM unlabeled GlaS-Fc in the untreated cells, the effect size was much smaller compared to the same groups in the H_2O_2 treated cells. *, $P < 0.05$; **, $P < 0.01$; ***, $P < 0.001$ ($n = 3$).

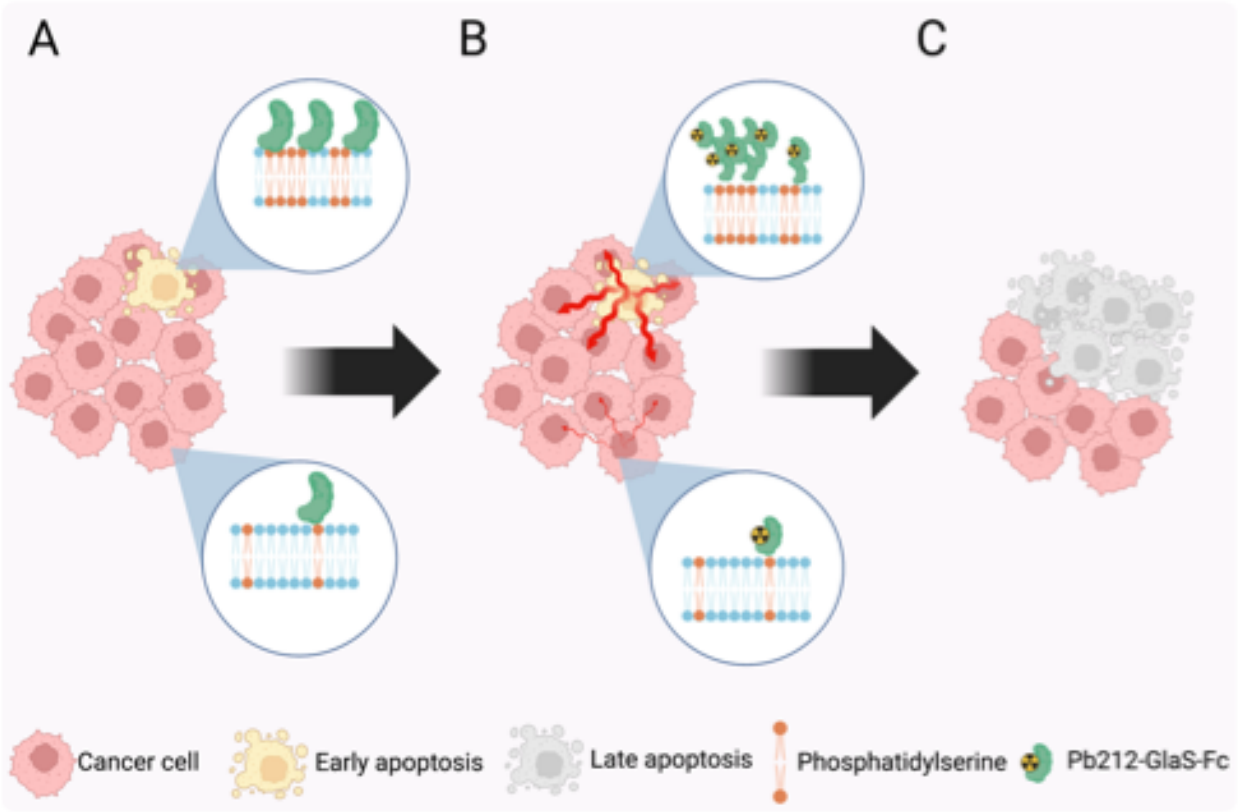

Figure 2.6 | Graphical overview of proposed oligomerization mechanism that could lead to increased radiotherapy efficacy. (A-C) In this representation of the cell culture treatment assay, a layer of cancer cells was treated with chemotherapy **(A)** but will have some sensitive cells that increase PS expression during apoptosis progression and other resistant cells that maintain basal PS expression. Following targeting with Pb-212-GlaS-Fc **(B)**, oligomerization is proposed to occur at areas with high PS density leading to increased total binding of Pb-212-GlaS-Fc. This would lead to increased total dose at the site of chemotherapy sensitive cells and allows for local crossfire into nearby chemotherapy resistant cells. This dose would therefore be enough to effectively treat nearby cells regardless of their individual chemotherapy sensitivity or PS expression **(C)**. Graphic created in BioRender.

Discussion

GlaS-Fc is a Protein S derivative that was created as a platform for delivering therapies to cells overexpressing PS at the cell surface. Our goal was to establish basic binding characteristics *in vitro* to prepare for imaging and therapy studies of cancer. While it is reported that Protein S binding to PS is amplified through oligomerization, [13] we initially did not design studies to investigate if GlaS-Fc worked similarly. Subsequently, we observed that unlabeled GlaS-Fc does not inhibit binding of labeled GlaS-Fc, but rather significantly increases it in a manner consistent

with cooperative binding. We believe GlaS-Fc oligomerizes following PS binding through the same mechanism as Protein S, and we are currently investigating this phenomenon.

The concentration of GlaS-Fc itself plays a critical role regardless of PS expression levels. In untreated groups with lower PS expression, addition of unlabeled GlaS-Fc still causes some increase in GlaS-Fc binding. Conversely, the binding of GlaS-Fc was not greatly increased between untreated and H_2O_2 treated cells in most of our studies. Only when unlabeled GlaS-Fc was included in H_2O_2 treated groups did we see a large spike in labeled GlaS-Fc binding. This indicates that there is synergy between the density of PS and the concentration of GlaS-Fc, where GlaS-Fc accumulates greatly on cells only when the concentration threshold is present.

Pb-212-GlaS-Fc was similarly efficacious in the untreated cells across all concentrations of unlabeled GlaS-Fc. Adding unlabeled did lead to slightly more killing, but the effect size shows that adding unlabeled did not improve the killing very much. Addition of unlabeled GlaS-Fc without any Pb-212-GlaS-Fc present did cause some reduced cell growth, but it was not concentration dependent. The samples in the untreated group had less cells after 24 hours compared to the completely untreated control group but were similar to each other. To control for this, the percent change of Pb-212-GlaS-Fc treated groups compared to the control version at each unlabeled GlaS-Fc concentration condition were calculated before comparing to the completely untreated control. In the untreated cells, addition of unlabeled only made a marginal difference compared to the untreated control. Therefore, addition of unlabeled GlaS-Fc did lead to some additional Pb-212-GlaS-Fc killing but it is an overall small effect size.

Only when H_2O_2 was stimulating PS expression was there an intense synergy leading to greatly increased cell death. When no unlabeled GlaS-Fc is present, there is no difference in cell number between control and Pb-212-GlaS-Fc in H_2O_2. This is completely opposite from the untreated group, where effective cell killing occurred via Pb-212-GlaS-Fc under no unlabeled added condition. This means that the H_2O_2 is leading to global cell growth reduction and Pb-212-GlaS-Fc is not binding in enough capacity to add any additional growth reduction. When the concentration is increased through addition of unlabeled GlaS-Fc, a difference in the Pb-212-GlaS-Fc treated cells and control cells occurs. Calculating the percent change compared to controls treated with the same unlabeled level then normalizing to the no unlabeled added control, a large effect size was apparent. Only when unlabeled is added is there enough additional Pb-212-GlaS-Fc driven cell growth reduction to achieve a difference compared to control.

There are limitations to the current study, particularly the radiotherapy survival assay. It is not known why the addition of unlabeled GlaS-Fc in the untreated condition caused reduced cell growth. It does not appear to be dose dependent as increased levels of unlabeled GlaS-Fc did not cause additional growth reduction. Further, the study was completed with a single lot of GlaS-Fc and only the 4T1 cell line. Although the flow cytometry and imaging studies reinforce the radiotherapy findings, further survival assays are needed. Repeating these results in an additional cell line, such as EO771, and with a different GlaS-Fc lot would confirm the findings.

The synergy between small changes in GlaS-Fc concentration and PS expression opens the possibility for an exciting nuclear imaging and therapy agent. The field of theranostics is constantly looking for agents that are specific for cancer, have minimal off-target activity, and operate at biologically tracer levels within the body. GlaS-Fc represents a platform to achieve all of these goals, and future studies will be performed to understand the mechanism behind the oligomerization and elucidate tumor targeting *in vivo*.

BIBLIOGRAPHY

1. Baghban, R.; Roshangar, L.; Jahanban-Esfahlan, R.; Seidi, K.; Ebrahimi-Kalan, A.; Jaymand, M.; Kolahian, S.; Javaheri, T.; Zare, P. Tumor microenvironment complexity and therapeutic implications at a glance. *Cell Commun Signal* **2020**, *18*, 59, doi:10.1186/s12964-020-0530-4.

2. Hanahan, D. Hallmarks of Cancer: New Dimensions. *Cancer Discov* **2022**, *12*, 31-46, doi:10.1158/2159-8290.CD-21-1059.

3. Jin, M.Z.; Jin, W.L. The updated landscape of tumor microenvironment and drug repurposing. *Signal Transduct Target Ther* **2020**, *5*, 166, doi:10.1038/s41392-020-00280-x.

4. Budhu, S.; Giese, R.; Gupta, A.; Fitzgerald, K.; Zappasodi, R.; Schad, S.; Hirschhorn, D.; Campesato, L.F.; De Henau, O.; Gigoux, M.; et al. Targeting Phosphatidylserine Enhances the Anti-tumor Response to Tumor-Directed Radiation Therapy in a Preclinical Model of Melanoma. *Cell Rep* **2021**, *34*, 108620, doi:10.1016/j.celrep.2020.108620.

5. Chang, W.; Fa, H.; Xiao, D.; Wang, J. Targeting phosphatidylserine for Cancer therapy: prospects and challenges. *Theranostics* **2020**, *10*, 9214-9229, doi:10.7150/thno.45125.

6. Birge, R.B.; Boeltz, S.; Kumar, S.; Carlson, J.; Wanderley, J.; Calianese, D.; Barcinski, M.; Brekken, R.A.; Huang, X.; Hutchins, J.T.; et al. Phosphatidylserine is a global immunosuppressive signal in efferocytosis, infectious disease, and cancer. *Cell Death Differ* **2016**, *23*, 962-978, doi:10.1038/cdd.2016.11.

7. Gerber, D.E.; Hao, G.; Watkins, L.; Stafford, J.H.; Anderson, J.; Holbein, B.; Oz, O.K.; Mathews, D.; Thorpe, P.E.; Haasan, G.; et al. Tumor-specific targeting by Bavituximab, a phosphatidylserine-targeting monoclonal antibody with vascular targeting and immune modulating properties, in lung cancer xenografts. *Am J Nucl Med Mol Imaging* **2015**, *5*, 493-503.

8. Gerber, D.E.; Horn, L.; Boyer, M.; Sanborn, R.; Natale, R.; Palmero, R.; Bidoli, P.; Bondarenko, I.; Germonpre, P.; Ghizdavescu, D.; et al. Randomized phase III study of docetaxel plus bavituximab in previously treated advanced non-squamous non-small-cell lung cancer. *Ann Oncol* **2018**, *29*, 1548-1553, doi:10.1093/annonc/mdy177.

9. Gerber, D.E.; Spigel, D.R.; Giorgadze, D.; Shtivelband, M.; Ponomarova, O.V.; Shan, J.S.; Menander, K.B.; Belani, C.P. Docetaxel Combined With Bavituximab in Previously Treated, Advanced Nonsquamous Non-Small-Cell Lung Cancer. *Clin Lung Cancer* **2016**, *17*, 169-176, doi:10.1016/j.cllc.2016.02.003.

10. Anderson, H.A.; Maylock, C.A.; Williams, J.A.; Paweletz, C.P.; Shu, H.; Shacter, E. Serum-derived protein S binds to phosphatidylserine and stimulates the phagocytosis of apoptotic cells. *Nat Immunol* **2003**, *4*, 87-91, doi:10.1038/ni871.

11. Gierula, M.; Ahnstrom, J. Anticoagulant protein S-New insights on interactions and functions. *J Thromb Haemost* **2020**, *18*, 2801-2811, doi:10.1111/jth.15025.

12. Kauffman, N.; Morrison, J.; O'Brien, K.; Fan, J.; Zinn, K.R. Intra-Arterial Delivery of Radiopharmaceuticals in Oncology: Current Trends and the Future of Alpha-Particle Therapeutics. *Pharmaceutics* **2023**, *15*, doi:10.3390/pharmaceutics15041138.

13. Uehara, H.; Shacter, E. Auto-oxidation and oligomerization of protein S on the apoptotic cell surface is required for Mer tyrosine kinase-mediated phagocytosis of apoptotic cells. *J Immunol* **2008**, *180*, 2522-2530, doi:10.4049/jimmunol.180.4.2522.

APPENDIX

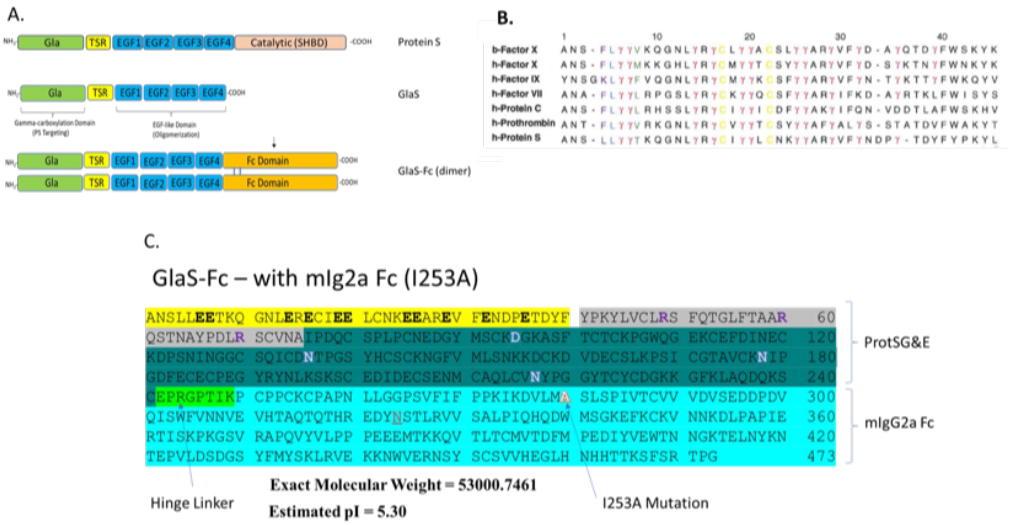

Figure S2.1 | Structure of Protein S, GlaS and GlaS-Fc and conserved Gla domain sequences. (A) Domain structures of Gla proteins: Protein S, GlaS and GlaS-Fc showing N-terminal Gla, thrombin sensitive (TSR), EGF or Kringle and catalytic or SHBG domains. GlaS-Fc is comprised of Gla, TSR, four EGF domains. The SBGB domain has been substituted with a C-terminal murine IgG2aFc with the I253A mutation to eliminate FcRn binding. GlaS-Fc exists as a disulfide-linked dimer. **(B)** Conserved sequence homology of the Gla domains of human coagulation factors. g indicates gamma-carboxylated glutamic acid residues. **(C)** Amino acid sequence of GlaS-Fc indicating Gla domain (yellow), TSR (grey), EGF domains (dark green), linker (green) and Fc domain (blue).

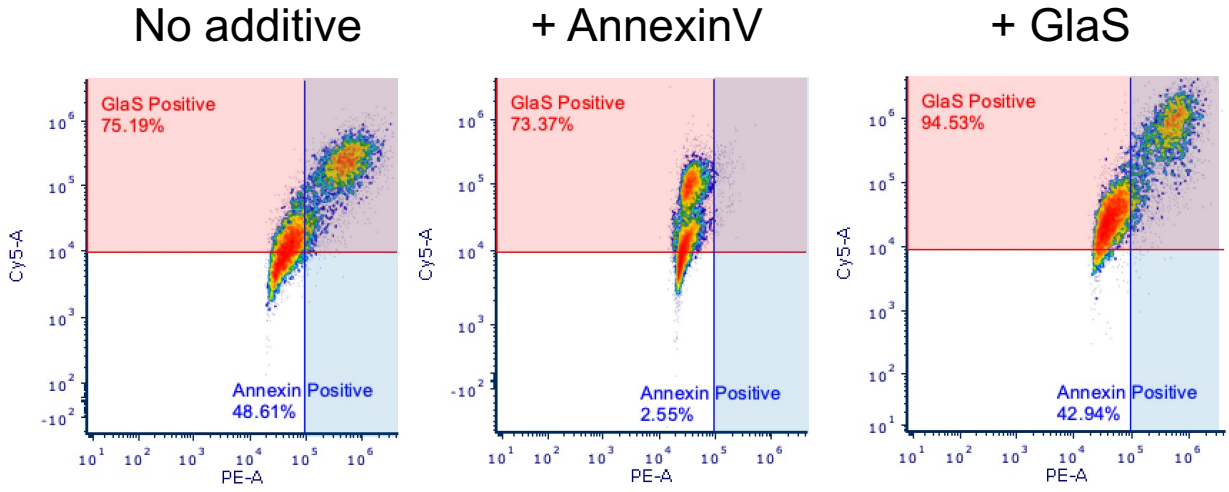

Figure S2.2 | Unlabeled GlaS increases Cy5-GlaS binding and does not completely block Annexin 5 binding. Flow cytometry of AnnexinV-PE and Cy5-GlaS show that unlabeled AnnexinV blocks AnnexinV-PE binding completely but has minimal effect on Cy5-GlaS binding. Unlabeled GlaS has a minimal effect on AnnexinV-PE binding but increases the total percent of positive cells and intensity of binding. This indicates different mechanisms for AnnexinV and GlaS binding, and suggests cooperation of GlaS with itself.

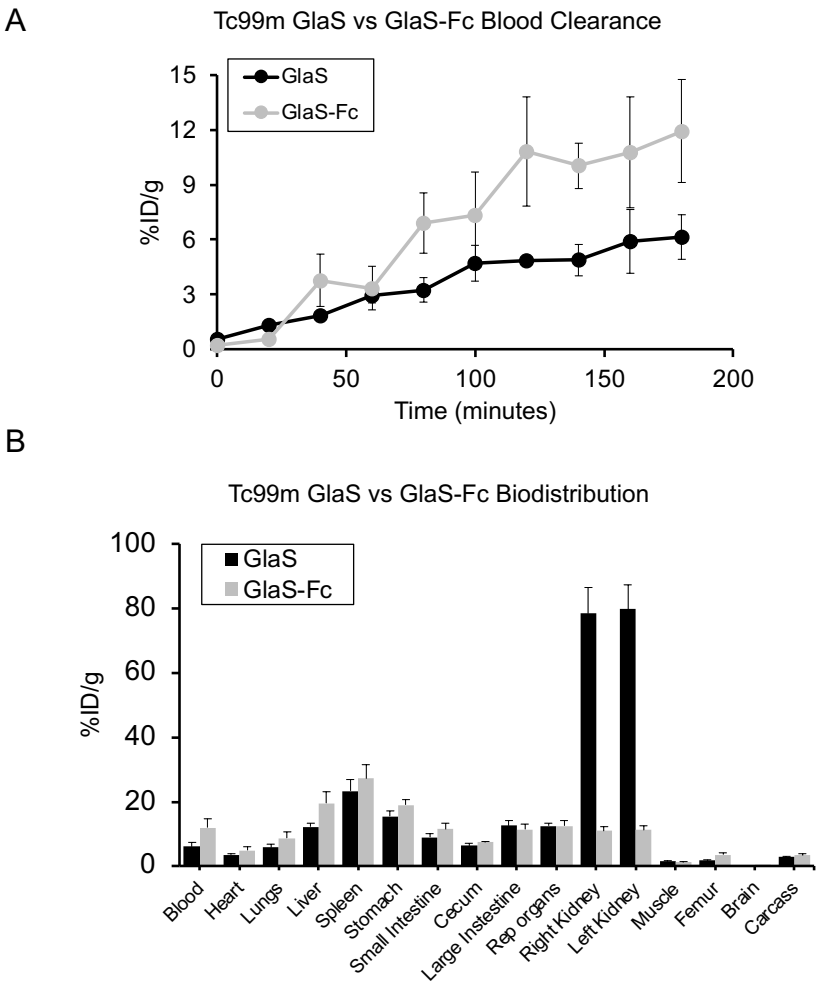

Figure S2.3 | GlaS-Fc has increased biological half-life compared to Gla. (A) Timecourse of Tc99m labeled Gla and GlaFc in healthy Balb/c mice (n =4 per group) showing increased levels of GlaFc in the blood after 3 hours. **(B)** A full biodistribution of tissues at 3 hours shows that GlaFc is not bound in the kidneys and is present in higher levels in the blood and bloody organs such as heart and lungs.

CHAPTER 3: EFFECTIVE THERAPY WITH BISMUTH-212 LABELED MACROAGGREGATED ALBUMIN IN ORTHOTOPIC MOUSE BREAST TUMOR MODELS

(Previously published as: Kauffman, N.; Singh, S.K.; Morrison, J.; Zinn, K.R. Effective therapy with Bismuth-212 labeled macroaggregated albumin in orthotopic mouse breast tumor models. Front Chem 2023, 11, 1204872, doi:10.3389/fchem.2023.1204872.)

Introduction

Radiation therapy has been essential for cancer management since its inception [1-3]. Many forms of radiation therapy exist, with each having unique properties and indications for use. Two forms of intravascular delivery of radiation therapy are well established in the clinical realm: peptide receptor radionuclide therapy (PRRT) and selective internal radiation therapy (SIRT). PRRT uses radiopeptides targeted against cancer-specific receptors to deliver radiation therapy, while SIRT uses selective intra-arterial (IA) infusion of radioembolics via tumor vasculature to irradiate tumors and stunt blood supply to tumors [4, 5]. Both methods rely on beta (β-)-emitting isotopes, namely Lutetium-177 (Lu-177) for PRRT and Yttrium-90 (Y-90) for SIRT [6]. β-particles are high-energy electrons that penetrate multiple millimeters into tissue. While the deep penetration allows for bystander treatment of non-targeted cancer cells, healthy cells surrounding the tumor also receive a large radiation dose [5, 7, 8]. This can lead to morbidity and toxicity.

Alpha (α)-particle emitting radionuclides are an exciting alternative to β-emitting radionuclides due to their high linear energy transfer (LET) and shorter range in tissue [7, 9, 10]. Alpha (α)-particle emitting nuclides such as Ac-225, Ra-223, At-211, Pb-212, and Bi-213 have been used in preclinical models and clinical trials to treat advanced-stage cancer where limited treatment options were available [10, 11]. Importantly, there are multiple reports where α-particle emitters were used to treat patients with β-radiation resistant tumors [12-14]. The large LET of α-particles compared to β-radiation resulted in double-stranded DNA breaks; free radical production was not required to kill cells. This means that radioisotopes emitting α-particles can be efficacious in situations of radioresistance, including hypoxia [15]. The poor commercial availability of radioisotopes with α-particle emissions has prevented them from becoming well translated into the standard of care [10, 11, 16]. Novel radiopharmaceutical combinations and delivery strategies can help translate more α-particle emitting radionuclides into the clinic [6, 13, 17, 18].

Interventional oncology is a field of medicine that utilizes image guidance to deliver cancer therapies directly into tumors [19]. The primary options for interventional oncologic therapies include percutaneous ablation and IA embolization. Selective Internal Radiation Therapy (SIRT),

also called Yttrium-90 microsphere (Y90) therapy or Trans-Arterial Radio-Embolization (TARE), is used extensively to treat hepatic cancers [20]. SIRT can reduce bulky liver tumors and bridge patients to surgical resection or transplantation options. SIRT relies on β-decay to deliver radiation therapy to tumors, which can have adverse effects due to the penetration of β-energy and effects on the nearby liver. Radiation and vascular damage also limit the ability to repeat treatment if there is a residual or recurrent tumor. It is important to retain as much healthy liver as possible, so the use of β-emitters may not be ideal. Additionally, few tumors in extrahepatic tissues have been explored for SIRT due to the penetration range of β-energy and the risk of the intervention blocking the blood supply to normal tissues. An internal locoregional therapy utilizing an α-particle emitting nuclide could improve tumor response and lower toxicity to healthy tissue. Currently, none exist.

FDA-approved macroaggregated albumin (MAA) are particles that range in size from 10-70 μm (90% of all particles) and can be labeled with Tc-99m for lung perfusion studies in nuclear medicine or for SIRT pre-treatment planning [21, 22]. MAA is similar in size to the microspheres used for SIRT and predicts deposition of the microspheres after delivery in the same arterial space. Other embolics such as lipiodol, have been used to test new SIRT delivery platforms, but few exist for MAA [23, 24]. MAA is attractive as a vehicle as it is semi-embolic, meaning it will be lodged into vasculature until it is eventually cleared naturally by the body. Combining the semi-embolic nature of MAA with a short-lived α-particle emitting radionuclide could allow for effective therapy in hepatic tumors but also other tissues more sensitive to radiation and reduction of blood supply. The current studies evaluated MAA as a vehicle for α-particle therapy delivery. Bismuth-212 (Bi-212), which was eluted from a Lead-212 (Pb-212) generator, was selected for binding to MAA due to availability from a generator system, short half-life, and decay scheme with α-particle emission. We also studied Bi-212 labeled MAA (Bi-212-MAA) efficacy in killing and inhibiting the growth of breast cancer cells *in vitro* and *in vivo*.

Methods

Pb-212 generator elution

The Ra-224/Pb-212 generators (5 mCi) were provided by Oak Ridge National Lab (The isotopes used in this research were supplied by the U.S. Department of Energy Isotope Program, managed by the Office of Isotope R&D and Production). Elution and preparation of the isotope was done similarly to as previously described [25]. The generator was washed with 500 μL of 2 M HCl upon receipt. Every day afterwards, Bi-212 was eluted from the generator with 800μL of

0.15M KI / 0.1 M HCl solution. The eluent was treated with 8 M HNO_3 and evaporated to dryness 3 times. The dried vials containing the Bi-212 were reconstituted with 100µL of 0.1 M HNO_3 for transfer to vials containing 10µL of 1 M NaOH for neutralization. To confirm the purity of the Bi-212 solution, a small sample from each elution was evaluated with a gamma counter (Wizard2, Perkin Elmer) for the energy peak corresponding to Bi-212 only (600 keV). Bi-212 purity was also confirmed by repeatedly measuring Bi-212 samples over time with a dose calibrator (CRC-25R, Capintec) to measure half-life.

Bi-212-MAA radiolabeling and quality control

FDA-approved MAA kits (Pulmotech) were purchased from Cardinal Health (East Lansing, MI). For radiolabeling MAA with Bi-212, 3 mg of the MAA kit (0.33mg MAA) was resuspended in 500µL 1X PBS (pH 7.0) and added to the neutralized Bi-212. The Bi-212-MAA solution was incubated for 10 minutes at 70 °C with 500 RPM shaking. Bi-212-bound MAA was purified by centrifugation at 1000g for 5 minutes with the pellet containing the Bi-212 bound MAA and the supernatant containing unbound Bi-212 that was easily removed. The percentage of Bi-212 bound to MAA was determined with instant thin layer chromatography (iTLC) on paper silica gel impregnated strips using 10 mM EDTA in 0.15 M NH_4OAc as the mobile phase.

Cell lines

4T1 and EO771 cells were purchased from ATCC. Cells were cultured in complete media (RPMI or DMEM with 10% FBS, 1% penicillin/streptomycin and 1% L-glutamine, respectively) and incubated at 37 °C with 5% CO_2. Cells were subcultured upon reaching 90% confluency and reseeded at 20% confluency.

For generation of stably luciferase expressing cell tines, both 4T1 and EO771 cells were transduced by PLV-10170-pLV-CAG-Firefly luciferase-PGK-Puro plasmid using lentivirus (Cellomics Technology) and luciferase positive clones were selected using puromycin (Thermo Fisher Scientific).

Clonogenic and survival assays

The clonogenic assay was performed as previously described [26]. In this assay, $1x10^3$ 4T1 and EO771 Luc+ cells were seeded into 6-well plates 12 hours prior to treatment. Cells were treated in triplicate with 0, 5, 10 and 20 µCi Bi-212-MAA and incubated for 1 week. Bland, unlabeled MAA particles were used as 0 uCi condition (control group) to match the number of particles used for the highest treated condition (20 µCi). For IVIS imaging and quantification, cells

had media removed and replaced with 150 μg/mL luciferin diluted in complete media. Cells were imaged using IVIS Lumina bioluminescence imaging (BLI) with autoexposure setting. Data were analyzed using ROI and radiance (photon/second). After imaging, colonies were stained with crystal violet and manually counted for the total number of colonies per well. Colonies were considered for clusters with greater than 50 cells.

For the survival assay, $5x10^4$ 4T1 and EO771 Luc+ cells were seeded into a 24-well plate. 12 hours later, cells were treated with 0, 2.5, 5, 10, or 20 μCi of Bi-212-MAA and incubated for 48 hours. Bland, unlabeled MAA was again used as the 0 μCi condition (Control group), with the number of particles matching those used in the 20 μCi condition. IVIS imaging and quantification were done identically to the clonogenic assay as described.

Animals

All animals were purchased from Charles River Laboratory. All animals used in the experiments were of standard Balb/c and C57BL/6 background (female) and 8 weeks of age. The animal studies were approved by the Institutional Animal Care and Use Committee (IACUC), and all animal experiments were conducted according to IACUC guidelines.

Bi-212-MAA imaging and biodistribution in Balb/c and C57BL/6 mice

Balb/c and C57BL/6 mice (8 weeks old) were implanted with $1x10^5$ 4T1 and EO771 cells (respectively) in the left 4th mammary gland using a 50:50 mixture of Matrigel and PBS in a total volume of 50 uL. After 10 days, 4 mice with 4T1 breast tumors were injected intratumorally (IT) with 11 μCi of Bi-212-MAA in 20 μL of 0.9% sterile saline using 25-gauge integrated needle syringes with zero dead volume. Similarly, after 11 days 4 mice with EO771 breast tumor were injected IT with 7 μCi of Bi-212-MAA. For EO771 tumors, 4 mice plus 1 additional untreated mouse with a breast tumor were then imaged 2 hours later using Cherenkov luminescence imaging (CLI) on IVIS for radiation localization. After imaging, all 5 mice were injected with luciferin (3 mg) intraperitoneally and imaged 5 minutes later using BLI for tumor localization. Mice from both 4T1 and EO771 groups were sacrificed and had organs removed for gamma counting. Injection data and gamma counted data were all decay corrected to the counting start time. Mice in the 4-hour group underwent biodistribution without an imaging session and were counted in the same fashion as the 2-hour group with proper decay correction.

Western blot analysis

Total protein was extracted by lysing the 4T1 cells using RIPA buffer (Thermo Fisher Scientific) with 1X proteinase inhibitor cocktail added (Abcam) and incubated at 4 °C for 30 min and vortexed 45 seconds every 10 min. Cell lysates were centrifuged at 30,000g for 30 min at 4 °C, and the supernatants were collected and stored at −80 °C for further use. Protein concentration was determined using the Bradford protein assay method. Protein samples were denatured by adding 4x Laemmli sample buffer (BioRad) and heating 95 °C for 5 mins. Further, 40 µg of proteins were run on 4-15% SDS-PAGE gels. Proteins were transferred onto the nitrocellulose membrane, followed by blocking with SuperBlock buffer (Thermo) for 1 hour at room temperature. Next, membranes were incubated with diluted primary antibody (1:1000) in a blocking buffer at 4 °C with gentle shaking for 1 hour. Membranes were washed three times with 1X TBST buffer and further probed with polyclonal anti-rabbit or anti-mouse IgG secondary antibodies conjugated to horseradish peroxidase (HRP) and incubated at room temperature for 1 h. After washing three times with 1X TBST buffer, enhanced chemiluminescence (ECL) solution (Thermo Fisher Scientific) on the top of the membrane, and protein bands were visualized using Chemidoc (BioRad).

Orthotopic mammary tumor treatment with Bi-212-MAA

Balb/c and C57BL/6 mice (8 weeks) were implanted with $1x10^5$ 4T1 and EO771 Luc+ cells (respectively) in the left 4^{th} mammary gland. After 7- and 10-days post-implantation, 4T1 and EO771 tumors, respectively, were injected IT with Bi-212-MAA or vehicle control (bland, unlabeled MAA). 4T1 mice received either 25 or 50 uCi of Bi-212-MAA or control, while EO771 mice received either 50 or 100 uCi Bi-212-MAA or control suspended in 20µL of 0.9% sterile saline using 25-gauge integrated needle syringes with zero dead volume. Mice were then tracked for tumor growth using digital caliper measurement. All groups were euthanized once the tumor size reached 2 cm in length in any group. Tumor volume was calculated using the equation (longest diameter x ((shortest diameter/2)^2)).

Statistical analysis

Statistical analysis was performed using GraphPad. One-way analysis of variance (ANOVA) with Dunnett's test was used to compare the experimental groups to the control group. Data are reported as mean ± standard error of the mean (SEM). P-values < 0.05 were considered statistically significant.

Results

Efficacy of MAA radiolabeling with Bi-212

Bi-212 was successfully eluted from the Ra-224 column (Pb-212 generator) and used for all assays. The decay scheme for Ra-224 and all daughters is shown in Figure 3.1. Bi-212 or short-lived Po-212 (0.3 μs) had the critical α-particle emissions and excludes the β-emission from Pb-212 decay. The commercially available MAA kits were radiolabeled using simple methods, as shown in Figure 3.1. This allows for quick use of the Bi-212-MAA and limits total decay of the activity. Many radiolabelings were performed throughout the life of the generator for the different assays. For example, on a day a week after the Pb-212 generator was received, the pure Bi-212 (484 ± 4 μCi) was added to 3mg MAA kit (n=3), incubated, and purified. The resulting Bi-212-MAA was 240 ± 1 μCi, indicating an efficiency of 50%. The MAA kits are 10% MAA particles and contain 4 million MAA particles. Approximately 667,000 MAA particles were contained within 3 mg of MAA kit, and it was assumed that all were retained after purification. This resulted in a specific activity of 240/0.3 μCi/mg of MAA particles, or 0.8 μCi/μg. The Bi-212-MAA used for treatment studies was labeled when the generator had higher activity with the highest being approximately 20 μCi/μg MAA particles. iTLC strips were used to determine purity and the strips were counted with either the dose calibrator or gamma counter depending on activity. IVIS-based CLI of an example iTLC strip is shown in Figure 3.1, with the EDTA mobile phase able to push free Bi-212 to the top of the strip while Bi-212 tightly bound to MAA remains at the bottom. To confirm the purity of the Bi-212 initial elution and the final Bi-212-MAA product, a sample was removed and counted on the gamma counter. Visualization of the peak at around 600 keV (orange window) and lack of a peak at 200 keV (blue window) confirms the presence of Bi-212 only.

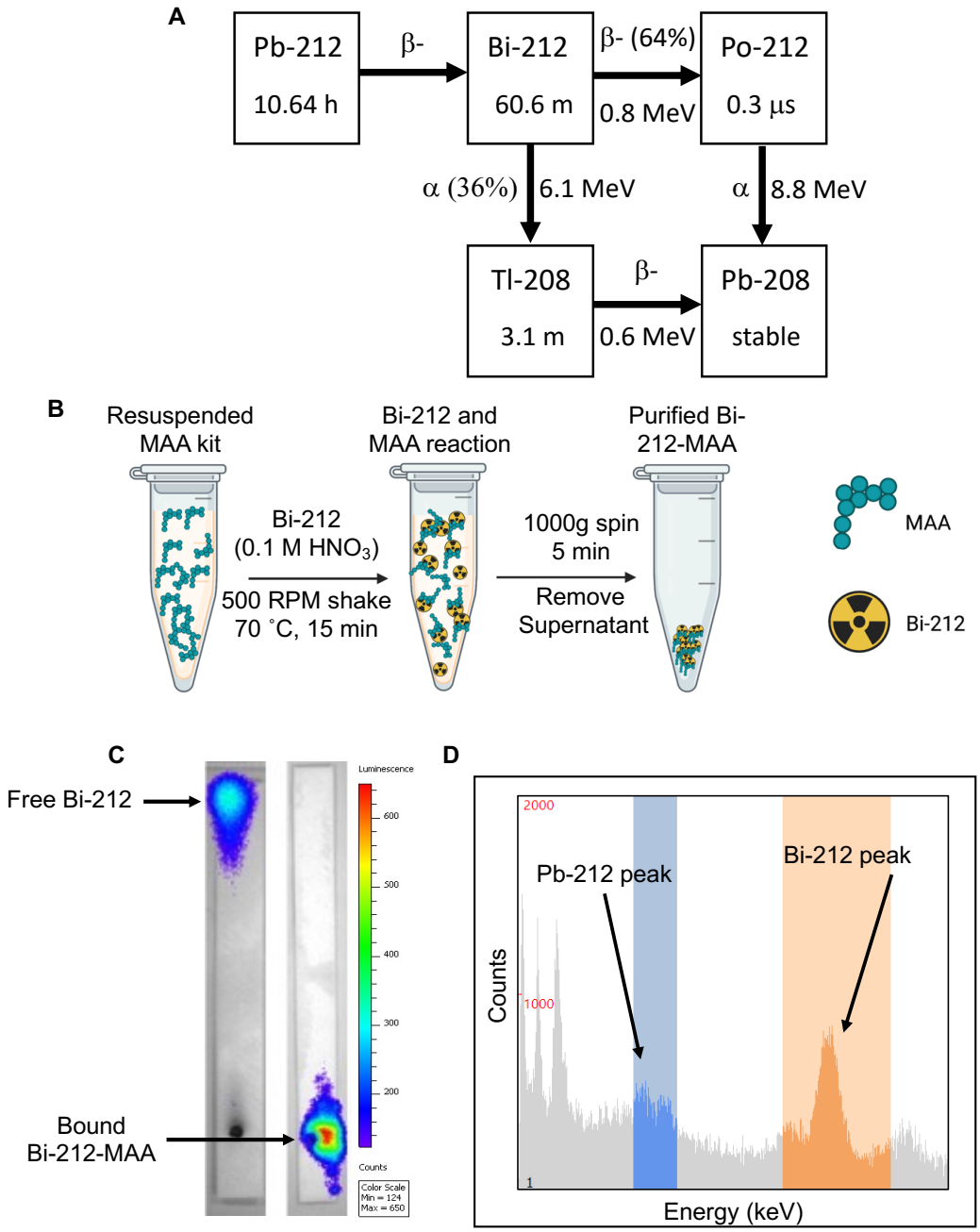

Figure 3.1 | Overview of radiolabeling and quality control protocols for Bi-212 MAA assays. **(A)** Decay scheme for Pb-212 available from Ra-224 parent. Bi-212 has a shorter half-life and avoids the beta decay emission arising from Pb-212. **(B)** Graphical overview of Bi-212-MAA radiolabeling procedure, highlighting the speed and simplicity of the procedure. **(C)** Representative CLI picture of developed iTLC strips of either pure Bi-212 (left) or purified Bi-212-MAA (right) using IVIS machine. Free Bi-212 moved to the top of the strip while Bi-212 bound to MAA remained at the bottom. **(D)** Representative gamma counting window present on Wizard gamma counter during a counting protocol. Bi-212 has a gamma peak around 600 keV (orange window) while Pb-212 has a peak at 200 keV (blue window) that can be used to discern the radionuclides in a sample.

Bi-212-MAA delivered radiation therapy and inhibited clonogenic potential, and killed breast cancer in vitro

MAA particles spread out evenly in solution and sink, allowing for treatment of monolayer cell cultures (Supplementary Figure 3.1). Previously, the treatment efficacy of radiotherapy was evaluated by clonogenic and survival assays for various cancer cells, with the clonogenic assay measuring the colony formation capacity of individual cancer cells and their ability to replicate [27]. In this study, we used Bi-212-MAA to treat $1X10^3$ 4T1 and EO771 breast cancer cells in a 6-well plate format to assess radiation therapy effectiveness on cancer cell clonogenicity. Increased levels of Bi-212-MAA led to significantly less total colony formation in both 4T1 and EO771 cells (Figure 3.2A-D). This was first assessed using BLI, which shows the total amount of signal in the plate and not the individual colony number. Afterward, cells were stained with crystal violet, and the number of colonies was manually counted. All treatment groups showed significantly decreased BLI signal when compared to bland MAA control for both 4T1 and EO771 cells (Figure 3.2A and C). After staining and counting, all treatment groups showed significantly decreased colony formation when compared to bland MAA control in both 4T1 and EO771 cells (Figure 3.2B and D). These results correlated well with a short-term survival assay (Figure 3.2E and F). Cells in a survival assay are grown at a higher confluency and thus are reactive to paracrine functions and other communications from neighboring cancer cells. They are also able to reach their exponential phase of growth more quickly compared to the clonogenic assay. Bi-212-MAA was added to cells in an increasing dose to identify the sensitive dose range. After 48 hours, there was a significant decrease in the total number of cells in all treatment conditions compared to the bland MAA control, which indicates that even the lowest dose of 2.5 μCi was sufficient to kill or prevent reproduction in most cells.

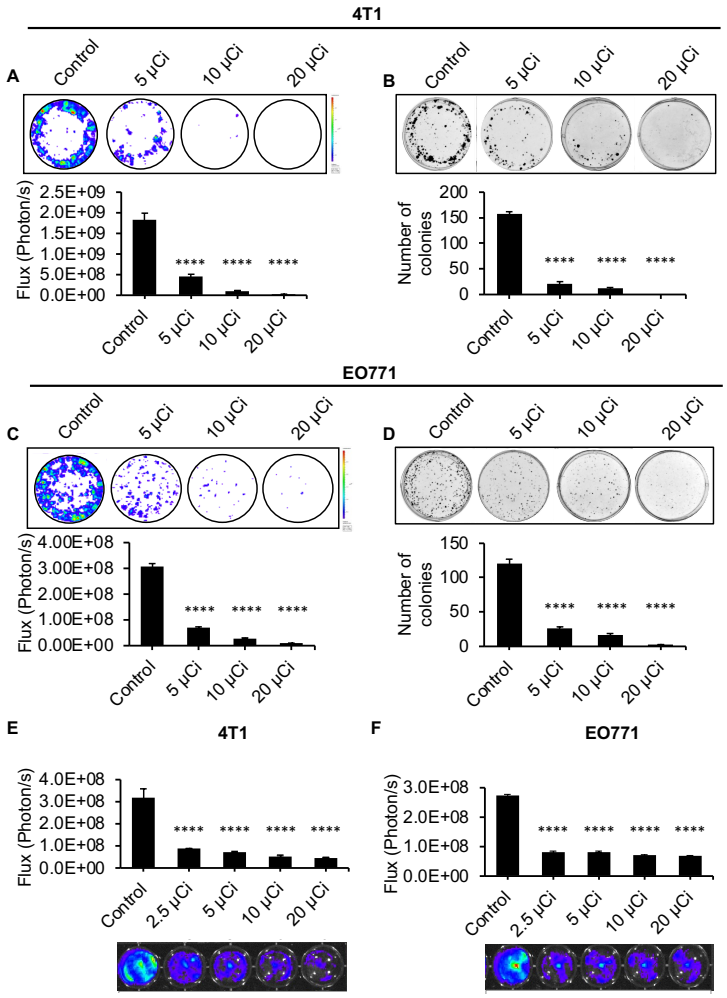

Figure 3.2 | Effective killing of 4T1 and EO771 cells in vitro with Bi-212-MAA. (A-D) Representative images of BLI and crystal violet staining of the clonogenic assay for 4T1 **(A,B)** and EO771 **(C,D)** showed a specific dose response in cancer cell reproductive death (n=3). **(E,F)** Representative images of BLI of the survival assay 48 hours after treatment with Bi-212-MAA showed dose specific reduction in 4T1 **(E)** and EO771 **(F)** cell growth (n=4). ****, $P < 0.0001$ compared to control.

Bi-212-MAA upregulated DNA damage and cell death markers in 4T1 cells

The clonogenic and survival assays showed that Bi-212-MAA was effectively killing breast cancer cells and preventing cell growth. Therefore, to find out the downstream molecular markers involved in cell death, a DNA damage marker and a cell death marker were evaluated. H2AX phosphorylation (γH2AX) is a well-known marker of an early cellular response to DNA double-strand breaks, and Caspase 3 is a key molecule involved in cell death [28, 29]. In this study, western blot analysis showed that Bi-212-MAA treatment induced H2AX phosphorylation in 4T1-treated

cells (Figure 3.3A). Further, a higher expression of cleaved Caspase-3 was found in Bi-212-MAA treated 4T1 cells compared to control cells (Figure 3.3B).

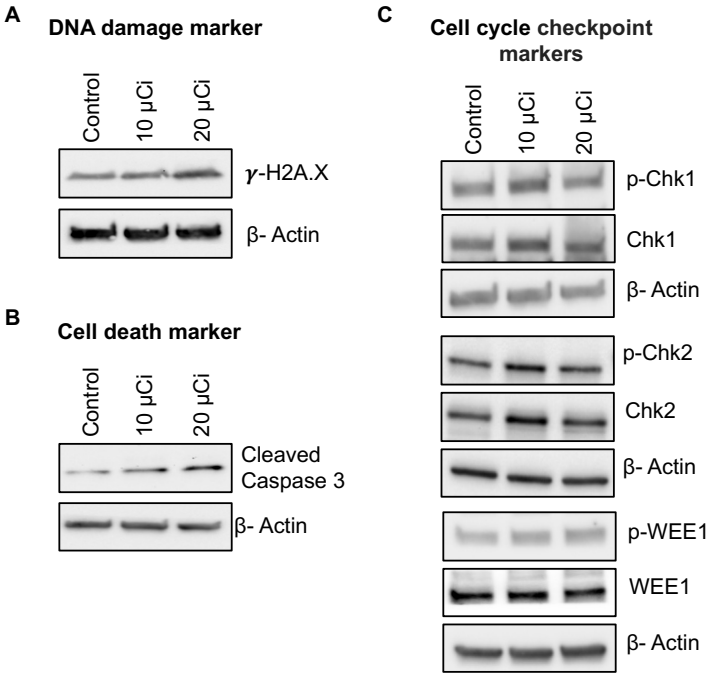

Figure 3.3 | Bi-212-MAA treatment induces DNA damage, apoptosis, and cell cycle pathways in mouse breast monolayer cancer cell culture. **(A-C)** Western blots showing Bi-212-MAA treatment results in induction of DNA damage **(A)** and apoptosis markers **(B)** and comparable effect on cell cycle checkpoint markers **(C)** in higher Bi-212 activity group compared to control.

Next, the expression of cell cycle checkpoint markers was studied to elucidate if 4T1 cells could effectively initiate DNA damage repair response [30]. The results showed that at a lower dose of Bi-212-MAA, there was increased activation of cell cycle checkpoint markers Chk1, Chk2, and Wee1; however, at higher dose levels, Chk1, Chk2, and Wee1 activation were comparable to control (Figure 3.3C). These findings suggest that Bi-212-MAA treatment to 4T1 cells caused DNA damage and killed breast cancer cells without activating cell cycle checkpoint markers at a higher dose which could avoid cell senescence and potential radioresistance.

Bi-212-MAA was safely delivered to orthotopic breast tumors in mice via intratumoral injection and significantly decreased tumor growth

Mice are too small to use IA delivery of drugs into tumor vasculature, so direct IT injection was needed for delivery of radioembolics into tumor tissue. It is well known that large particles can be retained in solid tumors after injection [23, 31, 32]. Mice with orthotopic EO771 tumor were injected IT and imaged 2 hours later. CLI showed that Bi-212-MAA stayed within the tumor

space (Figure 3.4B-D). This is indicated by the CLI data (Bi-212-MAA radiation) margins being within the BLI data (Luc+ EO771 tumor cells) margins. At 2 and 4 hours post-injection, greater than 90% of the total injected dose remained within the tumor for both 4T1 and EO771 (Figure 3.4I and J). A full biodistribution of the mice revealed minimal leakage out of the tumor and into the lungs, which was the expected destination for any Bi-212-MAA that entered post-tumoral venules (Figure 3.4E-H).

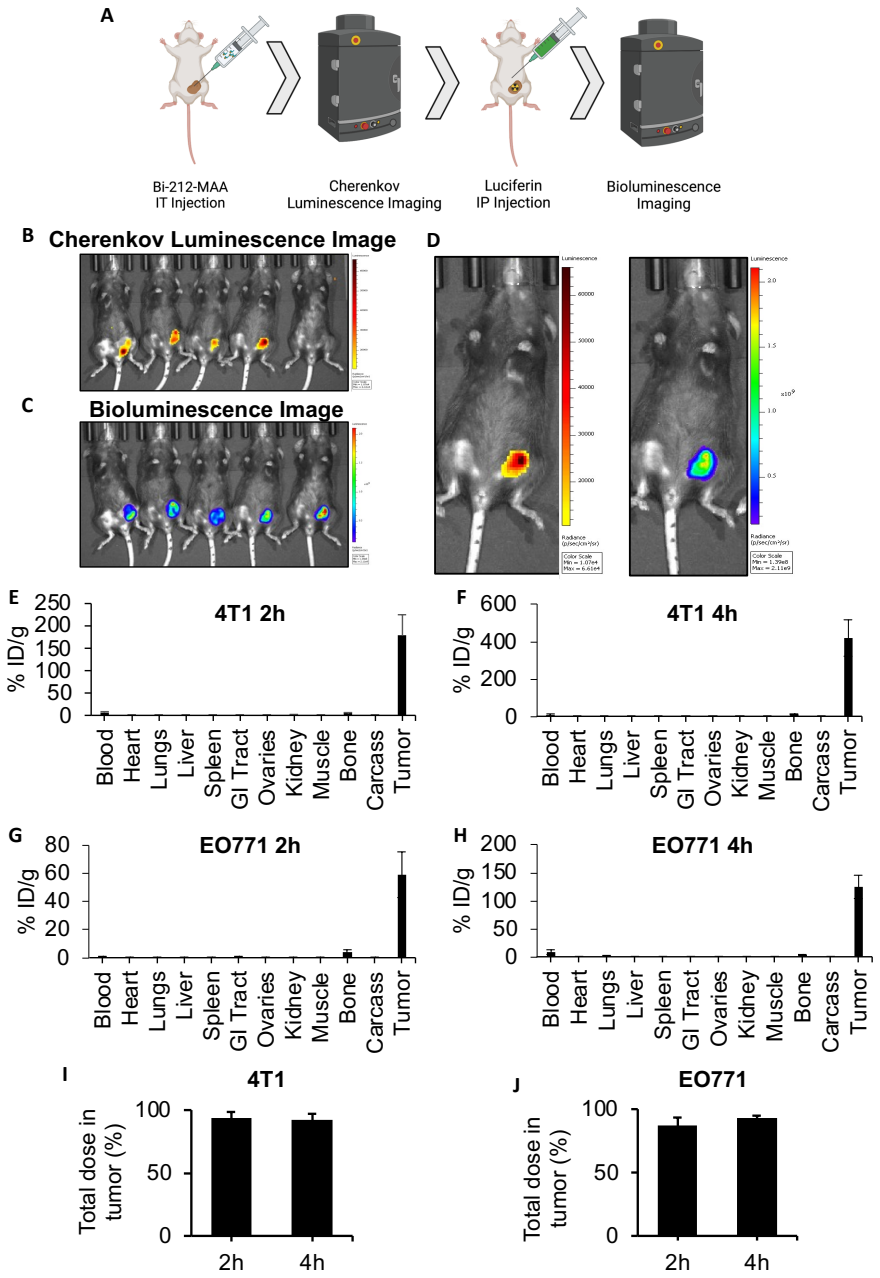

Figure 3.4 | Intratumorally injected Bi-212-MAA was stably retained in the tumoral space. **(A)** Mice used for the Bi-212-MAA imaging and biodistribution were treated as indicated. **(B,C)** Bi-212-MAA remained within tumor as shown by the CLI **(B)** picture and tumor tissue was confirmed with BLI **(C)** of Luc+ EO771 cells comprising the tumor. **(D)** Blow up of representative CLI and BLI images of the same mouse confirmed overlay of both data sets. **(E-H)** Complete biodistributions indicated most of the injected Bi-212-MAA remains in the tumor at 2 and 4 hours in both the 4T1 **(E,F)** and EO771 **(G,H)** tumors (n=4). Some radiation signal in the blood and bone potentially indicated free nuclide while minimal signal in lungs indicated minimal escape of Bi-212-MAA from the tumor. **(I,J)** The percentage of the total dose within the 4T1 **(I)** and EO771 **(J)** tumors indicated minimal leakage of Bi-212-MAA into healthy organs (n=4).

Further, to evaluate the effectiveness of Bi-212-MAA in killing breast cancer cells *in vivo*, 4T1 and EO771 tumors in Balb/c and C57BL/6 mice, respectively, were treated with Bi-212-MAA by injecting IT. The Bi-212-MAA caused a significant reduction in total growth compared to bland MAA-treated controls in both 4T1 and EO771 tumors (Figure 3.5A and B). These results indicated that IT injection was a viable route for Bi-212-MAA delivery. Additionally, these results indicated that Bi-212-MAA effectively reduced breast cancer cells growth in the mouse orthotopic models.

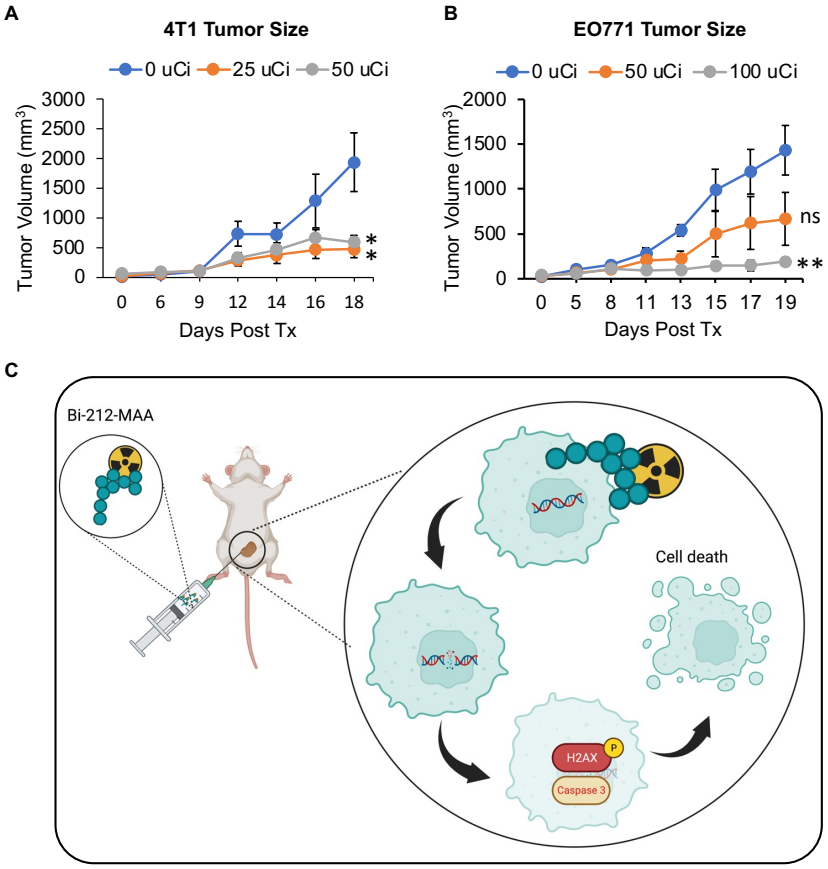

Figure 3.5 | Intratumoral delivery of Bi-212-MAA prevented orthotopic breast tumor growth. (A,B). Tumor volume growth was decreased in both 4T1 **(A)** and EO771 **(B)** orthotopic breast cancer models (n=4)**. (C)** Schematic picture showing potential mechanism involve in Bi-212-MAA therapy mediated breast cancer cell death. ns, not significant; *, $P < 0.05$; **, $P< 0.01$ compared to control.

Discussion

A standard commercially available MAA kit was rapidly labeled with Bi-212 and easily purified. The purification method was easier compared to other methods, that can take additional time, and the product can be lost during the process. The decay scheme of Pb-212 and easy elution

of Bi-212 allowed for easy labeling and quantification of Bi-212-MAA. The process can be improved further later on by using clinical grade generators.

Due to its size and density, MAA sank in solution and thus contacted cells in monolayer cell culture when added. With the short range of α-particles, it was unknown whether the MAA would bring the Bi-212 close enough to cells to deliver an effective therapy. However, the results clearly indicate that the Bi-212-MAA was an effective therapeutic against mouse breast cancer cells *in vitro* in both the clonogenic and survival assays. Importantly, we can perform further *in vitro* studies to study the molecular effects of α-particle radiation on cancer cells.

It was found that classic markers of apoptosis and general DNA-damage response were elevated with increasing levels of Bi-212-MAA. Further, no change was seen in markers of radioresistance, specifically proteins involved in cell cycle checkpoint control. It is known that increased radiation dose can lead to cell cycle arrest and cell survival, making it critical to find a sensitive dose [28-30]. Alpha (α)-particle therapy works through direct double-stranded DNA breaks, thus leaving the cell with very few options for resistance and survival. Other forms of radiation, including photon and β-, rely on single-stranded breaks and the generation of free radicals for cell destruction. These are much easier to overcome compared to double-stranded breaks and allow ample opportunity for cancer cell escape.

The large size of MAA allows it to remain in tumor when delivered IT as seen with our biodistribution studies. The 2 and 4 hour time points both showed high levels of MAA retention. These time points represented 75% and 94% of the total decay of Bi-212, respectively. The low dose present in healthy tissues shows that MAA stayed lodged within the tumor and that the radiopharmaceutical was stable and not releasing Bi-212. Further timepoints were not needed as greater than 90% of the dose was still present in the tumor at the 94% decay point. The biodistribution data were corroborated using CLI and BLI.

Both 4T1 and EO771 tumors showed a response to IT delivery of Bi-212-MAA. This is an impressive result since the MAA is likely not distributed uniformly throughout the tumor and is therefore not leading to a complete tumor tissue dose. Although the CLI data shows retention of Bi-212-MAA in tumors, it does not cover the margins of the BLI data, indicating a smaller area of localization at the injection site. In an IA delivery model, the distribution would be much more uniform. Additionally, the expected range of α-particles from Bi-212 decay would span multiple cell diameters, allowing for a local crossfire effect in the tumor without causing toxicity to

surround healthy parenchyma. Mice vessels were too small to utilize image guidance; however, there was precedence for direct injection of drugs into tumors to study therapy. With the short half-life of Bi-212, Bi-212-MAA only needed to remain within the tumor for a few hours to deliver a large radiation dose to tumors, which explains the success therapy of our studies.

Due to Bi-212-MAA being agnostic to tumor receptor presence or density, it can be used to explore the effects of α-particles on any solid tumor model. Critically, it was recently found that fractionated external beam radiation therapy combined with immunotherapy led to an abscopal response in mice [33]. Systemic immune response against cancer induced by radiation therapy would be an excellent treatment outcome and is a worthy goal sought. Bi-212-MAA can be used to explore its own effects on pan-cancer immunogenicity *in vitro* because of its agnostic targeting, similar to external beam radiation. Further, the short half-life of Bi-212 allows for a similar fractionated therapy schedule compared to the external beam, while long-lived isotopes such as Y-90 will continually dose the tumor once delivered [34].

Bi-212-MAA also represents an easily translatable α-particle emitting radiopharmaceutical. As MAA and Ra-224/Pb-212 generators are already used in clinical trials, Bi-212-MAA has great promise for translation to human studies as an IA delivered drug. SIRT is a widely used treatment option for reducing hepatic tumor size and bridging patients to either surgical or transplantation options. The recent success of SIRT in the prostate highlights the potential for radioembolization in tissues outside of the liver [35]. The breast represents another tissue that may be amenable to IA therapies [36]. Bi-212-MAA could be used not only to improve results in hepatic tumors but also safely explore new treatment options for prostate and breast cancers.

In this study, we were able to effectively radiolabel MAA with the short-lived α-particle emitter Bi-212. Additionally, Bi-212-MAA was successfully used to inhibit mouse breast cancer growth in monolayer cell culture and in orthotopic breast cancer models. Bi-212-MAA represents a widely applicable platform for studying the effects of α-particle therapy on cancer cells, including molecular mechanisms of radioresistance and immunogenicity. Further, Bi-212-MAA is uniquely poised to be translated into clinical trials due to all reagents and its required delivery method being FDA approved.

BIBLIOGRAPHY

1. Baskar R, Lee KA, Yeo R, Yeoh KW. Cancer and radiation therapy: current advances and future directions. Int J Med Sci. 2012;9(3):193-9.

2. Ma L, Men Y, Feng L, Kang J, Sun X, Yuan M, et al. A current review of dose-escalated radiotherapy in locally advanced non-small cell lung cancer. Radiol Oncol. 2019;53(1):6-14.

3. Razvi Y, Chan S, Zhang L, Tsao M, Barnes E, Danjoux C, et al. A review of the Rapid Response Radiotherapy Program in patients with advanced cancer referred for palliative radiotherapy over two decades. Support Care Cancer. 2019;27(6):2131-4.

4. Arslan N, Ince S, Okuyucu K, San H, Alagoz E, Karadurmus N, et al. Yttrium-90 (Y-90) resin microsphere therapy for patients with unresectable hepatocellular carcinoma. Identification of successful treatment response predictors and patient selection. Ann Ital Chir. 2021;92:623-31.

5. Bodei L, Cremonesi M, Grana CM, Fazio N, Iodice S, Baio SM, et al. Peptide receptor radionuclide therapy with (1)(7)(7)Lu-DOTATATE: the IEO phase I-II study. Eur J Nucl Med Mol Imaging. 2011;38(12):2125-35.

6. Kauffman N, Morrison J, O'Brien K, Fan J, Zinn KR. Intra-Arterial Delivery of Radiopharmaceuticals in Oncology: Current Trends and the Future of Alpha-Particle Therapeutics. Pharmaceutics. 2023;15(4).

7. Morris ZS, Wang AZ, Knox SJ. The Radiobiology of Radiopharmaceuticals. Semin Radiat Oncol. 2021;31(1):20-7.

8. Ravi Kumar AS, Hofman MS. Mechanistic Insights for Optimizing PSMA Radioligand Therapy. Clin Cancer Res. 2020;26(12):2774-6.

9. Sgouros G, Roeske JC, McDevitt MR, Palm S, Allen BJ, Fisher DR, et al. MIRD Pamphlet No. 22 (abridged): radiobiology and dosimetry of alpha-particle emitters for targeted radionuclide therapy. J Nucl Med. 2010;51(2):311-28.

10. Tafreshi NK, Doligalski ML, Tichacek CJ, Pandya DN, Budzevich MM, El-Haddad G, et al. Development of Targeted Alpha Particle Therapy for Solid Tumors. Molecules. 2019;24(23).

11. Sgouros G, Bodei L, McDevitt MR, Nedrow JR. Radiopharmaceutical therapy in cancer: clinical advances and challenges. Nat Rev Drug Discov. 2020;19(9):589-608.

12. Kratochwil C, Bruchertseifer F, Giesel FL, Weis M, Verburg FA, Mottaghy F, et al. 225Ac-PSMA-617 for PSMA-Targeted alpha-Radiation Therapy of Metastatic Castration-Resistant Prostate Cancer. J Nucl Med. 2016;57(12):1941-4.

13. Kratochwil C, Giesel FL, Bruchertseifer F, Mier W, Apostolidis C, Boll R, et al. (2)(1)(3)Bi-DOTATOC receptor-targeted alpha-radionuclide therapy induces remission in neuroendocrine tumours refractory to beta radiation: a first-in-human experience. Eur J Nucl Med Mol Imaging. 2014;41(11):2106-19.

14. Shi M, Jakobsson V, Greifenstein L, Khong PL, Chen X, Baum RP, et al. Alpha-peptide receptor radionuclide therapy using actinium-225 labeled somatostatin receptor agonists and antagonists. Front Med (Lausanne). 2022;9:1034315.

15. Muz B, de la Puente P, Azab F, Azab AK. The role of hypoxia in cancer progression, angiogenesis, metastasis, and resistance to therapy. Hypoxia (Auckl). 2015;3:83-92.

16. Strosberg J, Herrmann K, Bodei L. The Future of Targeted alpha-Therapy Is Bright, but Rigorous Studies Are Necessary to Advance the Field. J Nucl Med. 2023;64(2):219-20.

17. Autenrieth ME, Seidl C, Bruchertseifer F, Horn T, Kurtz F, Feuerecker B, et al. Treatment of carcinoma in situ of the urinary bladder with an alpha-emitter immunoconjugate targeting the epidermal growth factor receptor: a pilot study. Eur J Nucl Med Mol Imaging. 2018;45(8):1364-71.

18. Meredith RF, Torgue JJ, Rozgaja TA, Banaga EP, Bunch PW, Alvarez RD, et al. Safety and Outcome Measures of First-in-Human Intraperitoneal alpha Radioimmunotherapy With 212Pb-TCMC-Trastuzumab. Am J Clin Oncol. 2018;41(7):716-21.

19. Degrauwe N, Hocquelet A, Digklia A, Schaefer N, Denys A, Duran R. Theranostics in Interventional Oncology: Versatile Carriers for Diagnosis and Targeted Image-Guided Minimally Invasive Procedures. Front Pharmacol. 2019;10:450.

20. Spyridonidis T, Papathanasiou N, Spyridonidis J, Ntzoumani C, Spyropoulou D, Katsanos K, et al. (90)Y-microsphere radioembolization: The method, clinical evidence and perspective. Hell J Nucl Med. 2020;23(3):330-8.

21. Amor-Coarasa A, Milera A, Carvajal D, Gulec S, McGoron AJ. Lyophilized Kit for the Preparation of the PET Perfusion Agent [(68)Ga]-MAA. Int J Mol Imaging. 2014;2014:269365.

22. Hamami ME, Poeppel TD, Muller S, Heusner T, Bockisch A, Hilgard P, et al. SPECT/CT with 99mTc-MAA in radioembolization with 90Y microspheres in patients with hepatocellular cancer. J Nucl Med. 2009;50(5):688-92.

23. Bakker RC, Lam M, van Nimwegen SA, Rosenberg A, van Es RJJ, Nijsen JFW. Intratumoral treatment with radioactive beta-emitting microparticles: a systematic review. J Radiat Oncol. 2017;6(4):323-41.

24. Bozkurt MF, Salanci BV, Ugur O. Intra-Arterial Radionuclide Therapies for Liver Tumors. Semin Nucl Med. 2016;46(4):324-39.

25. Baidoo KE, Milenic DE, Brechbiel MW. Methodology for labeling proteins and peptides with lead-212 (212Pb). Nucl Med Biol. 2013;40(5):592-9.

26. Sinha S, Singh SK, Jangde N, Ray R, Rai V. p32 promotes melanoma progression and metastasis by targeting EMT markers, Akt/PKB pathway, and tumor microenvironment. Cell Death Dis. 2021;12(11):1012.

27. Hu T, Zhou R, Zhao Y, Wu G. Integrin alpha6/Akt/Erk signaling is essential for human breast cancer resistance to radiotherapy. Sci Rep. 2016;6:33376.

28. Chen H, Han Z, Luo Q, Wang Y, Li Q, Zhou L, et al. Radiotherapy modulates tumor cell fate decisions: a review. Radiat Oncol. 2022;17(1):196.

29. Widjaja L, Werner RA, Krischke E, Christiansen H, Bengel FM, Bogdanova N, et al. Individual radiosensitivity reflected by gamma-H2AX and 53BP1 foci predicts outcome in PSMA-targeted radioligand therapy. Eur J Nucl Med Mol Imaging. 2023;50(2):602-12.

30. Chan Wah Hak CML, Rullan A, Patin EC, Pedersen M, Melcher AA, Harrington KJ. Enhancing anti-tumour innate immunity by targeting the DNA damage response and pattern recognition receptors in combination with radiotherapy. Front Oncol. 2022;12:971959.

31. Morsink NC, Nijsen JFW, Grinwis GCM, Hesselink JW, Kirpensteijn J, van Nimwegen SA. Intratumoral injection of holmium-166 microspheres as neoadjuvant therapy of soft tissue sarcomas in dogs. Front Vet Sci. 2022;9:1015248.

32. Rosemurgy A, Luzardo G, Cooper J, Bowers C, Zervos E, Bloomston M, et al. 32P as an adjunct to standard therapy for locally advanced unresectable pancreatic cancer: a randomized trial. J Gastrointest Surg. 2008;12(4):682-8.

33. Vanpouille-Box C, Alard A, Aryankalayil MJ, Sarfraz Y, Diamond JM, Schneider RJ, et al. DNA exonuclease Trex1 regulates radiotherapy-induced tumour immunogenicity. Nat Commun. 2017;8:15618.

34. Aicher A, Sindrilaru A, Crisan D, Thaiss W, Steinacker J, Beer M, et al. Short-Interval, Low-Dose Peptide Receptor Radionuclide Therapy in Combination with PD-1 Checkpoint Immunotherapy Induces Remission in Immunocompromised Patients with Metastatic Merkel Cell Carcinoma. Pharmaceutics. 2022;14(7).

35. Mouli SK, Raiter S, Harris K, Mylarapu A, Burks M, Li W, et al. Yttrium-90 Radioembolization to the Prostate Gland: Proof of Concept in a Canine Model and Clinical Translation. J Vasc Interv Radiol. 2021;32(8):1103-12 e12.

36. Zhang W, Liu R, Wang Y, Qian S, Wang J, Yan Z, et al. Efficacy of intraarterial chemoinfusion therapy for locally advanced breast cancer patients: a retrospective analysis of 28 cases. Onco Targets Ther. 2013;6:761-5.

APPENDIX

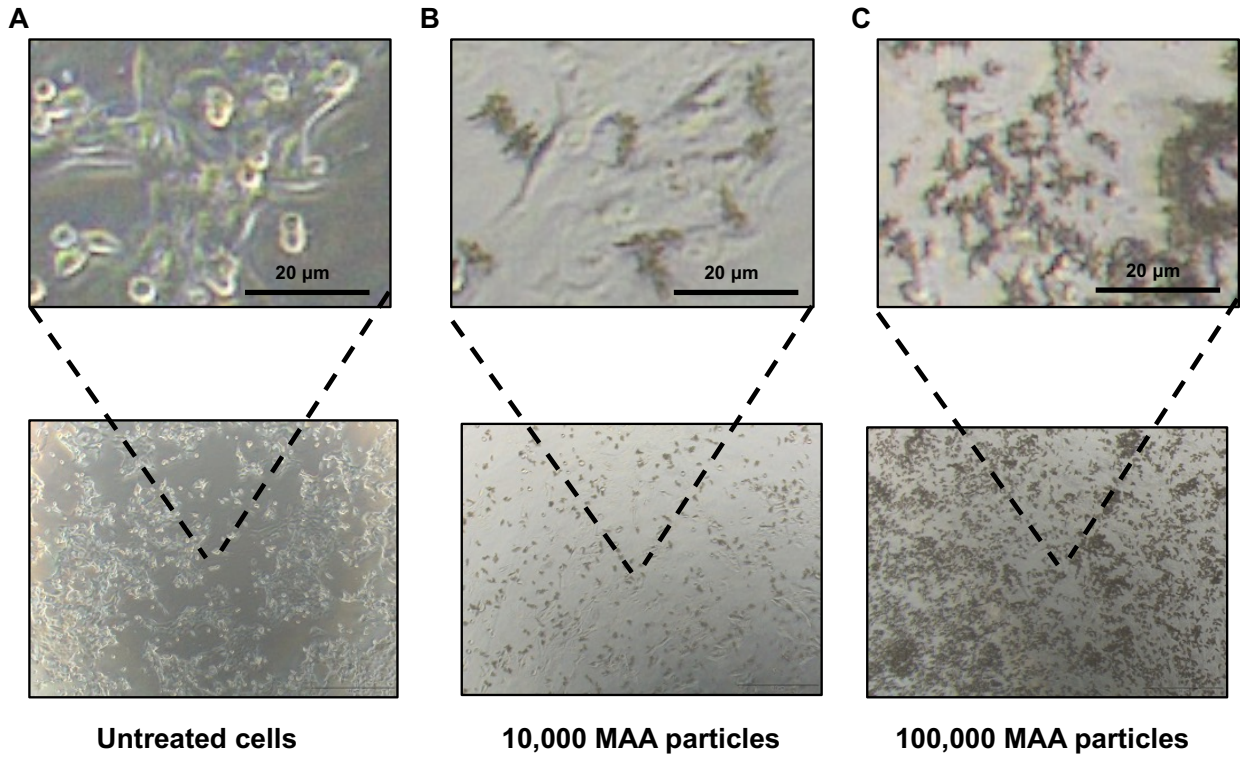

Figure S3.1 | MAA distributes evenly throughout cell culture plates. (A-C) 4T1 cancer cells in a 24-well plate **(A)** are well covered by MAA regardless of lower **(B)** or higher **(C)** amounts of MAA particles.

CHAPTER 4: USE OF FRACTIONATED BI-212-MAA FOR ABLATIVE ALPHA-PARTICLE THERAPY

Introduction

Radiopharmaceuticals for therapeutic purposes are typically injected systemically and use vascular routes to target cancer from inside the body [1-3]. Like radiation emitting brachytherapy devices that are placed internally adjacent to cancer, these radiopharmaceutical drugs emit beta (β-) radiation, negatively charged electrons that are emitted during radioactive decay and penetrate several millimeters into tissue [4-6]. Recently, alpha (α)-particle radiation has been applied for cancer therapy. While α-particle decay is usually accompanied by β- decay, the α-particles deliver significantly more radiation dose over a shorter penetrating range than the β-particles [4-6]. The α-particles are emitted when unstable high atomic number radioisotopes decay. While only one α-emitting radiopharmaceutical is FDA-approved (Ra-223 dichloride), many others are under evaluation in clinical trials [6,7].

The current paradigm that all these α-emitting radiopharmaceuticals share is often referred to as an “in vivo generator” approach which means that the injected drug contains a “parent” radioisotope that decays to a radioactive "daughter” that is also radioactive and the “daughter” releases the radioactive α-particles. The “parent” component may have an extremely long or shorter half-life. Radium-223 and Actinium-225 are examples of radioisotopes with long half-lives (11.4 d and 10 d, respectively) and emit four α-particles in their decay chains. In comparison, shorter-lived Pb-212 (10 hr half-life) decays to Bi-212 (1 hr half-life) which emits one α-particle in its decay chain. Both approaches operate under the same paradigm in that the “parent” radioisotope can be delivered one time and will continuously generate the shorter-lived “daughter” radioisotopes that emit the α-particles. While this “in vivo generator” strategy is attractive, it can lead to large radiation doses to healthy tissue that can preclude higher or repeated long-term doses. It also makes multiple dosings over shorter time intervals, such as 24 hours, an impossible strategy.

An alternate approach is to administer the shorter-lived α-emitting “daughter” radioisotope to reduce potential side effects and allow for repeated short-term dosing. The best example of this is the use of Bismuth-213 for α-particle therapy, which has been used widely in many different studies [8]. Use of Bi-213 goes against the established paradigm in that Bi-213 has a significantly shorter half-life (45 min) than Ra-223, Ac-225 or even Pb-212, and the decay of Bi-213 directly emits an α-particle rather than through a more complex decay scheme. While

the “in vivo generator” paradigm insinuates long-term production of α-particles, Bi-213 can be seen as a more ablative approach (Figure 4.1). Use of Bi-213 separately from selective elution of an Ac-225 generator has led to impressive results in the clinical setting, which has established the ablative approach as a valid option [9-12]. The use of an ablative approach could lead to a reduction in side effects while still maintaining the efficacy of tumor reduction. Further, it allows for short-term fractionated dosing of tumors, similar to the dosing schedule for well-established and efficacious external beam radiation therapy.

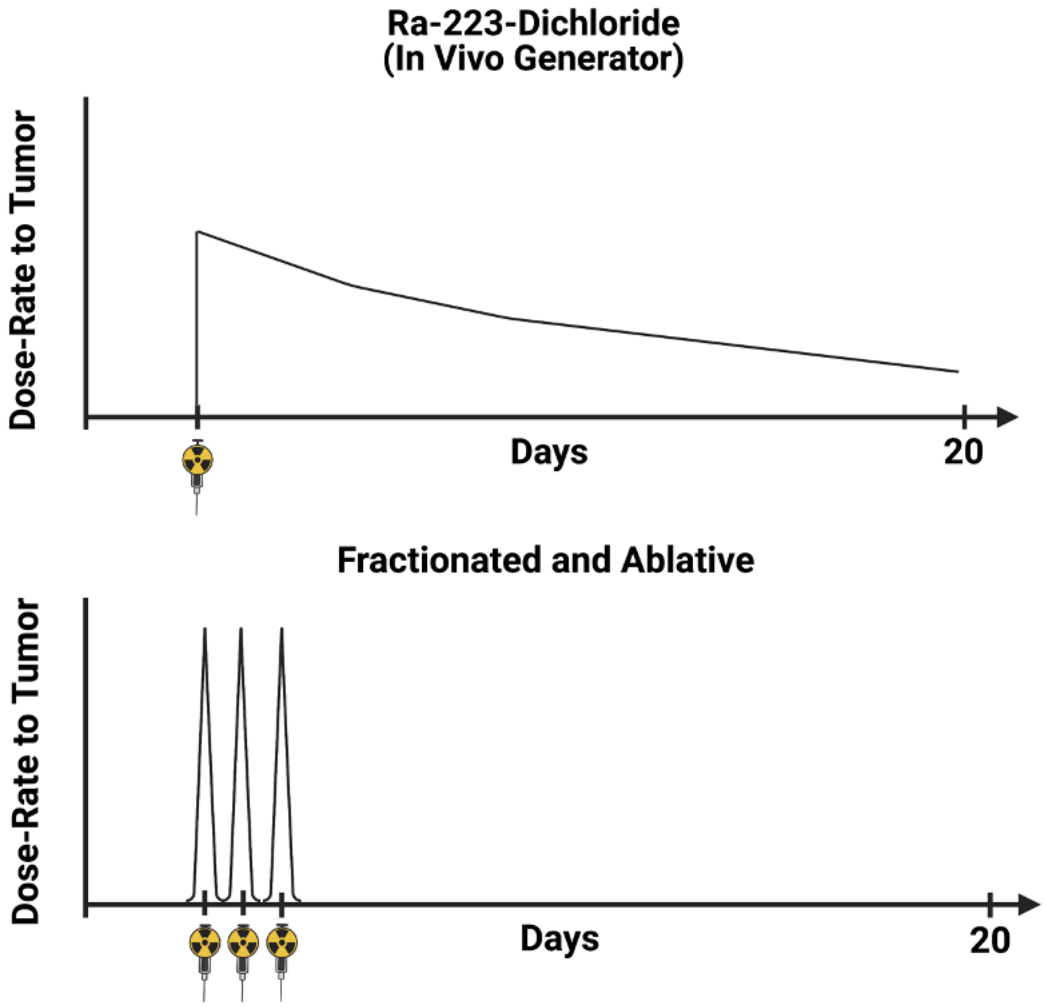

Figure 4.1 | In vivo generator vs. fractionated and ablative dosing. In this graphical example, the decay and dose to tumor (and healthy organs) is shown. Ra-223-dichloride is used as the example here as it is the only approved α-emitting radiopharmaceutical. Due to its long half-life, there will be dose remaining in the patient long after injection. Conversely, the ablative approach gives a higher initial dose but decays away quickly, allowing for short term repeat treatments. Graphic made on Biorender.

Another short-lived, α-emitting radioisotope is Bi-212. Bi-212 is similar to Bi-213 in half-life and α-particle energy. For the current research, Bi-212 was available by selective elution of a Ra-224/Pb-212 generator. Bi-212 has not been widely applied for preclinical studies, and to best of our knowledge, we were the first to report its potential in preclinical breast cancer treatment [13]. In the current report, the efficacy of Bi-212-MAA for fractionated radiation therapy was evaluated in preclinical models of breast cancer. The study also investigated the effect of Bi-212 α-particle radiation therapy on molecular pathways of cancer.

Methods

Pb-212 generator elution

The Ra-224/Pb-212 generator (10 mCi) was provided by Oak Ridge National Lab (The isotopes used in this research were supplied by the U.S. Department of Energy Isotope Program, managed by the Office of Isotope R&D and Production). Elution and preparation of the isotope was done similarly to as previously described [13]. The generator was washed with 500 µL of 2 M HCl upon receipt. Every day afterward, Bi-212 was eluted from the generator with 800µL of 0.15M KI / 0.1 M HCl solution. The eluent was treated with 8 M HNO_3 and evaporated to dryness 3 times. The dried vials containing the Bi-212 were reconstituted with 100µL of 0.1 M HNO_3 for transfer to vials containing 10µL of 1 M NaOH for neutralization. To confirm the purity of the Bi-212 solution, a small sample from each elution was evaluated with a gamma counter (Wizard2, Perkin Elmer) for the energy peak corresponding to Bi-212 only (600 keV). Bi-212 purity was also confirmed by repeatedly measuring Bi-212 samples over time with a dose calibrator (CRC-25R, Capintec) to measure half-life.

Bi-212-MAA radiolabeling and quality control

FDA-approved MAA kits (Pulmotech) were purchased from Cardinal Health (East Lansing, MI). For radiolabeling MAA with Bi-212, 4.5 mg of the MAA kit (0.5 mg MAA) was resuspended in 450µL 0.2 M sodium acetate (pH 4.3) and added to the neutralized Bi-212. The Bi-212-MAA solution was incubated for 10 minutes at 70 °C with 500 RPM shaking. Bi-212-bound MAA was purified by centrifugation at 5000g for 1 minute with the pellet containing the Bi-212 bound MAA and the supernatant containing unbound Bi-212 that was easily removed. The percentage of Bi-212 bound to MAA was determined with instant thin layer chromatography (iTLC) on paper silica gel impregnated strips using 10 mM EDTA in 0.15 M NH_4OAc as the mobile phase.

Cell lines

4T1 and EO771 cells were purchased from ATCC. Cells were cultured in complete media (RPMI or DMEM with 10% FBS, 1% penicillin/streptomycin and 1% L-glutamine, respectively) and incubated at 37 °C with 5% CO_2. Cells were subcultured upon reaching 90% confluency and reseeded at 20% confluency.

For the generation of stably luciferase-expressing cell tines, both 4T1 and EO771 cells were transduced by PLV-10170-pLV-CAG-Firefly luciferase-PGK-Puro plasmid using lentivirus (Cellomics Technology) and luciferase positive clones were selected using puromycin (Thermo Fisher Scientific).

In vitro survival assay

For the survival assay, $5x10^4$ 4T1 and EO771 Luc+ cells were seeded into a 24-well plate. 12 hours later, cells were treated with 0, 10, 50, or 100 μCi of Bi212-MAA and incubated for 48 hours. Bland, unlabeled MAA was used as the 0 μCi condition (Control group), with the number of particles matching those used in the 100 μCi condition. Cells were imaged using IVIS Lumina bioluminescence imaging (BLI) with autoexposure setting at 24- and 48-hours post treatment. Data were analyzed using ROI and radiance (photon/second).

Animals

All animals were purchased from Charles River Laboratory. All animals used in the experiments were of Balb/c and C57BL/6 background (female) and 8 weeks of age. The animal studies were approved by the Institutional Animal Care and Use Committee (IACUC), and all animal experiments were conducted according to IACUC guidelines.

Orthotopic mammary tumor treatment with Bi-212-MAA

Mice that were 8 weeks old were implanted with $1x10^5$ 4T1 (Balb/c mice) and EO771 (C57BL/6 mice) Luc+ cells (respectively) in the left 4^{th} mammary gland. After 7- and 10-days post-implantation, 4T1 and EO771 tumors, respectively, were injected intratumoral (IT) with Bi-212-MAA or vehicle control (bland, unlabeled MAA). Mice with 4T1 and EO771 tumors received 0, 25, 50, 100, 25 (3 times) or 50 (3 times) μCi of Bi-212-MAA suspended in 20 μL of 0.9% sterile saline using 25-gauge integrated needle syringes with zero dead volume. The doses given 3 times were 24 hours apart. Mice were then tracked for tumor growth using digital caliper measurement. All groups were euthanized once the tumor size reached 2 cm in length in any

group. Tumor volume was calculated using the equation (longest diameter x ((shortest diameter/2)^2)).

Treated mouse organ toxicity assays

After completion of the tumor treatment study, sacrificed mice bearing 4T1 tumors had blood and organs removed for analysis. Blood was removed using cardiac puncture with syringes lined with EDTA. Blood samples were then transferred to lavender top EDTA lined collection tubes and were delivered to Michigan State University Veterinary Diagnostic Laboratory for complete blood count analysis. Removed organs were placed in formalin buffer overnight and then transferred to 40% ethanol. These samples were then mounted and H&E stained at the Michigan State University Histopathology Core. Images of tissue slides were taken on Nikon Eclipse Ci-L microscope using 40x magnification. Slides were evaluated by a board-certified veterinary pathologist.

Gene expression analysis

For gene expression analysis, $5x10^5$ 4T1 cells were plated into 6-well plates. After 24 hours, cells were treated with 0, 5, 10, 25, 50 or 100 μCi of Bi-212-MAA. 24 hours after treatment, cells were removed using 1 mL of Trizol reagent and stored in -80 °C for further use. Frozen stocks were thawed, and RNA was prepped using an RNA isolation kit (Invitrogen). cDNA was created using a High-Capacity cDNA Reverse Transcription Kit (Thermo Fisher Scientific). cDNA stocks were diluted for use in a 96-well PrimePCR Assay (BioRad). 20x PrimePCR SYBR Green Primers from BioRad were used with the following Assay ID's: TREX-1 (qMmuCED0061616), CHOP (qMmuCID0005629), Fos (qMmuCED0001023), CXCL1 (qMmuCED0003898), CCL5 (qMmuCID0021047), CCL9 (qMmuCED0003898), MX-1 (qMmuCID0023356), IFN-β (qMmuCED0050444), and GAPDH (qMmuCED0027497). RT-PCR was completed on a QuantStudio 5 Real-Time PCR machine (Thermo Fisher Scientific). CT values were normalized to GAPDH for each sample and fold change compared to 0 μCi control was calculated using $2^{-\Delta\Delta CT}$.

Western blot analysis

For Western blot analysis, $5x10^5$ 4T1 cells were plated into 6-well plates. After 24 hours, cells were treated with 0, 25, 50, 100, 25 (3 times, every 24 hours), or 50 (3 times, every 24 hours) μCi of Bi-212-MAA. 24 hours after treatment, total protein was extracted by lysing the 4T1 cells using RIPA buffer (Thermo Fisher Scientific) with 1X proteinase inhibitor cocktail added (Abcam)

and incubated at 4 °C for 30 min and vortexed 45 seconds every 10 min. Cell lysates were centrifuged at 30,000g for 30 min at 4 °C, and the supernatants were collected and stored at −80 °C for further use. Protein concentration was determined using the Bradford protein assay method. Protein samples were denatured by adding 4x Laemmli sample buffer (BioRad) and heating 95 °C for 5 mins. Further, 40 µg of proteins were run on 4-15% SDS-PAGE gels. Proteins were transferred onto the nitrocellulose membrane, followed by blocking with SuperBlock buffer (Thermo) for 1 hour at room temperature. Next, membranes were incubated with diluted primary antibody (1:1000) in a blocking buffer at 4 °C with gentle shaking for 1 hour. Membranes were washed three times with 1X TBST buffer and further probed with polyclonal anti-rabbit or anti-mouse IgG secondary antibodies conjugated to horseradish peroxidase (HRP) and incubated at room temperature for 1 h. After washing three times with 1X TBST buffer, enhanced chemiluminescence (ECL) solution (Thermo Fisher Scientific) on the top of the membrane, and protein bands were visualized using Chemidoc (BioRad).

Cytokine array

For cytokine quantification, $5x10^5$ 4T1 cells were plated into 6-well plates. After 24 hours, cells were treated with 0, 5, 10, 25, 50 or 100 µCi of Bi-212-MAA. 24 hours after treatment, total protein was extracted by lysing the 4T1 cells using RIPA buffer (Thermo Fisher Scientific) with 1X proteinase inhibitor cocktail added (Abcam) and incubated at 4 °C for 30 min and vortexed 45 seconds every 10 min. Cell lysates were centrifuged at 30,000g for 30 min at 4 °C, and the supernatants were collected and stored at −80 °C for further use. Protein concentration was determined using the Bradford protein assay method. Protein samples were then added to prepared glass slides according to the Mouse Cytokine Array Q5 protocol (RayBiotech). RayBiotech then analyzed the slides. Mean minus background fluorescence values were calculated for each cytokine for each sample and used to compare cytokine levels between treated groups and control.

Statistical analysis

Statistical analysis was performed using GraphPad. One-way analysis of variance (ANOVA) with Dunnett's test was used to compare the experimental groups to the control group. Data are reported as mean ± standard error of the mean (SEM). P-values < 0.05 were considered statistically significant.

Results

Fractionated Bi-212-MAA was non-toxic and effective for therapy in mouse breast cancer

MAA was radiolabeled with Bi-212 in high purity, with specific activity averaging above 2 μCi/μg (2.1 ± 0.4 SE). *In vitro* dose escalation assays confirmed the efficacy of cell killing with higher doses compared to our previous studies. (Figure 4.2A and B). There was the efficacy of treatment even at a lower dose of 10 μCi, as seen by the large reduction in total cell signal after 48 hours. Although there was more killing of both cell lines at 100 μCi dose, the 50 μCi dose performed similarly and was comparable to the 100 μCi dose. These results indicated that the Bi-212 was stably attached to MAA and was able to deliver effective therapy. If the Bi-212-MAA complex was not stable, no therapy would be conferred.

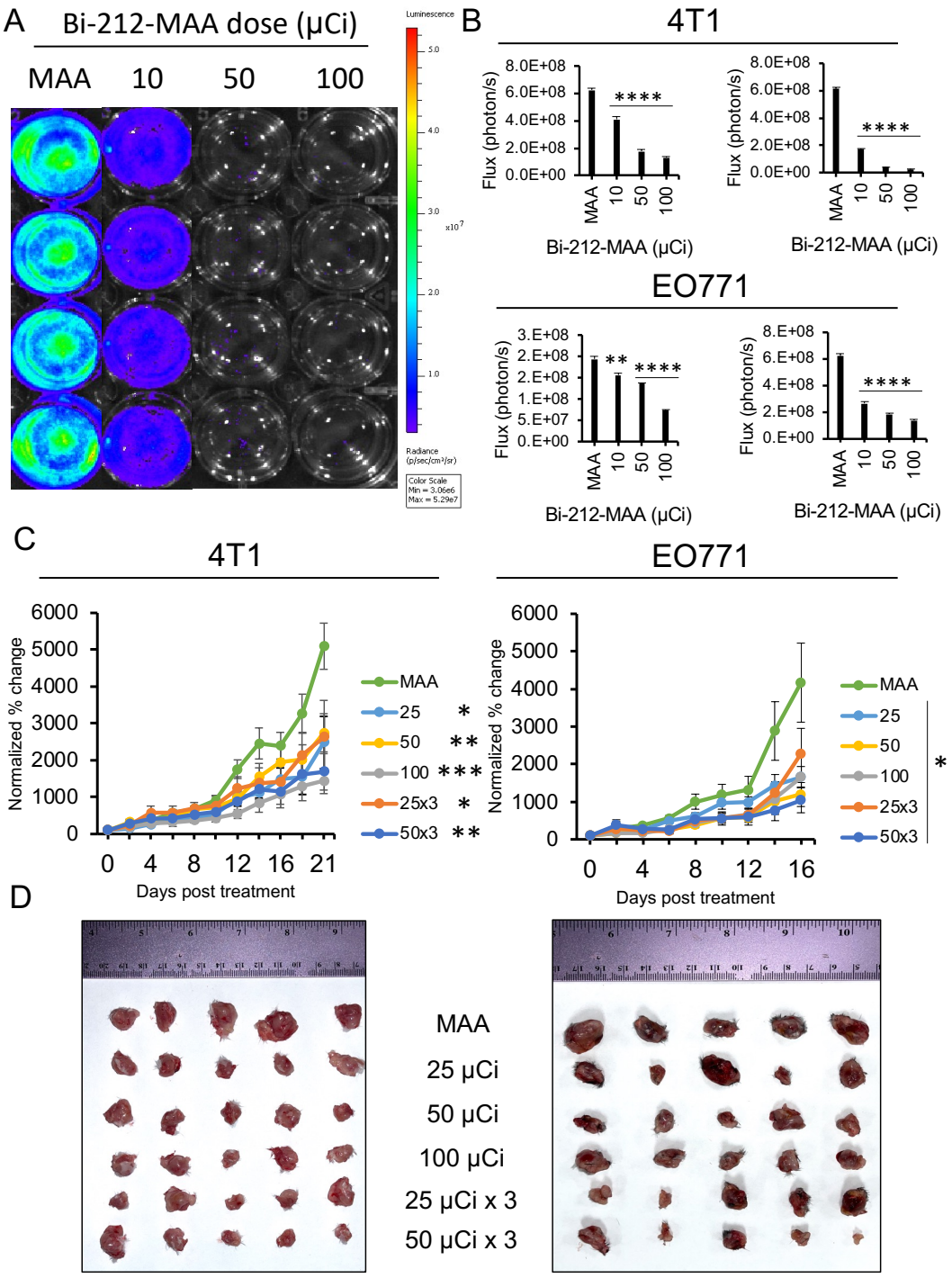

Figure 4.2 | Both high-dose single and fractionated Bi212-MAA treatment decreased mouse tumor growth compared to control. (A,B) Luciferase survival assay imaging with IVIS **(A)** showed significant differences between MAA control and treated groups **(B)** after 24 (left) and 48 (right) hours in both 4T1 and EO771 cells (n = 4). **(C,D)** Caliper measurement of tumors show that growth was reduced when normalized to tumor size at the start of the study **(C)** and final tumor size decreased **(D)** in both 4T1 and EO771 models (n = 5). *, $P < 0.05$; **, $P < 0.01$; ***, $P < 0.001$; ****, $P < 0.0001$.

After confirming efficacy *in vitro*, mice with orthotopic breast tumors were treated with IT-delivered Bi-212-MAA and tracked for tumor size and weight changes. All treatments showed a statistically significant reduction in tumor size compared to MAA control (Figure 4.2C and D) after 21 and 16 days for 4T1 and EO771, respectively. The 4T1 and EO771 tumors did not respond the same for the different dose conditions. The 100 μCi treatment showed the greatest efficacy for the treatment of 4T1 tumors. However, for the EO771 tumors, the best treatment regimen was 50 μCi x 3. However, the differences between these two treatment groups were not statistically significant for either 4T1 or EO771 models. Other doses showed efficacy compared to the control but did not have as much growth reduction compared to the highest treated conditions. These results indicate that fractionating the treatment with a lower dose per individual treatment can achieve similar efficacy.

Mouse weights were followed throughout the study to determine if the fractionated therapy was causing adverse effects in the mice (Figure 4.3A). Although mice with 4T1 and EO771 tumors in the 50 μCi x 3 treatment groups did show a reduction in weight initially, there was no significant difference compared to untreated control at any point in the study. At the end of the study, blood and tissues were collected from 4T1 tumor-bearing mice for complete blood counts and H&E staining, respectively. There were significant histological changes reported for all tissues, regardless of the treatment group. These included extramedullary hematopoiesis, bone marrow hyperplasia, and pneumonia. There were no histologic differences observed between MAA control and any of the treated groups in any organs (Figure 4.3B). Additionally, no significant changes were seen in RBC, platelet, or WBC counts (Figure 4.3C), indicating no bone marrow toxicity. These findings together indicate that the radiation did not cause any toxicity and that any histological changes in these tissues were due to tumor burden, which all mice shared.

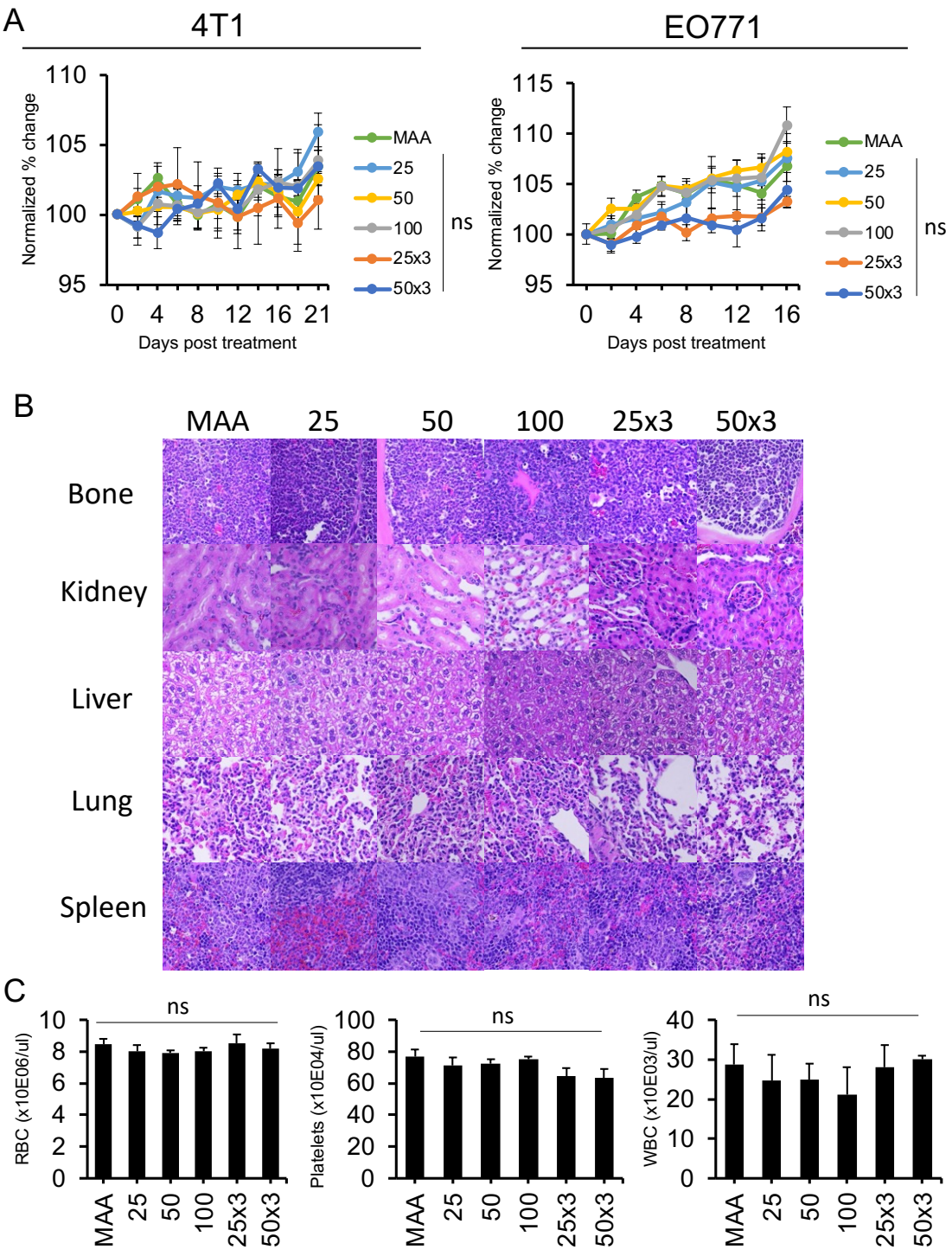

Figure 4.3 | Bi-212-MAA does not cause systemic toxicities in high-dose single or fractionated treatments. No significant change was seen in mouse weights (n = 5) at any timepoint during the study in either 4T1 or EO771 tumor bearing mice **(A)**. Analysis of 4T1 tumor bearing mice shows no changes in normal organ histologic structure **(B)** or blood count analysis **(C)** compared to control samples (n = 5). ns, not significant.

Fractionated Bi-212-MAA treatment increased cell death markers in vitro

After establishing tumor efficacy and safety in mice, investigations were done to evaluate the cellular effects of radiation on a molecular level. Gene expression and protein levels were measured to investigate different signaling pathways of radioresistance in Bi-212-MAA treated 4T1 cells. Treatment with Bi-212-MAA showed only slightly increased gene expression of Trex1 and Fos while CHOP (DDIT3) had significantly decreased levels (Figure 4.4A).

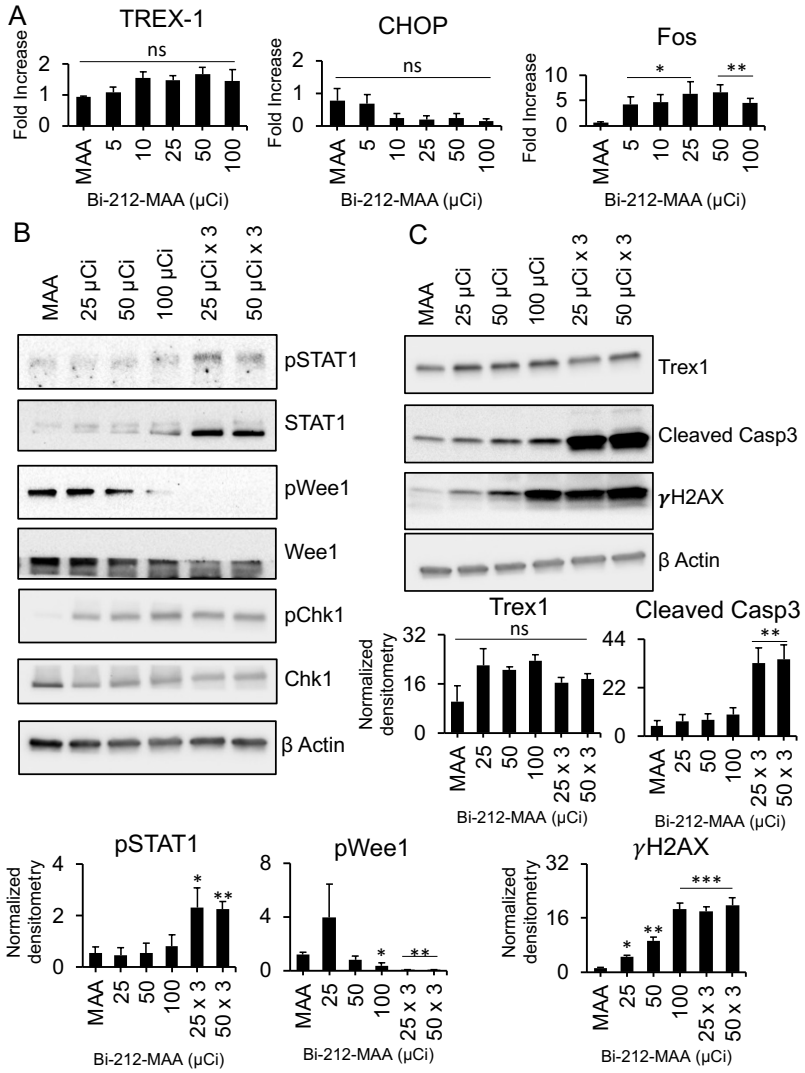

Figure 4.4 | Molecular pathways of cell death and radioresistance after Bi-212-MAA treatment in vitro. Gene expression analysis using qPCR reveals dose response of 4T1 cancer cells (n = 3) *in vitro* **(A)**. **(B,C)** Protein level analysis using western blot confirms varied expression of cell cycle **(B)** and apoptosis **(C)** markers after treatment (n = 3). Graphs are densitometric measured averages of triplicate western blot samples. ns, not significant; *, $P < 0.05$; **, $P < 0.01$; ***, $P < 0.001$.

Western blot analysis of 4T1 cells treated with both single and fractionated Bi-212-MAA showed a variety of responses in regulators of cell cycle (Figure 4.4B). Phosho and total STAT1 levels were increased in the fractionated groups. Phospho and total WEE1 levels were decreased in the highest single dose (100 μCi) and the fractionated groups. Phospho CHK1 was increased in all groups compared to control while total CHK1 levels were decreased. Western blotting of apoptosis-related regulators was also performed (Figure 4.4C). No differences were found in Trex1 levels for any treatment condition compared to control. Cleaved caspase3 was greatly increased in both fractionated conditions compared to control while the single dose treatment did not cause significant changes. $\boldsymbol{\gamma}$H2AX was significantly increased for the highest dose conditions and had an overall linear dose-response with increasing levels of Bi-212-MAA. All of the results reported here are based on densitometric analysis of triplicate samples.

Bi-212-MAA treatment increased cytokine production in vitro

To continue elucidating the intrinsic effects of Bi-212-MAA on cancer cells, 4T1 cells were treated with Bi-212-MAA *in vitro* to investigate the changes in cytokine production in response to increasing dose levels. A cytokine panel revealed varied production in response to dose for many different cytokines (Figure 4.5A). To confirm the increase in production of select cytokines CXCL1, CCL5, and CCL9, qPCR was used to quantify gene expression changes. Lower Bi-212-MAA doses led to increased gene expression, but all 3 cytokines eventually had gene expression trending downward at higher doses (Figure 4.5B). The largest increase in gene expression compared to baseline occurred at 10 μCi for CCL5 and CCL9, while 50 μCi led to the most CXCL1 expression. The 100 μCi dose never caused the greatest increase in gene expression for any of the evaluated cytokines. Similar results were found in the gene expression of MX1 and IFN-β, two important regulators of the interferon pathways. The 25 and 50 μCi Bi-212-MAA treatment groups showed the greatest increases in gene expression compared to baseline of MX1 and IFN-β, respectively (Figure 4.5C).

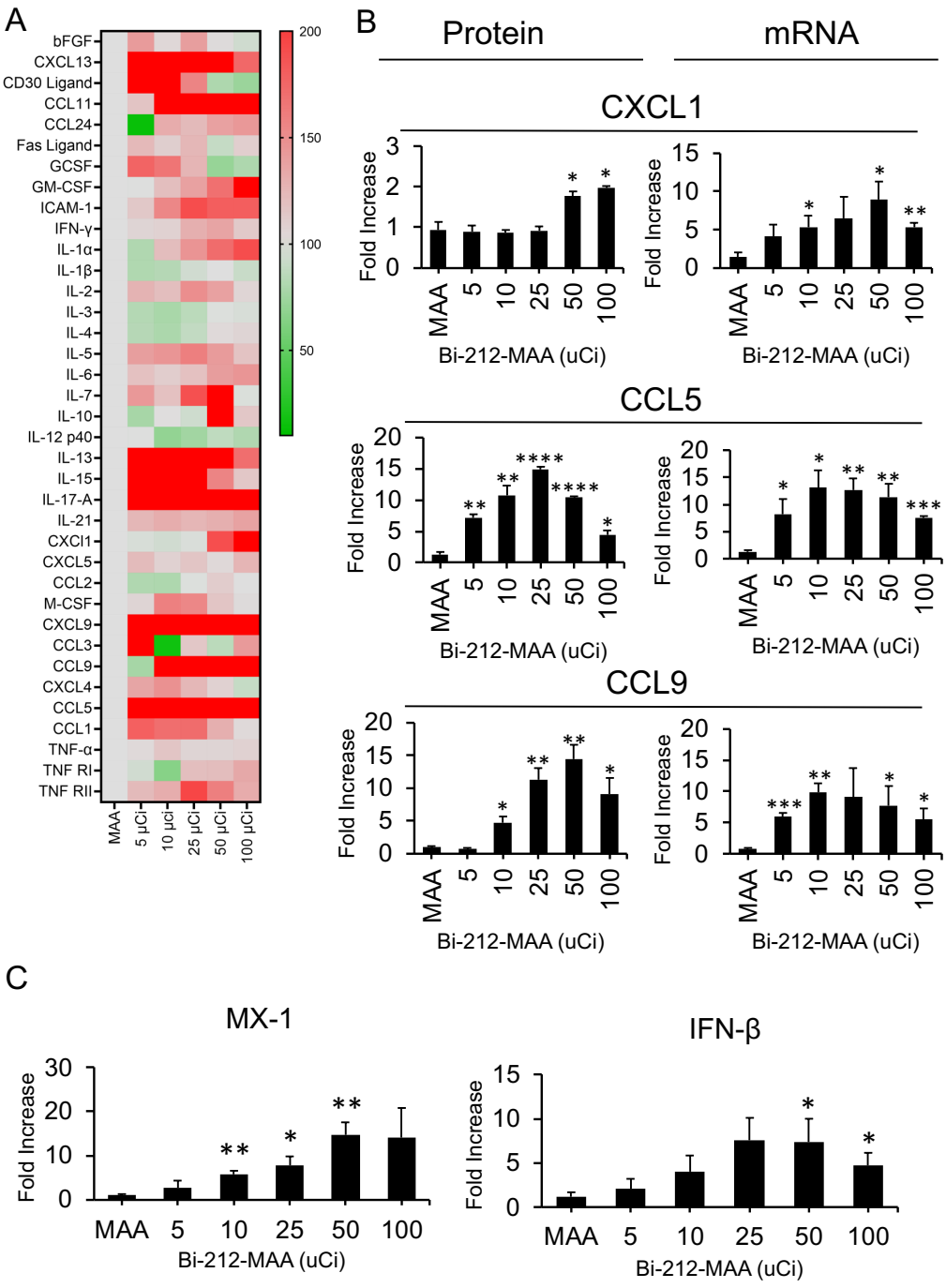

Figure 4.5 | Bi-212-MAA regulates the production of different cytokines involved in tumor suppression at single higher-dose or fractionated treatments. Cytokine panel array reveals varied production of multiple cytokines across treatment conditions (n = 3) **(A)**. Change in expression was confirmed with gene expression analysis using qPCR to compare to the levels of cytokines analyzed in the pane (n = 3) **(B)**. Gene expression analysis was also performed on two other genes of interest that were not included in the panel (n = 3) **(C)**. *, $P < 0.05$; **, $P < 0.01$; ***, $P < 0.001$.

Discussion

Bi-212 was delivered in a fractionated, ablative approach that combined high amounts of radiation and multiple short-term treatments. This approach differs from the "in vivo generator" paradigm, which uses long-lived radioisotopes to deliver radiation doses to tumors over a longer time. The long-lived radioisotopes have potential to cause damage to normal tissues that cause dose limiting toxicity that limits the levels of radiation that can be initially injected. Results presented here demonstrate that delivering 50 μCi levels of the Bi-212-MAA multiple times did not lead to dose limiting toxicity. Therapeutic efficacy using Pb-212-labeled antibodies was reported by other investigators with 15 μCi dose levels, but toxicity in bone marrow was reported with only 5 μCi [14,15]. Based on our studies with Bi-212-MAA it appears the dose can be increased even further without compromising healthy tissues. The IT delivery model may be the reason we did not find differences between the treatment groups. It was difficult to get global and well distributed dosing of the tumor using this method versus targeted systemic treatments. For human translation, the Bi-212-MAA could be more evenly distributed throughout the tumor by using an intra-arterial injection, as is currently accomplished with standard of care yttrium-90-labeled particles that are used for selective internal radiation therapy [16,17].

Various molecular responses to Bi-212-MAA therapy were characterized by measuring gene expression and protein levels of cell cycle regulators. Cell cycle regulators STAT1, Wee1, and CHK1 are critical in cancer defense against radiation damage [18,19]. High dose and fractionation appeared to cause increased expression of STAT1, while Wee1 levels were not increased. CHK1 was equally increased across all levels of Bi212-MAA therapy. The varied dose responses in these cell cycle regulators could inform which dose of Bi-212-MAA is optimal is targeting for synergy, particularly STAT1. STAT1 is well characterized as a radioresistant gene and it appears that Bi-212-MAA also leads to the same resistant response. Since it is already well characterized, inhibitors are available that can be used in combination with Bi-212-MAA to increase efficacy, particularly *in vivo*.

Cleaved caspase3, γH2AX, Trex1, CHOP, and Fos are known to be involved in apoptosis and cell proliferation [20-22]. While the highest doses caused the greatest increase in pro-apoptosis markers, cleaved caspase3 was greatly increased in the fractionated condition. This may indicate that the multiple doses continue to force cells to undergo planned death even more so than in high single dose conditions. The lack of increase in Trex1 and CHOP expression or

protein levels implied the cell was not able to utilize these pathways to resist radiation treatment. Fos interestingly was greatly increased in a dose-dependent manner up to the 50 μCi condition, but then 100 μCi treatment appeared to be trending back down towards control. While 100 μCi dose was still significantly increased compared to control, the downward trend could indicate that higher doses were directing the cell to utilize other pathways.

A limitation in these molecular analyses is lack of single dose conditions that were harvested for analysis at the same timepoint as the fractionated doses. Although single and fractionated doses were both analyzed 24 hours after the final treatment, the fractionated doses were harvested 72 hours after initial exposure. The longer timepoint after initial exposure could lead to increased expression of our targeted markers, regardless of repeated Bi-212 exposure.

A similar up and down trend was seen in our cytokine-related genes and cytokine panel array, other than CXCL1 which had conflicting results across the cytokine protein panel and gene expression. While IFN-β and MX1 are widely reported as being anti-tumor inflammatory markers, the other cytokines have conflicting findings [21,23-27]. CXCL1 is mainly reported as pro-tumor, however the conflicting results of the cytokine and mRNA analysis in the presented study makes it difficult to determine the effect of the dose on CXCL1 expression. CCL5 conversely had a consistent reaction to Bi-212-MAA across the cytokine and mRNA analyses while also being accepted as pro-tumor marker. In this case, it appears that the dose would not have to be tailored and that increasing the dose even further would continue to lower CCL5 expression. The CCL5 trend of increasing initially followed by decreased levels was found in multiple pathways, such as the radioresistance pathways. It may be that the high dose of Bi-212-MAA is so powerful that the cell is fully committed to apoptosis pathways and moves away from any of the pathways it had been initially using for defense.

Although MAA was used as the vehicle in this study, Bi-213 chelated to small molecules and antibodies have been used a systemic targeted therapy in clinical trials [8,10,12,28]. Systemic therapies may inherently lead to more retention in healthy organs meaning care must be taken in identifying the dose-limiting toxicity. The fractionated approach could still be used in these therapies as well as other clinical scenarios to reduce these effects. Understanding the timing and dose of the fractionated schedule is critical for maximizing tumor dosing while limiting healthy tissue toxicity and so should be investigated further in preclinical models for eventual clinical translation. Additionally, tailoring the schedule and dose levels based on

molecular mechanisms such as radioresistance and cytokine production can lead to better responses. Elucidating these mechanisms could reveal pathways that could then be targeted with combination therapies, leading to improved synergy and better overall response.

BIBLIOGRAPHY

1. Aboagye, E.O.; Barwick, T.D.; Haberkorn, U. Radiotheranostics in oncology: Making precision medicine possible. *CA Cancer J Clin* **2023**, doi:10.3322/caac.21768.
2. Degrauwe, N.; Hocquelet, A.; Digklia, A.; Schaefer, N.; Denys, A.; Duran, R. Theranostics in Interventional Oncology: Versatile Carriers for Diagnosis and Targeted Image-Guided Minimally Invasive Procedures. *Front Pharmacol* **2019**, *10*, 450, doi:10.3389/fphar.2019.00450.
3. Sgouros, G.; Bodei, L.; McDevitt, M.R.; Nedrow, J.R. Radiopharmaceutical therapy in cancer: clinical advances and challenges. *Nat Rev Drug Discov* **2020**, *19*, 589-608, doi:10.1038/s41573-020-0073-9.
4. Bodei, L.; Cremonesi, M.; Grana, C.M.; Fazio, N.; Iodice, S.; Baio, S.M.; Bartolomei, M.; Lombardo, D.; Ferrari, M.E.; Sansovini, M.; et al. Peptide receptor radionuclide therapy with (1)(7)(7)Lu-DOTATATE: the IEO phase I-II study. *Eur J Nucl Med Mol Imaging* **2011**, *38*, 2125-2135, doi:10.1007/s00259-011-1902-1.
5. Sgouros, G.; Roeske, J.C.; McDevitt, M.R.; Palm, S.; Allen, B.J.; Fisher, D.R.; Brill, A.B.; Song, H.; Howell, R.W.; Akabani, G.; et al. MIRD Pamphlet No. 22 (abridged): radiobiology and dosimetry of alpha-particle emitters for targeted radionuclide therapy. *J Nucl Med* **2010**, *51*, 311-328, doi:10.2967/jnumed.108.058651.
6. Tafreshi, N.K.; Doligalski, M.L.; Tichacek, C.J.; Pandya, D.N.; Budzevich, M.M.; El-Haddad, G.; Khushalani, N.I.; Moros, E.G.; McLaughlin, M.L.; Wadas, T.J.; et al. Development of Targeted Alpha Particle Therapy for Solid Tumors. *Molecules* **2019**, *24*, doi:10.3390/molecules24234314.
7. Kauffman, N.; Morrison, J.; O'Brien, K.; Fan, J.; Zinn, K.R. Intra-Arterial Delivery of Radiopharmaceuticals in Oncology: Current Trends and the Future of Alpha-Particle Therapeutics. *Pharmaceutics* **2023**, *15*, doi:10.3390/pharmaceutics15041138.
8. Ahenkorah, S.; Cassells, I.; Deroose, C.M.; Cardinaels, T.; Burgoyne, A.R.; Bormans, G.; Ooms, M.; Cleeren, F. Bismuth-213 for Targeted Radionuclide Therapy: From Atom to Bedside. *Pharmaceutics* **2021**, *13*, doi:10.3390/pharmaceutics13050599.
9. Allen, B.J.; Raja, C.; Rizvi, S.; Li, Y.; Tsui, W.; Graham, P.; Thompson, J.F.; Reisfeld, R.A.; Kearsley, J. Intralesional targeted alpha therapy for metastatic melanoma. *Cancer Biol Ther* **2005**, *4*, 1318-1324, doi:10.4161/cbt.4.12.2251.
10. Autenrieth, M.E.; Seidl, C.; Bruchertseifer, F.; Horn, T.; Kurtz, F.; Feuerecker, B.; D'Alessandria, C.; Pfob, C.; Nekolla, S.; Apostolidis, C.; et al. Treatment of carcinoma in situ of the urinary bladder with an alpha-emitter immunoconjugate targeting the epidermal growth factor receptor: a pilot study. *Eur J Nucl Med Mol Imaging* **2018**, *45*, 1364-1371, doi:10.1007/s00259-018-4003-6.
11. Kneifel, S.; Cordier, D.; Good, S.; Ionescu, M.C.; Ghaffari, A.; Hofer, S.; Kretzschmar, M.; Tolnay, M.; Apostolidis, C.; Waser, B.; et al. Local targeting of malignant gliomas by the diffusible peptidic vector 1,4,7,10-tetraazacyclododecane-1-glutaric acid-4,7,10-triacetic acid-substance p. *Clin Cancer Res* **2006**, *12*, 3843-3850, doi:10.1158/1078-0432.CCR-05-2820.

12. Sathekge, M.; Knoesen, O.; Meckel, M.; Modiselle, M.; Vorster, M.; Marx, S. (213)Bi-PSMA-617 targeted alpha-radionuclide therapy in metastatic castration-resistant prostate cancer. *Eur J Nucl Med Mol Imaging* **2017**, *44*, 1099-1100, doi:10.1007/s00259-017-3657-9.

13. Kauffman, N.; Singh, S.K.; Morrison, J.; Zinn, K.R. Effective therapy with Bismuth-212 labeled macroaggregated albumin in orthotopic mouse breast tumor models. *Front Chem* **2023**, *11*, 1204872, doi:10.3389/fchem.2023.1204872.

14. Kasten, B.B.; Gangrade, A.; Kim, H.; Fan, J.; Ferrone, S.; Ferrone, C.R.; Zinn, K.R.; Buchsbaum, D.J. (212)Pb-labeled B7-H3-targeting antibody for pancreatic cancer therapy in mouse models. *Nucl Med Biol* **2018**, *58*, 67-73, doi:10.1016/j.nucmedbio.2017.12.004.

15. Milenic, D.E.; Molinolo, A.A.; Solivella, M.S.; Banaga, E.; Torgue, J.; Besnainou, S.; Brechbiel, M.W.; Baidoo, K.E. Toxicological Studies of 212Pb Intravenously or Intraperitoneally Injected into Mice for a Phase 1 Trial. *Pharmaceuticals (Basel)* **2015**, *8*, 416-434, doi:10.3390/ph8030416.

16. Bakker, R.C.; Lam, M.; van Nimwegen, S.A.; Rosenberg, A.; van Es, R.J.J.; Nijsen, J.F.W. Intratumoral treatment with radioactive beta-emitting microparticles: a systematic review. *J Radiat Oncol* **2017**, *6*, 323-341, doi:10.1007/s13566-017-0315-6.

17. Spyridonidis, T.; Papathanasiou, N.; Spyridonidis, J.; Ntzoumani, C.; Spyropoulou, D.; Katsanos, K.; Apostolopoulos, D.J. (90)Y-microsphere radioembolization: The method, clinical evidence and perspective. *Hell J Nucl Med* **2020**, *23*, 330-338, doi:10.1967/s002449912210.

18. Chan Wah Hak, C.M.L.; Rullan, A.; Patin, E.C.; Pedersen, M.; Melcher, A.A.; Harrington, K.J. Enhancing anti-tumour innate immunity by targeting the DNA damage response and pattern recognition receptors in combination with radiotherapy. *Front Oncol* **2022**, *12*, 971959, doi:10.3389/fonc.2022.971959.

19. Liu, S.; Imani, S.; Deng, Y.; Pathak, J.L.; Wen, Q.; Chen, Y.; Wu, J. Targeting IFN/STAT1 Pathway as a Promising Strategy to Overcome Radioresistance. *Onco Targets Ther* **2020**, *13*, 6037-6050, doi:10.2147/OTT.S256708.

20. Chen, H.; Han, Z.; Luo, Q.; Wang, Y.; Li, Q.; Zhou, L.; Zuo, H. Radiotherapy modulates tumor cell fate decisions: a review. *Radiat Oncol* **2022**, *17*, 196, doi:10.1186/s13014-022-02171-7.

21. Vanpouille-Box, C.; Alard, A.; Aryankalayil, M.J.; Sarfraz, Y.; Diamond, J.M.; Schneider, R.J.; Inghirami, G.; Coleman, C.N.; Formenti, S.C.; Demaria, S. DNA exonuclease Trex1 regulates radiotherapy-induced tumour immunogenicity. *Nat Commun* **2017**, *8*, 15618, doi:10.1038/ncomms15618.

22. Widjaja, L.; Werner, R.A.; Krischke, E.; Christiansen, H.; Bengel, F.M.; Bogdanova, N.; Derlin, T. Individual radiosensitivity reflected by gamma-H2AX and 53BP1 foci predicts outcome in PSMA-targeted radioligand therapy. *Eur J Nucl Med Mol Imaging* **2023**, *50*, 602-612, doi:10.1007/s00259-022-05974-8.

23. Acharyya, S.; Oskarsson, T.; Vanharanta, S.; Malladi, S.; Kim, J.; Morris, P.G.; Manova-Todorova, K.; Leversha, M.; Hogg, N.; Seshan, V.E.; et al. A CXCL1 paracrine network links cancer chemoresistance and metastasis. *Cell* **2012**, *150*, 165-178, doi:10.1016/j.cell.2012.04.042.

24. Aldinucci, D.; Borghese, C.; Casagrande, N. The CCL5/CCR5 Axis in Cancer Progression. *Cancers (Basel)* **2020**, *12*, doi:10.3390/cancers12071765.

25. Huang, R.; Wang, S.; Wang, N.; Zheng, Y.; Zhou, J.; Yang, B.; Wang, X.; Zhang, J.; Guo, L.; Wang, S.; et al. CCL5 derived from tumor-associated macrophages promotes prostate cancer stem cells and metastasis via activating beta-catenin/STAT3 signaling. *Cell Death Dis* **2020**, *11*, 234, doi:10.1038/s41419-020-2435-y.

26. Kitamura, T.; Fujishita, T.; Loetscher, P.; Revesz, L.; Hashida, H.; Kizaka-Kondoh, S.; Aoki, M.; Taketo, M.M. Inactivation of chemokine (C-C motif) receptor 1 (CCR1) suppresses colon cancer liver metastasis by blocking accumulation of immature myeloid cells in a mouse model. *Proc Natl Acad Sci U S A* **2010**, *107*, 13063-13068, doi:10.1073/pnas.1002372107.

27. Lazarczyk, M.; Kurzejamska, E.; Mickael, M.E.; Poznanski, P.; Skiba, D.; Sacharczuk, M.; Gaciong, Z.; Religa, P. Mouse CCL9 Chemokine Acts as Tumor Suppressor in a Murine Model of Colon Cancer. *Curr Issues Mol Biol* **2023**, *45*, 3446-3461, doi:10.3390/cimb45040226.

28. Kratochwil, C.; Giesel, F.L.; Bruchertseifer, F.; Mier, W.; Apostolidis, C.; Boll, R.; Murphy, K.; Haberkorn, U.; Morgenstern, A. (2)(1)(3)Bi-DOTATOC receptor-targeted alpha-radionuclide therapy induces remission in neuroendocrine tumours refractory to beta radiation: a first-in-human experience. *Eur J Nucl Med Mol Imaging* **2014**, *41*, 2106-2119, doi:10.1007/s00259-014-2857-9.

CHAPTER 5: CONCLUSION AND FUTURE DIRECTIONS

Conclusion

Two separate radiopharmaceutical agents were investigated for cancer therapeutic applications based on radiation delivered during decay of the radioactive component of the agents. Pb-212-GlaS-Fc was developed for systemic targeted therapy and Bi-212-MAA for locoregionally delivered embolic therapy. Development of each agent highlighted the typical vertical paradigm of preclinical radiotheranostic development, which consists of three steps; target:vehicle identification, *in vitro* verification, and establishment of *in vivo* characteristics. The first step was identification of a mechanism for specific targeting of cancer using an entity designed to achieve that goal. Identification of PS as a biological target, design of PS targeting GlaS-Fc, and quality control testing of chelating and radiolabeling procedures were all parts of the first step. This first step required in depth knowledge of currently available vehicles, chelators, and radionuclides. These components were tailored to each project depending on the goal (imaging, therapy, both) and the specific biology that was targeted.

The second step involved *in vitro* validating steps for binding and cancer cell targeting and killing efficacy. This step is much more conserved across preclinically developed radiopharmaceuticals. After radiolabeling a ligand, it must be established that the ligand has not lost affinity for the target. If the radiopharmaceutical is for therapy, then efficacy against cancer cells in monolayer cell culture is required and is typically accomplished through clonogenic assays or survival assays. In the case of Bi-212-MAA, it was unknown if the MAA would bring the Bi-212 close enough to cells to deliver treatment. *In vitro* testing confirmed the dose needed to effectively kill cells. For the Bi-212-MAA clonogenic assays performed in a 6-well plate, 20 μCi was sufficient to kill all cells. These experiments proved that Bi-212-MAA could deliver radiation to cancer cells and that 20 μCi was sufficient for complete cell control.

Step three involved *in vivo* pharmacokinetics and imaging/therapy studies. These studies included biodistribution to determine the levels of the radiopharmaceutical in non-target tissues and survival studies to determine efficacy of therapy at a variety of doses. Normally the results of the clonogenic assay would educate the dose to be used in an *in vivo* model. Assuming the radiopharmaceutical of interest targets and binds to every single cancer cell, then the disease would be eradicated at that same dose. This never turns out to be the case, although many systemic targeted therapies perform very well using the dose found to be efficacious in cell

culture. In the case of Bi-212-MAA, a tumor receptor agnostic radiopharmaceutical, an increased dose was used to compensate for the lack of specific targeting. Excitingly, in our studies the higher dose conditions did not affect the mice negatively. Once a radiopharmaceutical has been shown to effectively treat tumors without delivering toxic doses to healthy tissues, then it can be considered for a translation to clinic for a Phase 1 study.

Each project presented in this dissertation stands at a different point in the preclinical development spectrum. Pb-212-GlaS-Fc will require more experiments to understand the biology and mechanism before moving to the *in vivo* models of targeting cancer. The next step in this project will need to focus on understanding the mechanism behind oligomerization to educate how the radiopharmaceutical should be delivered for *in vivo* models. If the oligomerization can be specifically controlled *in vitro*, then attempts should be made to capitalize on this effect *in vivo*. If not, then GlaS-Fc can simply be treated as any other systemic targeted radiopharmaceutical and be tested for pharmacokinetics and dynamics. While the oligomerization property is exciting, it may not be critical for delivering radiation to tumors. If there is a cancer specific target and a ligand that can be radiolabeled, then there remains potential for a valid radiopharmaceutical for imaging and therapy. Biodistribution and imaging studies in mice bearing tumors can be used to quickly uncover if GlaS-Fc is a viable therapeutic. The short biological half-life, as seen by low levels of Tc-99m-GlaS-Fc being present in the blood after only a few hours, may be difficult to overcome if there is not high enough PS expression in the tumor. This could be modified with first treating the tumor with a different modality to increase PS expression. The timing of PS expression and injection of the radiolabeled GlaS-Fc would need to be understood to utilize this effect. Additionally, IT or IA delivery of GlaS-Fc could improve tumor targeting further.

Bi-212-MAA conversely is ready for clinical translation. It was shown to be a stable radiopharmaceutical that was effective for treatment of tumors in mice without dose limiting toxicities. Bi-212-MAA could also be delivered using an IA procedure instead of IT like done in the presented mouse studies. This would greatly increase the efficacy of the treatment and likely lead to even higher levels of dose being retained in the tumor. A Phase 1 study for Bi-212-MAA would first need approval from the FDA as an Investigational New Drug (IND). This would require all of the preclinical data as provided in this dissertation, as well potentially additional data depending on the novelty of the radiopharmaceutical developed or specific side effects of

the ligand or cancer biology targeted (as determined by the IND review committee). While the preclinical data is crucial, the Phase 1 trial design must also be approved and is thus equally as important. For Bi-212-MAA, the design of the study would likely be a dose escalation study in patients that have already failed all standard of care treatments. A typical phase 1 design would include a total of 12 patients, with 3 different doses delivered and 3 patients in each cohort. The highest dose that does not see toxicity could then be expanded with 3 additional patients to confirm no toxicity. This would confirm safety of the IA delivery of Bi-212-MAA and potentially show efficacy as well, although efficacy is typically investigated in Phase 2/3 trials.

While initial Phase 1 studies are being explored, a further understanding of Bi-212-MAA's effects on cancer cells both *in vitro* and *in vivo* should be elucidated. The Phase 1 trial will determine maximum tolerable dose, but further pre-clinical studies can reveal what dose is best for combination therapy. Cancer treatment is rarely done with only a single drug or modality, meaning searching for synergistic combination therapies is critical. Very little is known about the molecular response of cancer cells after α-particle therapy. Most research has focused on solely on cytotoxicity and treatment efficacy, which is understandable. However, as is being seen with external beam radiation therapy, synergistic effects can be the better strategy overall. A concerted effort towards elucidating underlying molecular response of cancer cells and the tumor microenvironment is needed and should be sought after.

Use of short-lived α-emitting Bismuth radioisotopes for fractionated and ablative therapy is a very exciting prospect. The clinical performance of Bi-213 is already an example of what is possible. Initial testing of fractionated and ablative dosing should be done to achieve the most tumor targeting while minimizing dose to healthy tissue. This would be a major advancement for the field of α-particle therapeutics since the long half-life and strength of "in vivo generator" systems can lead to dose limiting toxicity in patients who still have disease that needs to be treated. While α-particle therapy in general needs more research into the molecular effects on cancer and potential synergies, it is believed that a fractionated approach would be more likely to cause targetable changes. This is because the tumor microenvironment will be radioactive for a shorter amount of time and will try to return to homeostasis or adjust survival strategies more quickly. This is when the tumor cell is most exposed, and synergy can be found. No current cancer therapy works perfectly in every single patient treated with it, necessitating the discovery of synergistic strategies to overcome resistance.

In conclusion, this dissertation outlines many of the basic assays required to move a radiopharmaceutical through preclinical development. Further, discovery of the oligomerization of GlaS-Fc and navigating the challenges of developing a drug without tumor specific biological targeting (Bi-212-MAA) highlights the unique skillset and open frame of mind required to carry out experiments in this area of research. Preclinical development of radiopharmaceuticals requires a multifaceted team with expertise in a variety of areas including cancer biology, nuclear physics, and radiochemistry. Additionally, the lack of availability of therapeutic radioisotopes, especially α-particle emitters, makes progress very slow. With increased access to the resources required to participate in this field, more α-particle emitting radiopharmaceuticals can be put through the preclinical development pipeline leading to more treatments being available to patients and overall better outcomes.